TAILORING BENZODITHIOPHENE CORE MOLECULES FOR ORGANIC ELECTRONIC APPLICATIONS

A Dissertation
Presented to
The Academic Faculty

by

Coralie Adèle Richard

In Partial Fulfillment
of the Requirements for the Degree
Doctor of Philosophy in the
School of Chemistry and Biochemistry

Georgia Institute of Technology
May 2014

TAILORING BENZODITHIOPHENE CORE MOLECULES FOR ORGANIC ELECTRONIC APPLICATIONS

Approved by:

Dr. John R. Reynolds, Advisor
School of Chemistry and Biochemistry
Georgia Institute of Technology

Dr. Elsa Reichmanis
School of Chemical and Biomolecular Engineering
Georgia Institute of Technology

Dr. Stefan France
School of Chemistry and Biochemistry
Georgia Institute of Technology

Dr. Zhiqun Lin
School of Materials Science and Engineering
Georgia Institute of Technology

Dr. David Collard
School of Chemistry and Biochemistry
Georgia Institute of Technology

Date Approved: March 03, 2014

“Go back?" he thought. "No good at all! Go sideways? Impossible! Go forward? Only thing to do! On we go!" So up he got, and trotted along with his little sword held in front of him and one hand feeling the wall, and his heart all of a patter and a pitter.”

— *J.R.R. Tolkien, The Hobbit*

To my parents and my family

ACKNOWLEDGEMENTS

When striving toward PhD studies, working hard is a necessary but not sufficient condition. Graduate school pushes our boundaries, and makes tenaciousness and diligence our two best friends. Fortunately, this journey is not lonely and is filled with people willing to help. I would like to recognize those who encouraged me through this challenging and exciting adventure.

My first acknowledgement goes to Professor John Reynolds. I am grateful that he accepted me into his group, and that he gave me the chance to move with him to the Georgia Institute of Technology. He has always pushed me to give my best, while still being understanding and comforting in moments of doubt. He guided me through the conception and development of a project, through grants, exams, manuscripts and cover letter writing, and provided me the opportunity of giving an oral presentation at a F-Pi conference. His dedication to the group is remarkable and commendable.

Moving from the University of Florida to the Georgia Institute of Technology gave me the opportunity to have two committees. At the University of Florida, I would like to acknowledge Professors Wagener, Veige, Xue and Christou, for advancing my general knowledge to a PhD candidacy level. At the Georgia Institute of Technology, I express my gratitude to Professors Reichmanis, France, Collard and Lin for helping me to carry my dissertation to completion, and for guiding me in the choice of my career.

I would like to thank my collaborators at the University of Florida: Professor Kirk Schanze and his group members, Zhenxing Pan, Hsien-Yi Hsu, Seda Cekli and Anand Parthasarathy. They all made my trips to Gainesville enjoyable and productive. I want to

express my gratitude to Keith Johnson, a brilliant undergraduate in the Reynolds' group. Working with him was highly enjoyable, and I wish him plenty of luck for the future.

Thank you to Drs. Jianguo Mei and Dan Patel, who guided me through the realm of organic synthesis. Upon my arrival, they took me under their wings, and patiently taught me the fundamentals of laboratory synthesis. A special thanks goes to Dr. Frank Arroyave, for both his crazy ideas and his invaluable friendship. I owe him more than I could give back. Jianguo, Dan and Frank's friendships are special to me: even when they are far away in distance, they are always a call away to guide me through chemistry and life.

I arrived at a special time in the Reynolds group, and I was fortunate to encounter wonderful people. I would like to thank Natasha Terán, my personality complement, Caroline Grand for "son amitié et nos fous rires partagés", Dr. Toan Pho, and his decision-making ability, and Dr. Mike Craig, for his useful tips and friendship. Also, I am grateful for all the cheerful moments and/or scientific discussions shared with Ray Bulloch, Gaëlle Deshayes, Aubrey Dyer, Leandro Estrada, Kenneth Graham, Jacob Jensen, Justin Kerszulis, Teresa Palazzo, Egle Puodziukynaite, Anna Salvati, Eric Shen, and finally Romain Stalder. My amount of gratitude for these people can't be well conveyed in these few lines. I also want to recognize the "new synthetic generation", Kin Lo, James Ponder, and Rylan Wolfe. Organic synthesis is a challenging science, and I wish them happiness and bright prospects.

Many thanks to Cheryl Googins and Sara Klossner at the University of Florida and Aeryal Herrod at the Georgia Institute of Technology for their incredible help and

their magic in making the group run smoothly. Their friendliness and caring was a warm breeze for me.

In a more personal note, I am thankful to my dear friends Marie Secco, Pauline Riche, Amélie Héricher, Katie Meese, Katherine Graham, Ivy Devitt, and Yangbae Park. Your support and friendship were tremendously precious to me, and helped me through my toughest time in the US. A very special thanks goes to Rylan for his support. It is incredible how a one dollar bill made such a difference in my life. Lastly, I would like to conclude this section by acknowledging the most special people in my life: my parents and my family. Merci for all the love and support you provided me, even 7454.48 km apart. Your sacrifices and unconditional love provided me the strength to face the world with cheerfulness, joy and hope. I am greatly indebted to you as I could have never made it without you.

TABLE OF CONTENTS

LIST OF TABLES

LIST OF FIGURES

LIST OF SCHEMES

LIST OF ABBREVIATIONS

A	Acceptor
ACN	Acetonitrile
Ag	Silver
AO	Atomic Orbital
APCE	Absorbed photon-to-current efficiency
BDT	Benzodithiophene
BDTD	Benzodithiophene-dione
CB	Conduction band
CV	Cyclic Voltammetry
D	Donor
D_2A	$(Donor)_2$-Acceptor
DBP	Dibenzophenazine
DCM	Dichloromethane
DFT	Density functional theory
DMF	Dimethylformamide
DPV	Differential pulse voltammetry
DSSC	Dye-sensitized solar cell
DTBT	Dithienyl-benzothiadiazole
DTP	Dithienophenazine
DTS	Dithienosilole
Fc	Ferrocene
fDA	fused donor-acceptor

FF	Fill factor
FTO	Fluoride-doped tin oxide
GTO	Gaussian type orbital
HOMO	Highest occupied molecular orbital
IPCE	Incident photon-to-current efficiency
Jsc	Short circuit current
J-V	Current density-voltage
LHE	Light harvesting efficiency
LUMO	Lowest unoccupied molecular orbital
OFETS	Organic field-effect transistors
OLED	Organic light emitting device
OPV	Organic Photovoltaics
PC	Propylene carbonate
$PC_{61}BM$	[6,6]-phenyl-C61-butyric acid methyl ester
$PC_{71}BM$	[6,6]-phenyl-C71-butyric acid methyl ester
PCE	Power conversion efficiency
PDI	Polydispersity index
ProDOT	Propylenedioxythiophene
$TBAPF_6$	Tetrabutylammonium hexafluorophosphate
TDDFT	Time-dependent density functional theory
TFA	Trifuoroacetic acid
TiO_2	Titanium dioxide
Voc	Open circuit voltage

SUMMARY

In this dissertation, the multiple facets of benzodithiophene (BDT) units are explored, with a focus on understanding how the isomerism of the BDT structure affects the macroscopic properties of the oligomeric and polymeric materials created. First, the story focuses on an overview of the BDT synthons and their applications in organic electronics. After describing the experimental methods used in this thesis, a straightforward synthesis of BDT and its derivatization to seven π-conjugated building blocks and seven polymers is presented. Notably, a structure:property relationship study of three isomeric polymers is described, and through computational and optoelectronic studies, shows that a small difference in the structural unit varies the absorption maxima from 447 to 508 nm, and the emission wavelength from 497 to 541 nm. Chapters 4 and 5 report a symmetric $(donor)_2$-acceptor (D_2-A) dye architecture for application in dye-sensitized solar cells. Two isomeric systems are studied: linear, where the conjugation pathway extends along a set of conjugated donors, and branched, where the conjugated donors are directly conjugated with the acceptor π-system. The branched dyes have a higher overlapping of the frontier orbital density, a smaller barrier for injection into titanium dioxide and a greater incident photon-to-current efficiency than the linear dyes. The nature of the core is also varied between dibenzophenazine to dithienophenazine. The sensitizer with the weakest accepting core displays the best photovoltaic performance, due to an increase in the open-circuit voltage of ~100 mV caused by the favorable shift of the metal oxide conduction band. Lastly, a study of the donating building blocks in these (D_2-A) sensitizers demonstrates that increasing the number of

donor units from two to six thiophene moiety doubles the solar cell performance, due to the improvement of the light harvesting ability.

CHAPTER 1

INTRODUCTION

1.1. Benzodithiophenes: Origin and Applications in Organic Electronics

In the last 60 years, more than 500 studies were reported on benzodithiophene (BDT). This section focuses on a concise review of the BDT units as building blocks for applications in organic field transistors and organic photovoltaics.

1.1.1 A Brief History of Benzodithiophene

The synthesis of BDT isomers were reported for the first time by Rao and Tilak in 1954.[2] The interest in these molecules originally lied in the difficult task of assigning the proper isomeric structure to BDT products or mixtures of BDT products. In 1969, Wynberg and Sinnige,[3] described the synthesis of BDT-quinones from intramolecular benzoin condensations of bithiophene-dicarbaldehydes. These ketones were an important stepping stone for the future as these synthons are straight-forward to synthesize and are the starting point for many derivatives. In parallel to these synthetic advances, a revolution was brewing in the field of conjugated polymers. After the preparation of polyacetylene in 1958 by Natta and co-workers,[4] Shirakawa, Heeger and MacDiarmid collaborated to synthesize halogen-doped polyacetylene with high conductivities ($\sim 10^3$ $S \cdot cm^{-1}$) in 1977.[5] Following this report, numerous molecules were subjected to polymerization and doping, in the hope to understand the properties and develop a library of conductive polymers. BDT was one of the synthons of interest, and the first polymerization of

benzo[2,1-b:3,4-b']dithiophene via electrochemistry was reported by Taliani *et al.* in 1987.[6] The following year, Kimura described the doping of poly(BDT) with AsF_6^-, leading to films that were stable in air but showed poor electrical conductivities of 3 $mS \cdot cm^{-1}$.[7] At this period, BDT-based polymer studies declined, and small molecules, such as BDT analogues of tetracyanoquinodimethane (compounds **1.1-1.3** presented in Figure 1) were investigated. These accepting derivatives, combined with electron donor molecules, formed electrically conductive charge-transfer complexes, with conductivities ranging from 0.001 to 25 $S \cdot cm^{-1}$, depending on the donor unit employed.[8–10]

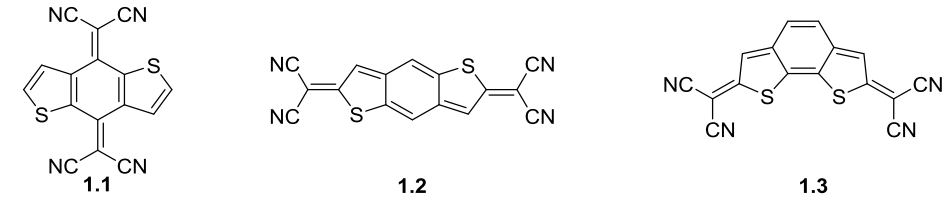

Kobayashi *et al.*,[8] 1988 Fujii *et al.*,[9] 1993 Yoshida *et al.*,[10] 1994

Figure 1: Structure of electron accepting benzothiophene analogue to tetracyanoquinodimethane: 2,2'-(benzo[1,2-b:4,5-b']dithiophene-4,8-diylidene)dimalononitrile (left), 2,2'-(benzo[1,2-b:4,5-b']dithiophene-2,6-diylidene)dimalononitrile (middle), 2,2'-(benzo[2,1-b:3,4-b']dithiophene-2,7-diylidene)dimalononitrile (right).

Due to their easy synthesis and good optoelectronic properties, the BDT moiety has been integrated into many organic electronic materials, as shown in the following sections.

1.1.2. Benzodithiophene Units in Organic Electronic Devices

1.1.2.1. Organic Field-Effect Transistors

Organic field-effect transistors (OFETs) behave as a capacitor with a conductive channel between a source and a drain electrode. The channel is constituted of organic

semiconductor and the voltage applied at the gate electrode controls the amount of charge carriers flowing through the system. Rubrene-based OFETs have the highest carrier mobility, ranging from 20 to 40 $cm^2 \cdot V^{-1} \cdot s^{-1}$.[11] Rubrene is an exception as most of the polymers and small molecules employed in OFETs have carrier mobilities varying from 0.001 to 6 $cm^2 \cdot V^{-1} \cdot s^{-1}$.[11]

BDT units were first employed in OFETs in 1997 by Laquindanum *et al.,*[12] who reported p-channel organic thin film transistors based on the BDT dimer **1.4** (Figure 2), with electron mobilities of 0.04 $cm^2 \cdot V^{-1} \cdot s^{-1}$. This type of molecule, without pendant chains, is inconvenient for large-scale device fabrication as it needs to be vacuum-deposited. This led to the synthesis by Xu and coworkers of solution-processable copolymers based on thiophene and benzo[2,1-b:3,4-b']dithiophene units, compound **1.5** in Figure 2. The FET devices gave a saturation mobility of 0.25 $cm^2 \cdot V^{-1} \cdot s^{-1}$, with a current on/off ratio of 10^5-10^6 when measured under ambient conditions.[13] Another advantage of this system is that it does not require thermal annealing after the layer deposition, making it highly convenient for roll-to-roll manufacturing process. The next milestone was reached in 2011 with the report of butterfly-shaped BDT molecules **1.6**, with amphiphilic pendant chains that yielded solution-transferable and free-standing bilayer films. The mobilities for such molecules were in the order of 0.02 $cm^2 \cdot V^{-1} \cdot s^{-1}$, with an on/off ratio of 10^5.[14]

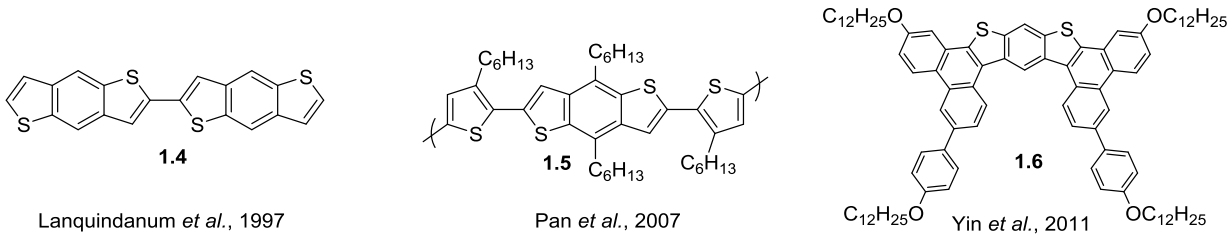

Figure 2: Molecular structures of BDT derivatives used in OFETs.

1.1.2.2. Organic Photovoltaics

In organic photovoltaics (OPV), benzo[2,1-b:3,4-b']dithiophene derivatives have become one of the units of choice for the donor moieties in p-type polymers. Table 1 presents a collection of copolymers using BDT, and their corresponding solar cell characteristics. In most of the studies, the BDT unit is alkylated with linear or branched chains, and the co-monomers are varied. The alkyl chains on BDT are of great importance, as they impact the resulting morphology when the polymer is blended with the n-type acceptor (generally fullerenes such as $PC_{61}BM$ or $PC_{71}BM$). The most efficient devices are obtained by fine tuning the structural properties of the polymers, such as the HOMO-LUMO levels, the energy gap, or the chain planarity and morphology. The energy gap is tuned by using different acceptor units (this will be discussed more in details in section 1.2), and the rows 1 to 8 in Table 1 illustrate a range of synthons, effectively directing the overall PCE from 0.90 to 8.3 %. Another way to tailor the properties is to append thiophene and phenyl units on the 4- and 5- positions of the BDT (Table 1, rows 9-11) When co-polymerized with 4,7-di(thiophen-2-yl)benzo[c][1,2,5]thiadiazole, the resulting solar cells have efficiencies of 8.07% (Table 1, row 11.) Other isomers of BDT can be employed, and upon tuning the pendant chain and the morphology, lead to moderate to high efficiency devices (Table 1, rows 12-15.)

Table 1: Photovoltaic characterization of BDT polymers with varying side chains and acceptor co-monomers.

Row	Donor	R=	Co-monomers	Photovoltaic properties[a]	Ref
1	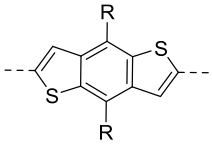	Dodecyloxy-		V_{oc}=0.75 J_{sc}=3.78 FF=0.56 PCE=1.60	[15]

Table 2 continued

2		Dodecyloxy-	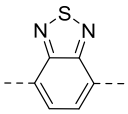	V_{oc}=0.68 J_{sc}=2.97 FF=0.44 PCE=0.90	15
3		Dodecyloxy-	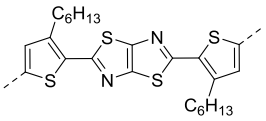	V_{oc}=0.76 J_{sc}=6.32 FF=0.57 PCE=2.72	16
4		Ethylhexyloxy-	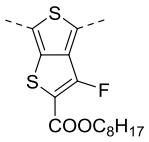	V_{oc}=0.74 J_{sc}=14.5 FF=0.69 PCE=7.40	17,18
5		Ethylhexyloxy-	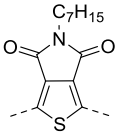	V_{oc}=0.97 J_{sc}=12.6 FF=0.70 PCE=8.30	19,20, 21
6	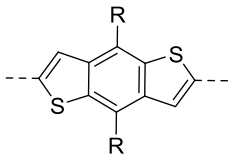	Propylnonyl	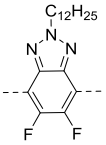	V_{oc}=0.79 J_{sc}=11.8 FF=0.73 PCE=6.81	22
7		Dodecyloxy-	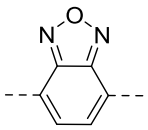	V_{oc}=0.89 J_{sc}=13.6 FF=0.51 PCE=6.05	23
8		Ethylhexyloxy-	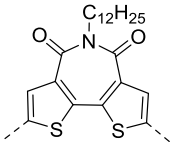	V_{oc}=0.92 J_{sc}=9.62 FF=0.62 PCE=5.50	24
9	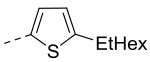		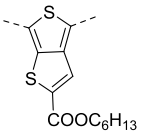	V_{oc}=0.74 J_{sc}=17.5 FF=0.59 PCE=7.59	25
10	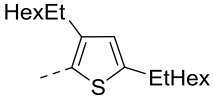		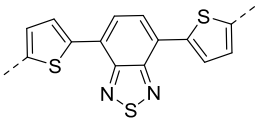	V_{oc}=0.92 J_{sc}=10.7 FF=0.58 PCE=5.66	26

Table 3 continued

11		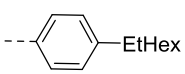	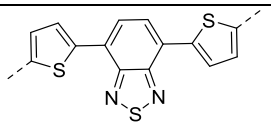	V_{oc}=0.88 J_{sc}=12.3 FF=0.71 PCE=8.07	27
12	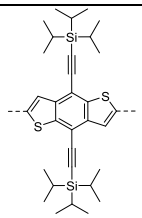		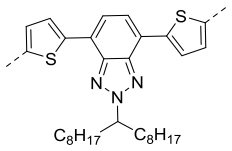	V_{oc}=0.80 J_{sc}=12.7 FF=0.55 PCE=5.53	28
13	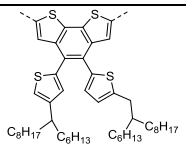		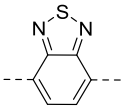	V_{oc}=0.72 J_{sc}=2.06 FF=0.42 PCE=0.60	29
14	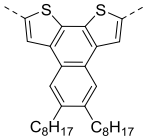		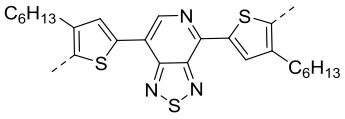	V_{oc}=0.71 J_{sc}=14.2 FF=0.62 PCE=6.20	30
15	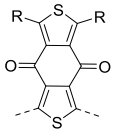	Ethylhexyl-	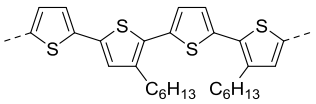	V_{oc}=0.83 J_{sc}=11.6 FF=0.71 PCE=6.88	31

[a]For the photovoltaic results, V_{oc} (open circuit voltage) is in V, J_{sc} (short circuit current) is in $mA \cdot cm^{-2}$ and the PCE (power conversion efficiency) is in %

To note, BDT units are also used in processable small molecules OPV, generating devices with efficiencies up to 7.1% and 7.6%.[32,33]

1.2 Donor-Acceptor and Fused Donor-Acceptor Molecules

1.2.1. Donor-Acceptor Approach

In organic electronics, it is crucial to have access to materials that have tunable energy levels. In semiconductors, the top of the valence band corresponds to the highest occupied molecular orbital (HOMO) and the bottom of the conduction band to the lowest

unoccupied molecular orbital (LUMO). The ability to adjust the HOMO and LUMO levels allows control of the energy gap of the system, as well as its electron affinity and ionization potential. To manipulate these frontier orbital levels, several tactics have been employed. The most common one, developed by Havinga *et al.*[34] and exploited in our group for more than ten years,[35,36] is to covalently couple a donor and an acceptor fragment into a conjugated system, as illustrated in Figure 3. The energy gap of the resulting molecule is reduced because its LUMO is now related to the LUMO of the acceptor, and its HOMO is correlated to the HOMO of the donor. This is known as the donor-acceptor approach, or the push-pull method.

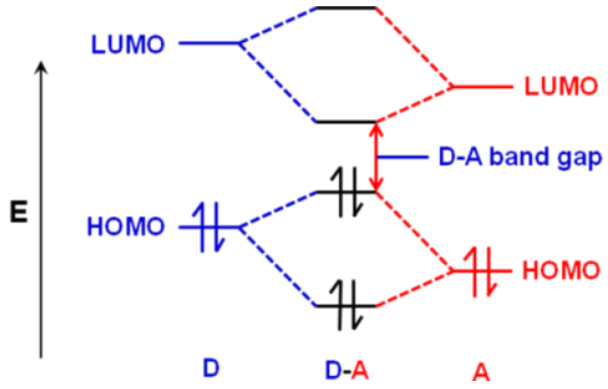

Figure 3: Molecular orbital energy diagram showing interaction between a conjugated donor-acceptor pair in close proximity. Figure adapted from reference 37.

The reduction of the band gap is due to the improvement of electron delocalization and the reorganization to a quinoid mesomeric structure (D-A ↔ D^{+}=A^{-}). Intramolecular charge transfer also leads to an extended absorption, and can be probed by simple spectroscopy experiments, as the absorption maxima of the resulting materials are solvent-dependent.

This D-A method has been widely used in the organic electronic community, and is so far the most successful method of controlling energy levels. In our group, this methodology

has led to spray-processable electrochromic polymers, whose colors change according to the acceptor used,[38] and to D-A-D oligomers and polymers with application in organic photovoltaics.[39,40]

1.2.2. Fused Donor-Acceptor Approach

The donor-acceptor approach permits tuning of the energy levels and control of the amount of light that can be absorbed by the material. In organic electronics, another key parameter to control is charge transport, notably for OFETs applications. In the last decade, reports have shown that fusing aromatic systems together allows for flat and rigid frameworks that permit better packing and stronger π- π interactions, resulting in materials with higher carrier mobilities.[41] Specifically, a lot of interest has been generated on fusing electron donating molecules, such as thiophenes. Fusion of donor and acceptor molecules, as portrayed in Figure 4 with benzothiadiazole and thiophene units, can integrate both the tuning of the energy gap, and the improvement of electron transport.

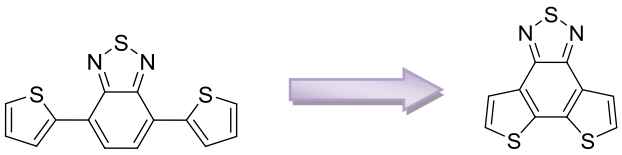

1.7 **1.8**

Figure 4: From a D-A-D system to a fused D-A (fDA) system for 4,7-di(thiophen-2-yl)benzo[c][1,2,5]thiadiazole (left) and dithieno[3',2':3,4;2",3":5,6]benzo[1,2-c][1,2,5]thiadiazole (right).

Figure 5 illustrates a representation of the frontier orbitals obtained for the D-A-D and the fused D-A (fDA) molecules by computations. In this figure, it is observed that while the orbital density shapes are similar for the frontier orbitals, the HOMO and LUMO values

differ. The HOMO level for the fDA system is lower than for the D-A-D system, and the LUMO level for the fDA is higher than for the D-A-D system.

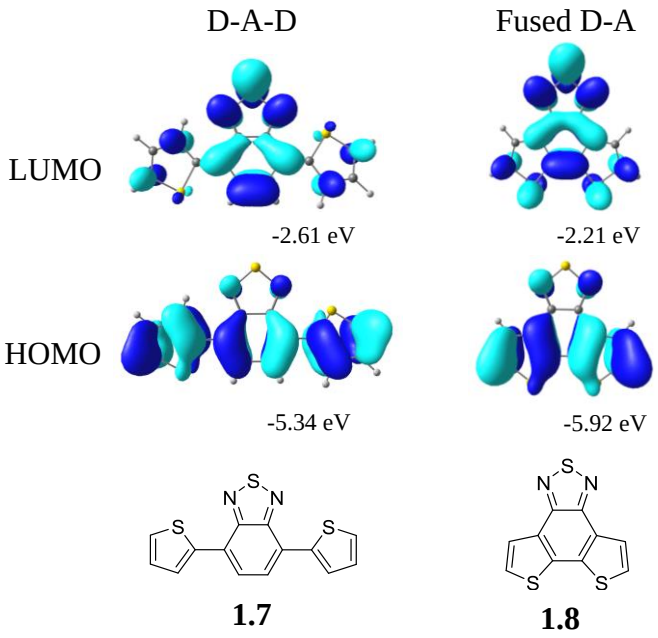

Figure 5: Illustration of the frontier orbitals and molecular structures for 4,7-di(thiophen-2-yl)benzo[c][1,2,5]thiadiazole (left) and dithieno[3',2':3,4;2",3":5,6]benzo[1,2-c][1,2,5]thiadiazole (right), obtained at the B3LYP/6-31G* theory in vacuum.

Figure 6 illustrates the simulated absorption spectra for the D-A-D and fDA systems. The energy gap is indeed higher for the fDA systems, and the D-A-D systems show higher oscillator strength and bathochromic transitions. Fusing the systems gives rise to another visible peak, which is mainly of HOMO → LUMO +2 character.

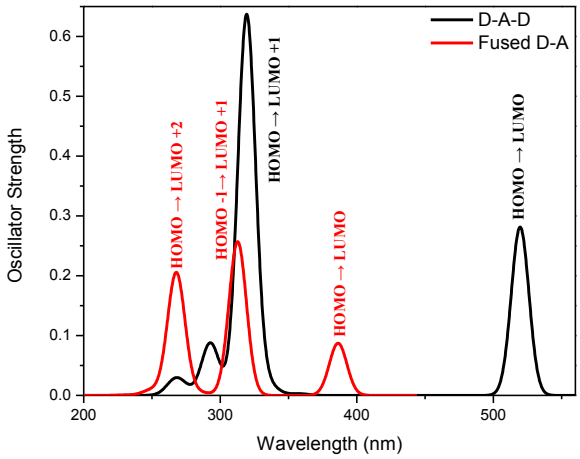

Figure 6: Simulated absorption spectra structures for 4,7-di(thiophen-2-yl)benzo[c][1,2,5]thiadiazole and dithieno[3',2':3,4;2",3":5,6]benzo[1,2-c][1,2,5]thiadiazole determined by TDDFT at the B3LYP/6-31G* theory in vacuum, and their respective transitions.

1.2.3. "There is nothing either good or bad, but thinking makes it so".[1]

Comparing the D-A and fDA approaches, and declaring one to be better than the other is difficult. Indeed, depending on the application chosen, D-A-D molecules can be more desirable for their lower band gap and higher light harvesting capabilities, whereas the increase in the system planarity and the deepening of HOMO level of the fDA system can serve well in other applications.

For example, Mei *et al.*[42] reported recently the comparison between benzodithiophene (BDT) and dithienyl-benzothiadiazole (DTBT) co-polymers, with fused and non-fused DTBT for organic solar cells. The polymers structures are presented in Figure 7.

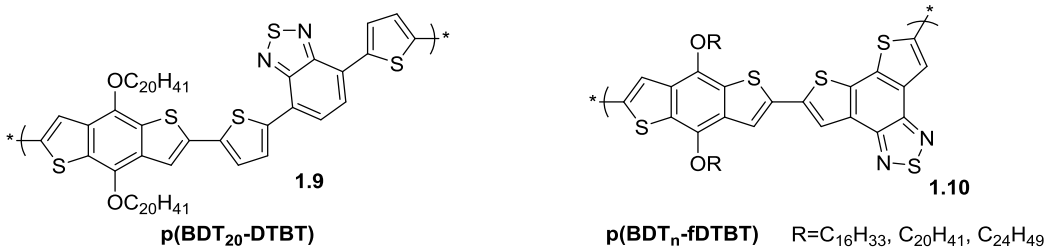

Figure 7: Structure of the polymers p(BDT_n-fDTBT) (n=16, 20, 24) and p(BDT_{20}-DTBT) to compare D-A and fDA effects. Adapted from reference 42.

To summarize their results, the fused BDT-DTBT shows a hypsochromic absorption peak compared to the D-A-D system (Figure 8, blue triangle *vs.* the other curves), in agreement with the computations discussed in section 1.2.2. Interestingly, the absorption coefficients were similar for these fused and non-fused polymers.

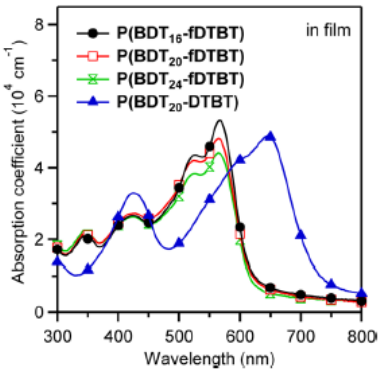

Figure 8: UV-visible absorption spectra at room temperature of p(BDT_n-fDTBT) (n=16, 20, 24) and p(BDT_{20}-DTBT) in films. Reproduced with permission from reference 42. Copyright 2013 American Chemical Society.

When integrated into solar cells, the solubilizing chains on the BDT units have the highest impact on the J_{sc}: the shorter hexyldecyl alkyl chains (black circles in Figure 9) have a J_{sc} of approximately 7 $mA \cdot cm^{-2}$, whereas the longer octyldodecyl and decyltetradecyl chains (green and red squares on Figure 9) have a Jsc of 1 and 2 $mA \cdot cm^{-2}$, respectively. The effect of the solvent (chlorobenzene or dichlorobenzene, full and empty circles on Figure 9) also influences on the current density value: an increase of

1 mA·cm^{-2} is observed when dichlorobenzene is employed. The improvement of the J_{sc} upon optimization of the polymer pendant chains and of the solvent is caused by the improved morphology of the films upon blending with the $PC_{61}BM$ acceptor. On the other hand, the fused systems always have a greater V_{oc} (up to 100 mV higher) than the D-A-D system. This is due to the lower HOMO levels for the BDT-fDTBT polymers. The BDT_{16}-fDTBT polymer has an efficiency of 4.4%, whereas the PCE for BDT_{20}-DTBT is of 3.9%.

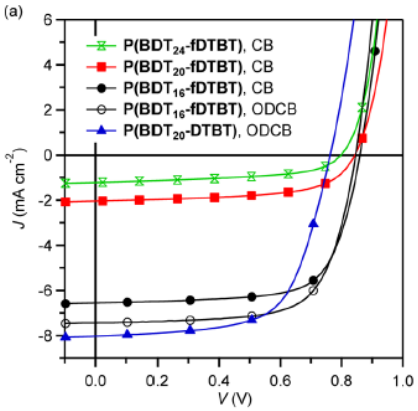

Figure 9: J-V responses of the solar cells devices based on blend of p(BDT_n-fDTBT) (n=16, 20, 24) or p(BDT_{20}-DTBT) with $PC_{61}BM$. Reproduced with permission from reference 42. Copyright 2013 American Chemical Society.

In conclusion, this study shows the complexity of comparing fused and non-fused systems in organic electronic applications. While the D-A-D polymers have a broader light absorption, the non-fused systems have lower HOMO levels. With proper control of morphology, the fused systems lead to more efficient OPV devices than the D-A-D systems. This fDA approach directs to new synthons that deserve to be studied in organic electronics.

1.3. Dye-sensitized Solar Cells: Here comes the sun.

1.3.1. Creation and Development of DSSCs

The story of dye-sensitized solar cells (DSSCs) began with the report of O'Reagan and Grätzel in 1991 describing mesoporous nanoparticles of titanium dioxide (TiO_2) sensitized with ruthenium-polypyridine dyes, and integrated into electrodes containing a redox shuttle based on iodine.[43] It was not the first report of metal oxides sensitized with dyes for photovoltaic applications. Previous work involved studies of phthalocyanine and porphyrine dyes on a smooth surface semiconductor, resulting in efficiencies below 1%.[44–46] O'Reagan and Grätzel "coup de génie" was the use of mesoporous semiconductor electrode, with a high internal surface area.

With this change, efficiencies of the devices improved to 7.9%, which at the time was the record for hybrid solar cells (Figure 10). Following this discovery, the next two decades gave rise to the development of an incredible number of dyes: several thousands of inorganic, organic or polymeric sensitizers were reported.[47–49] Moreover, hundreds of electrolytes were described, and the review by Wu *et al.* illustrates the breadth of work that has been accomplished in this field.[50] Lastly, mesoporous films have also received considerable attention. Varying the morphology of the titanium dioxide to nanowire or nanotubes permits up to a two-fold increase in the efficiency of the devices.[51–53] With the understanding of the mechanisms and processes involved in light absorption, electron injection and electron regeneration, more questions have arisen. As a consequence, efficiencies have stagnated around the bar of 10% for twenty years, which is illustrated in Figure 10, with the efficiency plateau from 1998 to 2011. In 2012, a new record

efficiency of 12.3% was reached by using a redox couple based on a cobalt complex as well as a cocktail of dyes (of inorganic and organic nature).[54]

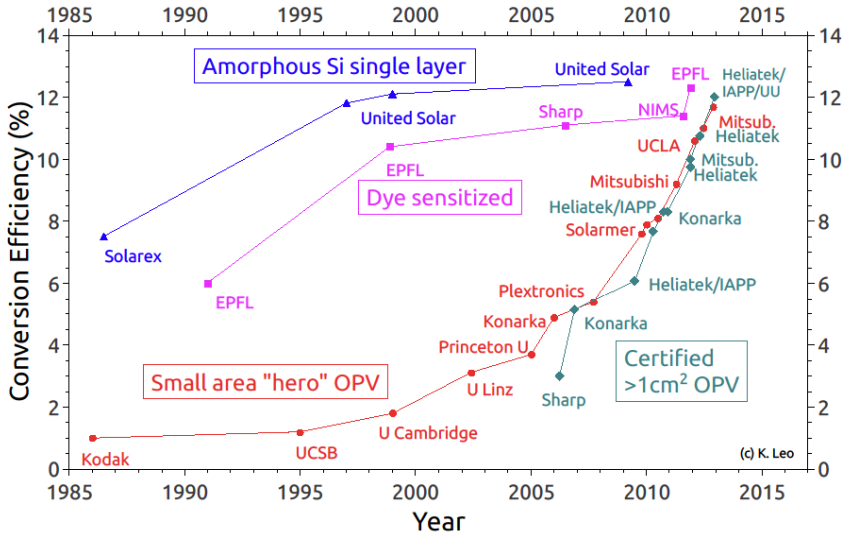

Figure 10: Organic photovoltaics research cell efficiency records. Retrieved from orgworld.de with permission.

1.3.2 DSSC Operation Principles Overview

Figure 11 illustrates a traditional DSSC set-up, composed of mesoporous oxide layer constituted of a network of TiO_2 particles, ranging from 10-30 nm in diameter. The nanoparticles are sintered to establish electronic conduction, leading to films of ~ 10 μm thickness. This layer is deposited on a fluorine-doped tin oxide (FTO) slide, usually by doctor-blading. Dyes are adsorbed at the surface of the TiO_2 particles by dipping the TiO_2 films into a solution of the dye. An electrolyte, generally consisting of the iodine/triiodide redox system, and a cathode made of FTO slide coated with a thin layer of platinum, complete the cell.

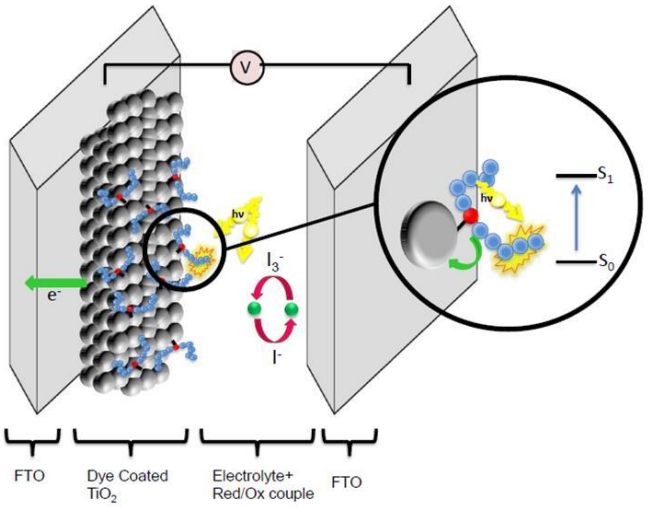

Figure 11: Schematic overview of a DSSC.

The overall chemical processes are summarized in Figure 12. This picture is simplified, but useful for an understanding of the mechanisms occurring in DSSCs. The first step is the photoexcitation of the dye via absorption of a photon. With the energy acquired, one of the electrons of the dyes is promoted from the ground state to an excited state (equation 1). Following this excitation is an ultrafast (on the femtosecond range) electron injection of the excited electron onto the titanium dioxide conduction band (TiO_2 CB) (process 2). The electron hops from one crystallite site to the next, until encountering the anode (process 3). The dye, which was left in its oxidized state, is restored to its ground state by electron transfer from the electrolyte, commonly the iodine/triiodide redox system (eqution 4). During this step, the oxidized dye combines with the generated electron traveling from the anode through the electrolyte, and the generated iodine molecule is reduced to regenerate the triiodide anion.

In the schematic illustration in Figure 12, the processes described above, in green, are favorable to electron injection and regeneration. The red arrows depict the recombination routes that are detrimental to the cell operation. The two main loss mechanisms

associated with the cell are the electron recombination between the injected electrons of the metal oxide and the hole in the dye (process 5) and the electron recombination between the injected electrons of the metal oxide and the redox couple (process 6). The latter is dependent on the electrolyte used, and can be reduced with the use of a co-adsorbent to limit the proximity of the redox mediator to the TiO_2.

$S + h\nu \rightarrow S^*$ (1)

$S^* \rightarrow S^+ + e^- (TiO_2)$ (2)

Electron transport through TiO_2. (3)

$I_3^- + 2\ e^- \rightarrow 3\ I^-$ (4)

$S^+ + e^- \rightarrow S$

$I^- \rightarrow 2\ e^- + I_3^-$

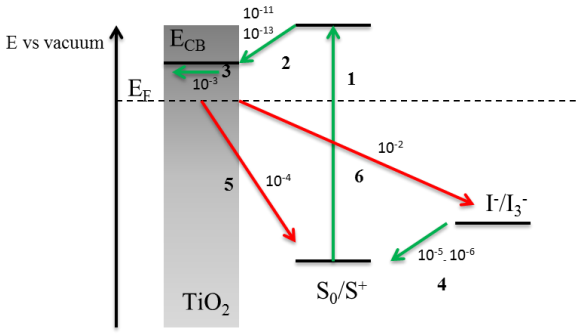

Figure 12: DSSC processes, simplified energy level diagram with favorable (green) and unfavorable (red) processes, and their associated timescale (in seconds). Adapted from references 47 and 48.

1.3.3 Figures of Merit and Their Relation to the Sensitizers

To characterize the solar cells, current density-voltage (J-V) and incident photon-to-current efficiency (IPCE) responses are employed. The photovoltaics figures of merit are composed of the short circuit photocurrent density (J_{sc}), the open circuit voltage (V_{oc}), the fill factor (FF) and the overall power conversion efficiency (PCE). Experimentally, these parameters are obtained from the J-V curves, as depicted in Figure 13. J_{sc} is the photocurrent per unit area when the applied bias potential is zero, and V_{oc} is the voltage when there is no current flowing through the cell. FF and PCE are related by equations (5) and (6). The FF is the maximum rectangle area obtained inside the J-V curve, and the

PCE is the ratio of the power output to the power input. The maximum output power of the cell is found where the product |J×V| reaches a maximum.

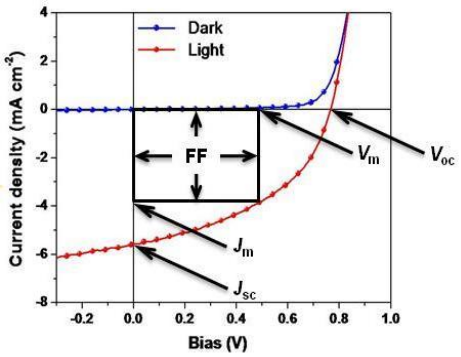

Figure 13: Typical J-V curves and figure of merits for a DSSC, adapted from reference 55.

The relations linking the different parameters are presented in equations (5) and (6).

$$FF = \frac{J_m \times V_m}{J_{sc} \times V_{oc}} \quad (5)$$

$$\eta = \frac{P_{out}}{P_{in}} = FF \frac{Jsc \times Voc}{P_{in}} \quad (6)$$

1.3.3.1 Open Circuit Voltage

Contrary to organic photovoltaics, where the V_{oc} is directly related to the frontier orbital levels of the active materials, in DSSCs, the frontier orbitals of the sensitizers do not directly determine the V_{oc} of the device. Indeed, equation (7) shows the expression of the V_{oc} as the difference between the potential of the Fermi-level of the redox couple ($E_{f,redox}$) and the potential of the Fermi-level of TiO_2 ($E_{f,n}$).[48] As the $E_{f,redox}$ does not vary if the same electrolyte is used,[56] the main change in Voc is dictated by $E_{f,n}$, which depends largely on its environment. For instance, additives from the electrolyte can raise its

level,[56] and this influence can be rationalized by equation (8), where the TiO_2 Fermi-level energy is the sum of the TiO_2 CB potential and an additive factor.

$$Voc = E_{f,redox} - F_{f,n} \quad (7)$$

$$E_{f,n} = E_{CB} + k_b T \ln \frac{n_c}{N_c} \quad (8)$$

kb is the Boltzmann constant, T is the temperature, n_c is the free electron density and N_c is the density of accessible states in the CB.

The TiO_2 CB potential (E_{CB}) and the free electron density (n_c) are the two variable parameters of the system. E_{CB} is determined by the surface charge on TiO_2. Any change in the surface charge will shift the conduction band edge position.[57] The free electron density n_c is determined by the balance between electron injection and electron recombination.

The relationship between the dye structures and the V_{oc} of the devices is quite intricate. When comparing two different sensitizers without changing the electrolyte, it is reasonable to approximate that the main difference in V_{oc} is due to the shift in the TiO_2 CB. Recently, Ronca *et al.*[58] managed to unravel the electrostatic effect and the charge transfer effect for a dye bound to a semiconductor surface. In their study, they expressed the total TiO_2 shift as a combination of various contributions such as the solvent, the ions present in the electrolyte, the electrostatic field of the dyes and the amount of dye to semiconductor charge transfer:

$$\Delta CB_{TOT} = \Delta CB_{solv} + \Delta CB_{ions} + \Delta CB_{EL} + \Delta CB_{CT} \quad (9)$$

With this equation, the terms associated with the dyes ($\Delta CB_{EL} + \Delta CB_{CT}$) can be directly related to the V_{oc}. By computing each of the effects separately, and comparing the results

to experiments, Ronca *et al.* were able to demonstrate that an extensive charge rearrangement accompanies the dye-TiO_2 interactions. They also prove that the conduction band shifts can be decomposed into contributions directly related to the sensitizer properties, and the effect of the electric field generated by the dye on the semiconductor conduction band amounts to *ca.* 40% of the total shift.

1.3.3.2 Short Circuit Current Density and Incident Photon-to-Current Efficiency

J_{sc} can be linked to another figure of merit, IPCE. The IPCE is the J_{sc} produced in the circuit under monochromatic illumination of the cell ($\varphi(\lambda)$), divided by the photon flux that strikes the cell, as pictured in equation (10).

$$\mathrm{IPCE} = \frac{J_{sc}(\lambda)}{e\varphi(\lambda)} = 1240\frac{J_{sc}(\lambda)}{\lambda P_{in}(\lambda)} \qquad (10)$$

with e being the elementary charge, λ being the wavelength

Consequently, J_{sc} can be further expressed as a function of the IPCE, as shown in equation (11). Experimentally, once the IPCE is recorded, the integral of the spectra (*i.e.* the area under the curve) should match with the experimental value of J_{sc}. As the J_{sc} depends mainly on the IPCE, a higher IPCE will increase the J_{sc}.

$$J_{sc} = \int \mathrm{IPCE}(\lambda).\mathrm{e}.\varphi_{\mathrm{phAM1.5G}(\lambda)}\mathrm{d}\lambda \qquad (11)$$

Equation (12) expresses the parameters involved in the IPCE as the product of the absorbed photon-to-current efficiency (APCE) and the light harvesting efficiency (LHE). The latter is directly related to the amount of light that is absorbed by the dye, as described in equation (13). The APCE shows how efficiently the absorbed photons are

converted into current, and this is determined by three terms: the overall charge collective efficiency (η_{coll}), the regeneration efficiency (η_{reg}), and the overall electron injection efficiency (φ_{inj}). Calculations of the charge collection efficiency can be found in reference 59.

$$IPCE = APCE \times LHE = \varphi_{inj} \times \eta_{coll} \times \eta_{reg} \times LHE \quad (12)$$

$$LHE_{\lambda} = 1 - 10^{-A(\lambda)} \quad (13)$$

A is the absorbance of the dyes adsorbed on TiO_2 films

To understand the influence of the sensitizers on the APCE, and ultimately on the J_{sc}, a deeper look at the electron injection factors is essential. The electron injection (φ_{inj}) is related to the driving force ΔG_{inj} of electron injection from the excited states of dye molecules to the semiconductor substrate.[60] It can be estimated as:

$$-\Delta G_{inj} = -e\left(E^{dye*} - E_{CB}\right) = -e\left(E^{dye} - \frac{E_{0-0}}{e} - E_{CB}\right) \quad (14)$$

where E^{dye*} represents the oxidation potential of the excited dye, E^{dye} is the redox potential of the dye in its ground state, $E_{0\text{-}0}$ is the vertical transition energy and E_{CB} is the conduction band edge of the semiconductor. Both the redox potential of the ground state of the dyes and the vertical transition energy can be probed experimentally: E^{dye} is known through electrochemistry and $E_{0\text{-}0}$ through spectroscopic studies, as it is the crossing point between the absorption and emission spectra. The only parameter challenging to determine with precision is the conduction band edge of the semiconductor, as seen in the previous section. It can be measured,[61] or approximated to -0.5 V vs NHE.[60] With a higher electron driving force, the electron injection increases, cascading to an increase in

the short current density. However, Katoh *et al.*[60] demonstrate that the electron efficiency attain a plateau when $-G_{inj} > 0.5$ eV.

1.3.3.3 Fill Factor

The fill factor is determined via equation (5). However, the value is attenuated by the series resistance of the cells, determined by the device fabrication. To date, there is no direct observed correlation between fill factor and sensitizer.

1.3.4. Organic Sensitizers used in DSSC

A myriad of molecules have been studied and used for DSSCs. Multiple reviews have been written focusing on inorganic dyes[62], organic dyes [63,48,49] or a combination of both in a more extensive review.[47] In this section, the emphasis is placed on the sensitizer design rules, with some well-chosen examples shown.

One of the reasons behind the abundance of sensitizers is that their design criteria are defined, but are broad enough to be applied to numerous systems. The requirements for an ideal dye are:

- The sensitizer should bear a metal oxide adsorbing group. Carboxylic acid groups are widely used, but other acidic moieties, such as phosphonic acids have also been employed for stronger binding to the TiO_2 surface.[64–66]
- The sensitizer should exhibit a large light absorptivity, both in terms of extinction coefficients and in terms of wavelength. Molecules absorbing in the IR region are of interest as a greater amount of the solar photon flux can be absorbed.

- The LUMO of the dye should be more positive in energy than the CB of TiO_2, to assure electron injection. With the network of TiO_2 nanoparticles ranging from different nanoparticles sizes, there is no set value for the conduction band. Moreover, as seen in the previous section, the environment can shift the level of the CB. However, it is common and accepted to estimate the level at -0.5 V vs NHE (-4 eV *vs.* vacuum).[49]
- The HOMO of the dye should be more positive than the redox potential of the mediator. For iodine/triiodide, the value is 0.35 V vs NHE (-4.85 eV *vs.* vacuum).[49] The offset necessary to drive the reaction is still unclear, but it estimated to be above 0.4eV.[67] Complexes based on cobalt have received a lot of attention recently as they permit an increase of the V_{oc}, due to a deeper redox potential. For the Co $^{(II/III)}$tris(bipyridyl) couple, the redox potential is 0.86 vs NHE (-5.36 eV *vs*. vacuum).[68]
- Dye aggregation should be avoided as it leads to low conversion efficiency. The aggregation can be controlled by the help of molecular design (for instance, with the addition of branched alkyl chains), or by the addition of co-adsorbents in the dipping solution, before adsorption of the dyes onto TiO_2.
- The sensitizers should be electrically, thermally and optically stable. In that regard, adding alkyl chains to the main structure of the dye helps the stability of the dyes.[69,70]

In Table 4, a selected panel of dyes is shown. For a more thorough review of the sensitizers, the reader is directed to the reviews presented earlier in this section. In this table is represented the classic N3 dye that is to DSSC what P3HT is for OPV: a

reference dye that works well, and that was used to gain in-depth knowledge on the photophysics of DSSCs. The next row represents an example of a cocktail of judiciously selected dyes, leading to the record efficiency of 12.3%. In the rest of the table are presented sensitizers that hold an interest for this thesis. For example, the third row introduces some of the synthons used in Chapter 5, and the fourth row shows an example of a starburst arylamine, that is a related approach to the one that is described in Chapter 4. In each case, the photovoltaic parameters are given.

Table 4: Molecular structures, photovoltaic parameters, and references of remarkable sensitizers for DSSCs. The photovoltaic parameters reported are taken under P_{in} = 100 $mW \cdot cm^{-2}$

Sensitizer Structure	Figures of Merit	Notes	Ref.
N3 dye 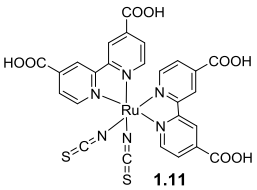 **1.11**	V_{oc}=0.72 V J_{sc}=18.2 $mA \cdot cm^{-2}$ FF=0.76 PCE=10.4 %	reference dye, used for comparison	71
Cocktail dyes:YD2-o-C8 +Y123 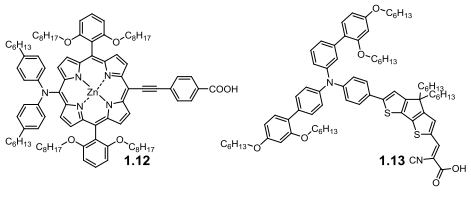 **1.12** **1.13**	V_{oc}=0.94 V J_{sc}=17.3 $mA \cdot cm^{-2}$ FF=0.74 PCE=12.3 %	Highest reported efficiency to date	54
C219 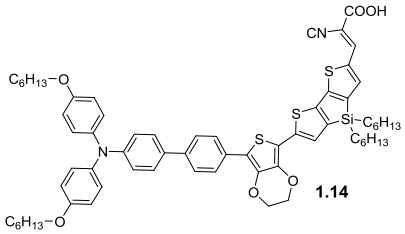 **1.14**	V_{oc}=0.69 V J_{sc}=15.0 $mA \cdot cm^{-2}$ FF=0.74 PCE=7.6 %	Triarylamine dye conjugated with ethylenedioxythiophene and dithienosilole	72

Table 2 continued

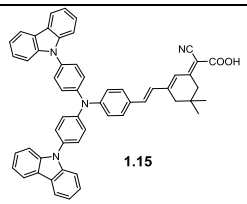 1.15	V_{oc}=0.63 V J_{sc}=13.8 mA·cm^{-2} FF=0.69 PCE=6.0 %	Starburst triarylamine sensitizers	73

To note, polymeric dyes have also been developed. While these systems fulfill all the criteria for a DSSC sensitizer, the device efficiencies decline with the augmentation of polymer molecular weight.[74,75] This has been explained by the aggregation of high molecular weight polymer on the metal oxide surface, hence inhibiting successful electron injection and electron regeneration.

1.3.5. Current and Future Challenges

To compete against current photovoltaic technologies, DSSCs still have some major challenges to overcome.

- Efficiency

In order to attain commercial viability, photovoltaics devices should meet the 15% efficiency bar. In the last decade, device efficiencies have been plateauing at 10-12%. Overcoming this challenge will likely focus more on the electrolytes and the semiconductor metal oxides than on the nature of the dyes. For instance, the maximum open circuit potential that can be obtained with the iodine/triiodide redox shuttle is 0.7-0.8 V. To further improve this V_{oc}, cobalt-based complexes have been used successfully.[68] These complexes have a deeper redox potential than the iodine-based

shuttle, hence raising the theoretical V_{oc} to 1.2-1.3 V. Similarly, studies with structured metal oxides have presented a promising increase in the efficiencies of the devices by increasing the surface available for dye absorption, and enhancing electronic properties.[51–53] Of course, there is still room of improvement on the dye structure, for example by extending absorption to low energy photons, or by separating the charge injection and charge recombination sites to minimize unfavorable electron recombination.

- Cost per watt

In order to be competitive with inorganic silicon photovoltaics modules, the cost of a DSSC element should be lower than \$0.70 W^{-1} (expected price for silicon modules in 2015).[76] The most expensive part of the cells lies in the ITO coated glass, so progress in glass replacement such as flexible coatings or foil should decrease the overall cost. To note, there are already a few applications based on DSSCs in the market. For example, G24Cell and Logitech have developed a solar keyboard, which prices range from \$50-200.[77]

- Stability

To be attractive to consumers, DSSCs need to be stable, and have a lifetime of 10-20 years. While a lot of progress has been made on the lifetime of the sensitizers, the liquid iodine-based electrolytes employed remain an issue, due to the potential leakage or volatilization of the liquid solvent. A possibility to consider is to employ solid-state DSSCs, which are composed of solid hole conductors, instead of liquid electrolytes. However, the efficiencies for these types of devices are still twice lower than with the common iodine/triiodide redox shuttle, and need to be improved upon.[78]

Lastly, it is worthy to mention that in the last few years, inorganic and organic dyes have seen their appeal diminish to the profit of perovskite cells, which present a more straight-forward synthesis as well as the promise of higher efficiencies.[79,80] However, the scale-up of these cells have not been demonstrated, and the race for cheap, efficient and stable solar technology is still open for all competitors.

In conclusion, the discovery of the sensitization of mesoporous titanium dioxide particles with dyes in 1991 led to a paradigm shift in the fields of photoelectrochemistry and photovoltaics. Twenty three years later, more than 20,000 papers and patents exploring dyes, redox couples, metal oxides and explaining the chemical and physical processes involved in the devices have been reported. This scientific enthusiasm is reflective of the promising technology of DSSCs. With the commercialization of theses photovoltaic devices in keyboards, backpacks and windows, the pathway for large-sale applications is wide open.

1.4. Thesis of this Dissertation

The organic electronics field may appear as a synthetically monotonous topic for a pure synthetic chemist: similar synthons are used for solar cell, electrochromic, OLED and OFET devices and they are often composed of derivatives of thiophene, such as alkyl-thiophenes, dioxythiophenes or dithienosilole. To improve on the systems and create new materials, pendant chains are varied, or the π-conjugated molecules or polymers are tuned with different donating or accepting units. In this thesis, we are exploring the multi-faceted applications that the BDT unit offers in organic electronics, with a focus on understanding how the isomerism of the BDT structures affects the macroscopic properties of the oligomeric and polymeric material created. After describing the toolbox

of characterization techniques and synthesis methods for a complete understanding of the directions taken in this work, Chapter 3 follows with an efficient synthesis of BDT, its modification to a wide range of synthons, and more particularly of dicarboxylic dithiophenes. Then, it details a comparative study of three isomeric polymers of BDT which are characterized in terms of their fundamental physical and electrochemical properties. A small difference in the structural unit varies the absorption maxima from 447 to 508 nm, and the emission maxima from 497 to 541 nm. The electrochromic properties of these isomeric polymers are also investigated and the variations in color and absorptivity upon oxidation can be related to the molecular structure and backbone rigidity of the polymers. In Chapter four, we apply the fused donor-acceptor approach presented in the introduction to synthesize carboxylate functionalized $(donor)_2$-acceptor (D_2-A) sensitizers for DSSCs, based on two isomers of BDT: linear, where the conjugation pathway extends along a set of conjugated donors, and branched, where the conjugated donors are directly conjugated with the acceptor π-system. Upon full investigation of their optoelectronic properties, the sensitizers are integrated into platform DSSCs for characterization of light harvesting and electron injection. This study demonstrates that the device characteristics are dependent on the dye geometry. The branched dyes have a higher overlapping of the frontier orbital density, a smaller barrier for injection into titanium dioxide and a greater incident photon-to-current efficiency than the linear dyes. The nature of the core is also varied between dibenzophenazine to dithienophenazine. The sensitizer with the weakest accepting core displays the best photovoltaic performance, due to an increase in the open-circuit voltage of ~100 mV caused by the favorable shift of the metal oxide conduction band. Building on this family

of D_2-A dyes, the sensitizers are manipulated by increasing the number of donor groups from two to six thiophene moiety to raise the light absorption ability of the sensitizers. Lengthening the oligomeric chain led to a two-fold increase of the cell characteristics. Finally, varying the nature of the donors shows that the strongest donating groups lead to cells with a greater light harvesting efficiency, but an overall decrease of the device performance is observed.

CHAPTER 2.

CHARACTERIZATION TECHNIQUES AND EXPERIMENTAL METHODS

Within the variety of techniques available to synthesize and characterize molecules, it is important to choose, understand and evaluate those that will provide insightful data on the properties of the material or molecule. In this chapter, the characterization techniques and experimental methods employed in this thesis are discussed. As seen below, an emphasis is placed on theoretical computations and microwave chemistry with the goal of guiding younger readers towards these useful techniques in mind.

2.1. Density Functional Theory Computations

Quantum mechanics calculations have been made available and popularized to synthetic chemists through programs such as Gaussian and Q-Chem. There are four different types of models regularly used to represent a molecule: molecular mechanics, semi-empirical, density functional, and ab initio. The choice of the method depends on the size and composition of the molecule and on the quality of the desired results. In general, the molecular mechanics approach is appropriate for large molecules (such as proteins) and gives a low level of accuracy. The semi-empirical method is adapted for large and medium-sized molecules, with a medium level of accuracy. The ab initio and density functional models are suitable for small (around 12 atoms) to medium (around 150 atoms) molecules, which encompass the molecules studied in this thesis. The ab initio and density functional methods are based solely on theoretical principles. They are

similar in approach, but differ in the approximations used to resolve quantum mechanics equations. The results obtained with the two models are comparable; however the computation time of the density functional theory is significantly shorter. The reason is that the ab initio approach uses a complex many-electron wave function to compute the energy whereas the density functional theory uses the electron density; hence going from 3N variables to a 3 variable problem. For this thesis, we used Density Functional Theory (DFT) and Time-dependent Density Functional Theory (TDDFT) to predict or explain optoelectronic properties of organic systems. An extensive description of the theory can be found in Laxman Pandey's dissertation.[81] This section will illustrate the practical aspects of the computations used in this thesis.

2.1.1. Some Theory, Basis Sets and Experimental Details

DFT found its roots in the Thomas-Fermi model,[82,83] which was then completed by the two Hohenberg-Kohn theorems.[84] In the first theorem, the ground state properties of a multiple electron system are uniquely controlled by an electron density depending on 3 spatial coordinates. Hence, the 3N variable problem can be reduced to a 3 variable problem, using functionals of the electron density. The functionals will be described in the next section. The second Hohenberg-Kohn theorem fixes an energy functional for the system and proves that the correct ground state electron density minimizes this functional. The minimal energy can be found with iterations in order to find the ground state electron density.

The same approach is taken for TDDFT calculations, using the Runge-Gross theorem,[85] which is the time-dependent analogue to the Hohenberg-Kohn theorem. TDDFT

computations are more complex as the time-dependent potential at any given time depends on the value of the density at all previous times. To reduce the time of calculation, the description of the mathematical equations are approximated.

A basis set is a group of wave functions that describes the shape of atomic orbitals (AOs). The accuracy level of the calculations is directly related to the basis set used. The caveat is that the more precise the basis set is, the more elaborate the calculations are. Consequently, a compromise needs to be found between accuracy and computing time. In this thesis, the molecules are small enough to use a precise basis set. Gaussian Type Orbitals (GTOs) were used to define the AOs, and more particularly, 6-31G (d) and 6-31G (d,p) sets were employed. 6-31G refers to the number of GTOs used to describe the core and valence electrons. For instance, with 6-31G, 6 GTOs are used to depict the inner shell, 3 GTOs are used to express the inner valence, and 1 GTO for the outer valence. This basis set can be further modified to obtain a better approximation of the system. Polarization effects can be added to allow the AOs to be distorted (be polarized) by the influence of the surroundings. Adding (d) to the 6-31G basis set adds a d-type function on atoms other than hydrogen, and adding (d, p) to the 6-31G basis set adds a p-type function to hydrogen and d-type functions on to all other atoms.

For all calculations, geometry optimizations were first carried out, and then frequency calculations were used to characterize the stationary point obtained. When needed, time-dependent density functional theory (TDDFT) calculations were done to probe the 10 first excited states of the molecules.

Calculations were done with the Gaussian03 program package[86], provided by the High Performing Computing Center at the University of Florida, and later the Gaussian09

package A.02[87], provided by the Partnership for an Advanced Computing Environment at the Georgia Institute of Technology. The orbitals were represented using the Chemcraft 1.6 sofware[88], with 0.03 *e*/bohr^3 as the isodensity value.

2.1.2. Functionals

To find the minimum energy of the molecule, the Kohn-Sham equations need to be resolved. For that, it is necessary to implement some approximations. Functionals are a class of approximations for the exchange-correlation energy functional (one of the terms composing the Kohn-Sham equation).[89] There is a gamut of functionals, each considering different approximations or corrections, some enclosing experimental data, and others uniquely based on theory. Using DFT with different methods will lead to different results. To compare the change of the orbital density with the type of the functional employed in our systems, we evaluated several functionals to the experimental data. Four hybrid methods were studied: B3LYP,[90,91] B3PW91,[92,93] CAM-B3LYP[93–95] and wB97xD[96]. This choice was based on the common hybrid functionals used in the literature. They are called hybrid as they incorporate a portion of the exact change for the Hartree-Fock theory with the exchange and correlation from empirical or ab initio sources.[89] B3LYP (Becke, three parameter, Lee-Yang Parr) is the most common functional seen in the literature. It uses corrections for both gradient and exchange correlations. B3PW91 (Becke, three parameter, Perdew-Wang-91) is a gradient-corrected method. CAM-B3LYP includes a long range corrected version of B3LYP. The wB97xD functional includes empirical dispersion. As all the calculations are considered in the gas phase, it was also interesting to probe the influence of placing the molecule in a solvent environment. For that, we used the SCRF solvent correlation parameters with CAM-

B3LYP and B3PW91.[97] Figure 14 presents quantitative and qualitative comparisons of the frontier orbitals obtained by computations and by electrochemistry (refer to section 2.5 of this chapter for details on electrochemistry).

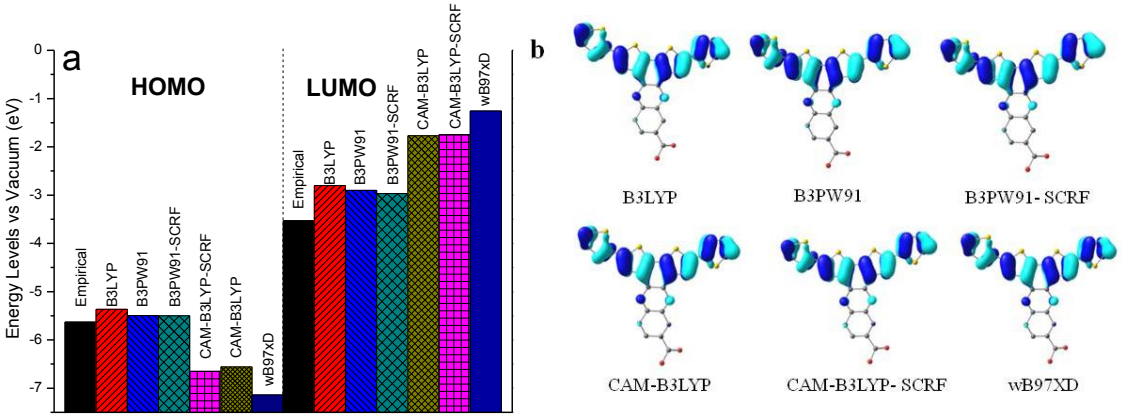

Figure 14: (a) Values of energy levels and (b) Illustration of HOMOs for 2,5-di(thiophen-2-yl)dithieno[3,2-a:2',3'-c]phenazine-9-carboxylic acid with B3LYP, B3PW91, B3PW91-SCRF, CAM-B3LYP, CAM-B3LYP-SCRF and wB97XD hybrid functionals.

In Figure 14a, B3LYP (red bars), B3PW91 (blue bars), and B3P91-SCRF (dark cyan bars) have the closest values to the experimental values (black bars) for the frontier orbital levels. The three other hybrid functionals CAM-B3LYP (dark yellow bars), CAM-B3LYP-SCRF (magenta bars), and wB97XD (navy bars) largely overestimate the values. Interestingly, when comparing the frontier orbitals graphical representation (Figure 14b), the electron density profile is essentially the same for all hybrid functionals. This difference in value when using different hybrid methods has also been reported recently by Guido *et al.*,[98] and comes from the approximations done when describing the exchange-correlation energy functionals. These examples are a good reminder that the computations do not quantitatively match the experimental values, particularly when describing donor-acceptor systems. For these systems, new methods are currently being developed, notably by the Brédas group, with the hope to match experimental values

more closely.[99] Yet, for the purpose of this thesis, the frontier orbital representations are more crucial, as the values of the frontier orbitals are determined experimentally. Therefore, the B3LYP hybrid functional was chosen for the good fitting obtained compared with the experimental data, and the numerous reports using this functional in the literature.

2.1.3. Alkyl Chains

In our systems, we excluded alkyl chains during the calculations, replacing them with hydrogen or methyl groups. The omission of long alkyl chains speeds up computations, and in most cases, does not influence the properties calculated. As a proof of concept, Figure 15 illustrates the HOMO orbitals for two compounds, used in Chapter 4, with hydrogen atoms, with methyl chains and with hexyl groups. It is apparent that the delocalization of the electrons is the same on the molecules. However, both the calculated HOMOs and the planarization differ slightly (Figure 15). The HOMOs differ by 0.1 eV between the non-alkylated and the alkylated compounds, but are the same between the methyl and hexyl alkylated molecules.

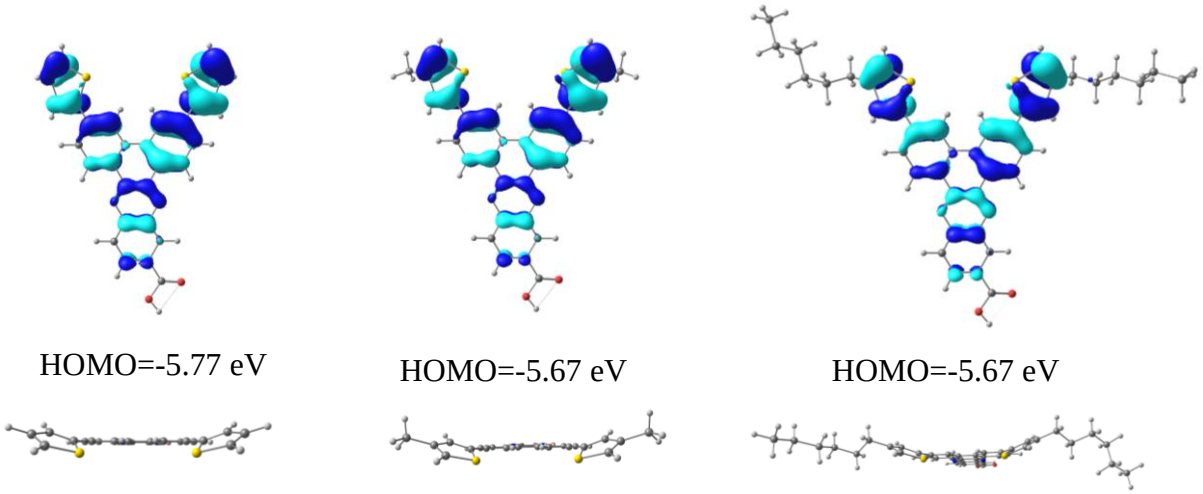

Figure 15: Top: HOMOs for 3,6-di(thiophen-2-yl)dibenzo[a,c]phenazine-11-carboxylic (left), 3,6-bis(4-methylthiophen-2-yl)dibenzo[a,c]phenazine-11-carboxylic acid (middle), 3,6-bis(4-hexylthiophen-2-yl)dibenzo[a,c]phenazine-11-carboxylic acid (right), and their calculated HOMO values. Bottom: Side view of the three molecules.

To further investigate the effect of the alkyl chains, UV-visible spectra were computed using TDDFT, and the results are presented in Figure 16. The oscillator strengths are similar, and some small differences can be seen in the wavelengths of the transitions. Interestingly, a bathochromic shift is predicted in the presence of alkyl chains both in the high energy region (around 300 nm and 350 nm) and in the low energy transitions (in the 450 nm region). When compared with the experimental spectra (dotted line in Figure 3), the similarity of shapes between computed and experimental spectra is striking, and demonstrates the validity of using TDDFT computations to simulate optical properties.

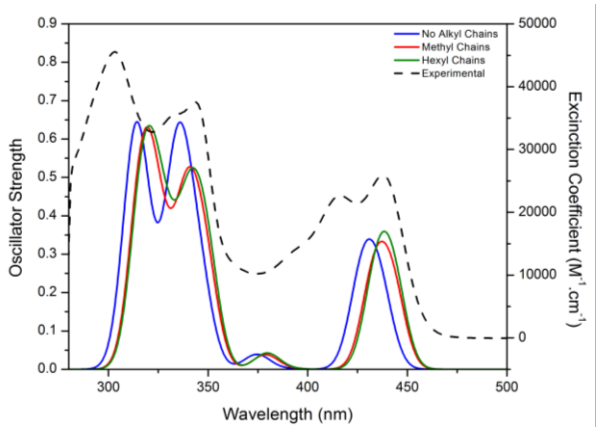

Figure 16: Simulated UV-Vis spectra with TDDFT of 3,6-di(thiophen-2-yl)dibenzo[a,c]phenazine-11-carboxylic (blue line), 3,6-bis(4-methylthiophen-2-yl)dibenzo[a,c]phenazine-11-carboxylic acid (red line), 3,6-bis(4-hexylthiophen-2-yl)dibenzo[a,c]phenazine-11-carboxylic acid (green line), and experimental UV-visible spectra in toluene for 3,6-bis(4-hexylthiophen-2-yl)dibenzo[a,c]phenazine-11-carboxylic acid (dotted black line).

Overall, the economy of time that the omission of alkyl chains offer outweighs the small differences in the properties calculated. It is recommended to replace alkyl chains with methyl group, and to use alkyl chains only if expressly needed.

In summary, while the results obtained with calculations often predict the properties correctly, they need to be thought upon. Does the optimization of the molecules seem chemically right? What hybrid functionals should be used, and does it matter? Should the pendant chains be omitted? More in-depth reasoning on the computations will enhance the computation time and the quality of the results, as well as increase the level of understanding of the studied system.

2.2 Microwave Heating *vs.* Conventional Heating

Over the past decade, the microwave reactor has become an essential tool in the synthesis lab and has been praised for its faster, simpler, cost-effective processes, leading to high-yielding and pure products.[100–104] The first use of microwave heating in chemical research

can be traced back to 1971.[105] In 1986, Gedye *et al*. published the first successful set of reactions using a conventional, domestic oven.[106] Despite a surge of interest catalyzed by reports describing up to 1000-fold increase in the reaction rates,[107,108] some reports of explosions using conventional microwave ovens have tarnished the image of microwave chemistry. Presently, microwave reactors, designed specifically for laboratory use, have made microwave heating convenient, easy and safe for scientists. In this thesis, a CEM microwave SP Discover was employed. Unless noted, the parameters were fixed on the dynamic set-up, with maximum power at 300 W and pressure of 250 PSI. The temperature and time used are specified for each experiment.

The advantages of microwave *vs.* conventional heating are still being discussed. In simple terms, conventional heating warms a reaction by convection, from the outside inwards, and the equilibration upon heating or cooling is long: on the timescale of minutes to hours. Microwave heating produces a localized heating that acts on all parts of the vessel, which can be heated and cooled down in the seconds to minutes timescale. This variation in heating is illustrated in Figure 17, that displays the temperature profiles for a tube heated conventionally (left) and by a microwave reactor (right) for 60 seconds.[109]

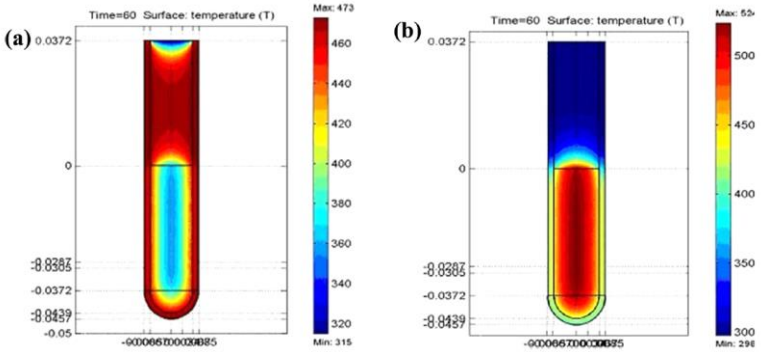

Figure 17: Difference in temperature profile of a tube heated (a) conventionally and (b) with microwave heating. The images shows a slice of a tube heated after 60 seconds in (a) a water bath and in (b) a CEM Discover microwave reactor. Figure adapted from reference 109.

Contrary to conventional heating, a microwave reactor encompasses several types of heating: direct, volumetric, instantaneous, and selective. Direct heating means that the microwave radiation interacts directly with the reaction components. In Figure 17, the contents inside the vessel are warmed whereas the rest of the vessel is not. Because the microwave radiation is equally propagated, the vessel can be heated volumetrically and homogeneously. The heating is also instantaneous, given the nature of the volumetric and direct heating. Moreover, some reactants interact more strongly with the microwave field, and can be heated selectively. One other advantage of a microwave reactor is that the system can be considered closed. By heating above the boiling point of the solvent, the rate of the reaction is higher, following the Arrhenius law (15):

$$k = A\, e^{\frac{-Ea}{RT}} \qquad (15)$$

with k, the rate constant of a chemical reaction, A the pre-exponential factor, E_a the activation energy, R the universal gas constant, and T the temperature.

In the literature, some glorify microwave's use, praising the reduction of reaction time, the success of couplings that do not proceed with conventional heating and the use of "green chemistry" conditions.[110,111] Others are wary of the harsh conditions employed for unstable compounds or of the relevance of using microwave heating.[112] There is an on-going discussion on microwave oven: is it just heating, or does it involve a non-thermal "microwave effect"? [113,114] Overall, any reaction working with conventional heat will likely proceed in a microwave reactor, in a shorter time. However, a non-working reaction in conventional heating is not assured to work in the microwave. Moreover, extra care is required for reactions needing water and oxygen free environments. To date, the usual procedure is to add all reagents into the microwave vessel while in an oxygen-

free and water-free glove-box, to cap the vessel, and to take it out of the glove-box to the microwave reactor. The microwave vessel does not have an impermeable cap, so the amount of oxygen that can enter in the vessel via the cap, before or during the reaction is unknown.

In this thesis, reactions known to work well under conventional heating (condensation, ring closing, Stille coupling) were used to our advantage in the microwave, reducing the time of sample preparation, the reaction time, and the quantity of solvent used. Figure 18 represents some reactions performed and a comparison of time and yield values for conventional and microwave heating.

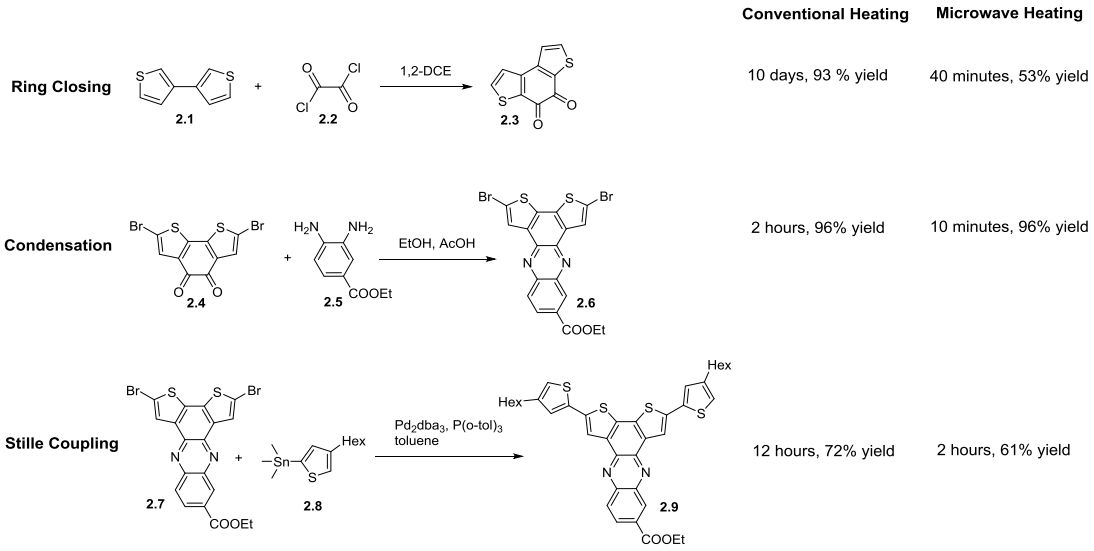

Figure 18: Illustration of three reactions performed with conventional and microwave heating and their corresponding reaction times and yields.

A microwave reactor was also used for polymerization, as described in more details in Chapter 3 of this thesis. Polymers can be obtained overnight, compared to several days in conventional heating, proving the utility of microwave reactor when considering scale-up processes for industry applications.

2.3. Material and Reagents

All starting materials and reagents were purchased from commercial sources, and used without further purification, unless otherwise noted. ^{1}H and ^{13}C NMR spectra were collected on a Mercury 300, Gemini 300, Bruker 400 or Inova 500. Chemical shifts are referenced to the residual solvent peaks: ^{1}H NMR δ =7.26 ppm and ^{13}C NMR δ =77.23 ppm for $CDCl_3$ and ^{1}H NMR δ =2.50 ppm for DMSO. High resolution mass spectrometry was performed by the spectroscopic services in the School of Chemistry and Biochemistry of the Georgia Institute of Technology. Fourier Transform Infrared (FTIR) spectroscopy was carried out on a Perkin-Elmer Spectrum One FTIR outfitted with a $LiTaO_3$ detector.

2.4 Structural and Polymer Characterization

At the University of Florida, gel permeation chromatography (GPC) was performed at 40°C using a Waters Associates GPCV2000 liquid chromatography system with an internal differential refractive index detector and two Waters Styragel HR-5E columns (10 μm PD, 7.8 mm ID, 300 mm length) using HPLC grade THF as the mobile phase at a flow rate of 1.0 mL/min. Injections were made at 0.05-0.07 % w/v sample concentration using a 220.5 μL injection volume. Retention times were calibrated against narrow molecular weight polystyrene standards (Polymer Laboratories; Amherst, MA).

At the Georgia Institute of Technology, Gel-Permeation Chromatography (GPC) was performed at 35 °C in THF to determine molecular weight(s). A combination of Waters HPLC pump 1515, UV-Vis Detector 2487, and a Refractive Index Detector 2414 were used. A Waters column (4.6 mm × 300mm; Styragel HR 5E) and polystyrene standards

from Fluka were used. The polymer solution (1 mg/mL in THF) was prepared and filtered through a Mini-UniPrep PTFE filter with a 0.45 μm filter. 20 μL of each polymer solution was injected and molecular weights were calculated using Waters Breeze II software.

2.5 Electrochemical Methods

Electrochemistry was employed to evaluate the electroactivity of the materials synthesized and presented in this dissertation. In this thesis, a general set-up consisting of a reference, a working, and a counter electrodes was used. CV and DPV experiments were performed using an EG&G Princeton Applied Research model 273A potentiostat-galvanostat in an argon filled dry-box. For all systems, the counter electrode was a platinum flag and the reference probe was based on an Ag/Ag^{+} redox couple. The background current was recorded before each sample to evaluate the electrochemical purity of the electrolyte. Scans were calibrated *vs.* a ferrocene/ferrocenium (Fc/Fc^{+}) reference, taken to be 5.12 eV below vacuum. Discussions for this value can be found in the thesis of Barry C. Thompson,[115] and reference [116]. For small molecules, the working electrode was a platinum button, and solutions were made from freeze-pump-thawed benzonitrile or DCM, using 0.1 M tetrabutylammonium hexafluorophosphate ($TBAPF_6$, 98% Acros, recrystallized from ethanol) as the supporting electrolyte. For polymers, materials were drop-casted from chloroform solution (1 mg/mL) onto a platinum electrode (0.8 cm^2). The supporting electrolyte was 0.1 M $TBAPF_6$ solution in ACN, which was taken from the solvent purification system, dispensed directly into the glovebox.

2.5.1 Cyclic Voltammetry and Differential Pulse Voltammetry

In cyclic voltammetry (CV), the working electrode potential is linearly increased and then reversed versus time. In Differential Pulse Voltammetry (DPV), a square-wave potential is applied versus time. Figure 19 shows the applied signal, and the usual response recorded for both CV and DPV experiments. More details on these experiments can be found in the dissertations of Jennifer A. Irvin[117] and Emilie E. Galand.[118]

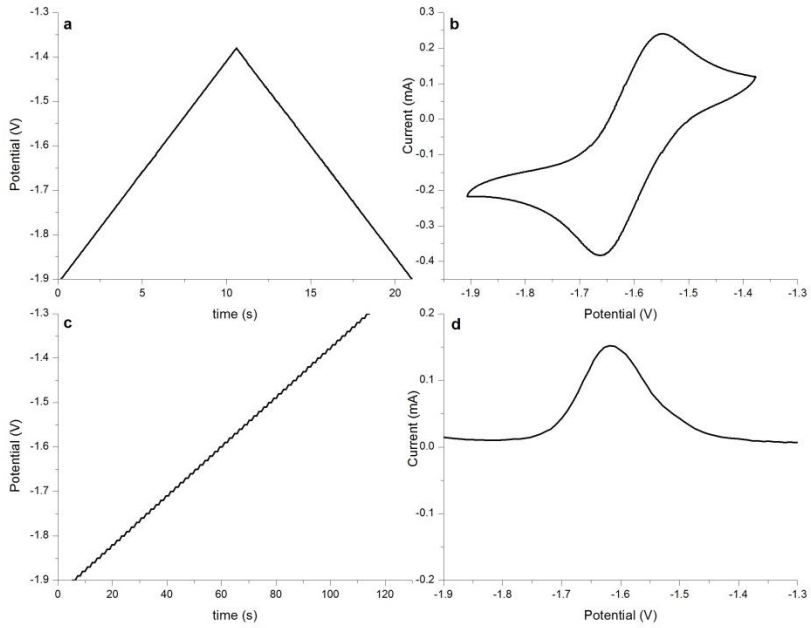

Figure 19: Potential applied (a, c) and current-potential response (b, d) for CV (a,b) and DPV (c,d) of ethyl dithieno[3,2-a:2',3'-c]phenazine-9-carboxylate.

In reversible systems, the half wave potential value on a CV experiment is equal to the peak potential value of a DPV experiment. In DPV, the major component of the current is faradic, due to the oxidation or reduction at the electrode surface. In a CV experiment, capacitive current, notably due to the charging of the electrode double layer, is also observed. DPV experiments are generally more defined, as the signal to noise ratio is increased compared to the CV experiment. For polymers, the onsets of the peaks were

used to determine the frontier orbitals, whereas for small molecules, the half wave potentials of CV curves and the peak potential of DPV responses were used.

2.5.2 Spectroelectrochemistry

For Chapter 3, spectroelectrochemistry was studied for different polymers to obtain the absorption variation upon oxidation and reduction of polymer thin-films. The polymer films were prepared by spray-casting polymer solutions (3-5 mg. mL^{-1} in toluene) onto ITO (Indium Tin Oxide) - coated glass slide (Delta Technologies, Ltd., 7 x 50 x 0.7 mm, sheet resistance, Rs=8-12 Ω/cm^2) using an air brush (GREX genesis xg or Itawa-eclipse HP-Bs) at 20 psi. The electrochemical oxidation of the films was carried out in 0.1 M of $TBAPF_6$ supporting electrolyte using the three cells set-up described previsously, with a platinum wire as a counter electrode in order to avoid blocking incident light. Absorption spectra were recorded using a Varian Cary 5000 Scan UV-Vis/NIR spectrophotometer, and the oxidation potentials were varied using the Corrware software. Pictures were taken with Nikon D90-18-105VR camera.

2.6 Optical and Spectroscopic Methods

2.6.1 Steady State UV-visible Absorption

Absorption spectra were obtained using a Varian Cary 5000 Scan UV-Vis/NIR spectrophotometer and quartz crystal cells (1 cm×1 cm×5.5 cm, Starna Cells Inc.). Solution spectra were recorded in HPLC grade solvents, the optical density at the maximum of absorbance being below 1. For thin film spectra, the molecules were drop-casted on a 1×1" glass slides from 10mg/mL chloroform or toluene solutions.

2.6.2 Fluorescence, Quantum Yield and Lifetime Fluorescence

Fluorescence spectra were taken at the University of Florida on a Jobin Yvon Horiba Nanolog, or at the Georgia Institute of Technology on a Fluorolog FL3C-21. Quantum yields were measured on the instrument used for the fluorescence in conjunction with the UV-Vis spectrometer, following the procedure reported by Würth *et al.*[119] HPLC grade solvents were used, and the actionometer was selected with the best match between the standard and sample absorption and emission spectra.

2.6.3 Singlet Oxygen

Singlet oxygen emission was determined on a PTI near-infrared emission spectrometer equipped with an InGaAs detector. Singlet oxygen quantum yields were determined from plots of $^1O_2$ emission intensity as a function of the optical density of the sensitizer at 337 nm using terthiophene ($\Phi_\Delta = 0.70$) as an actinometer.

2.6.4 Transient Absorption

Transient absorption measurements were conducted on a home-built apparatus, using a Continuum Surelite II Nd:YAG laser for excitation and PI-Max intensified CCD camera coupled with a spectrograph as a detector. The probe source was a Perkin-Elmer LS1130-3 pulsed xenon lamp. Excitation energies were ~6 – 7 mJ/pulse. Spectra were recorded in 12-mL quartz flow cell containing 10 mL of oligomer samples in toluene. The optical density (355 nm) was adjusted to 0.7 and the solutions were purged with argon for 30 min prior to transient absorption measurements. The initial decay was 70 ns, and the camera increment was 40 μs.

2.7 Dye-sensitized Solar Cells

The TiO_2 solution, TiO_2 electrodes and platinum cathodes were prepared according to literature procedures.[120,75] On the platinum cathodes, two holes (1 mm diam.) were drilled to later permit the injection of the electrolyte solution. A solution of 0.2 mM of dye in dimethylformamide (DMF) was stirred overnight, and the TiO_2 electrodes were immersed in the solution for 36 h. After rinsing the electrodes with DMF and acetone to remove the unbound dye, the electrodes were placed under vacuum for 2 hours. The TiO_2 electrodes and platinum cathodes were sealed together with surlyn (Solaronix Meltonix 1170-25). Electrolyte solution containing 0.05 M I_2, 0.1 M LiI, 0.6 M 1-methyl-3-(n-propyl)imidazolium iodide, and 0.5 M 4-tert-butylpyridine in butyronitrile was injected into the sealed device via the holes in the platinum cathodes. For IPCE characterization, an Oriel Apex monochromator illuminator (100 W xenon lamp) coupled with a ¼ m Oriel Cornerstone spectrometer was used to illuminate the cell with monochromatic light. The photocurrent response was recorded under short circuit conditions at 10 nm intervals using a Keithley 2400 source meter. The light intensity at each wavelength was calibrated with an energy meter (S350, UDT Instruments).

CHAPTER 3.

SYNTHONS AND POLYMERS DEVELOPED FROM BENZODITHIOPHENE.

3.1 Benzodithiophene Derivatization, Ring Opening and Polymers

3.1.1 Previous Methods and Importance of Precursors

In π-conjugated systems, the donor-acceptor approach – orbital mixing of alternating donor and acceptor units to decrease the electronic band gap- has become one of the most powerful strategies for band gap engineering.[37,121] Therefore, access to new donor and acceptor molecules is highly convenient since it can lead to new π-conjugated systems with tuned band gaps and properties. Aromatic diones are versatile starting materials that can generate a wide variety of monomers for the synthesis of π-conjugated materials. The ketone moiety can be easily converted into other organic functionalities leading to new molecules with desired properties and characteristics (*i.e.* electron donors or electron acceptors). Many of these transformations can be carried out in one or two steps, which demonstrate the usefulness of these intermediates. The research described in this chapter first focuses on the synthesis of the fused-aromatic dione benzo[1,2-b:6,5-b']dithiophene-4,5-dione (BDTD) and its conversion to new π-conjugated material precursors by different synthetic approaches. This methodology can be adapted to other aromatic diones, giving access to novel donor and acceptor molecules, which is crucial to generate new π-conjugated materials with improved physical and electronic properties.

Molecules such as BDTD offer various features that make them attractive for π-conjugated materials. These molecules inherit the wide range of electronic properties offered by thiophene-based materials,[122] and also offer the possibility for derivatization on the thiophene rings (*i. e.* halogenation, borylation, stannylation, etc.) and on the carbonyl groups. Due to these features, various syntheses and uses for BDTD have been reported.[3,123–125]

3.1.2 BDTD Synthesis and Derivatization

Initially, to make BDTD, we used the synthetic route shown in Scheme 1. This route employs the commercially available 2-bromothiophene as the starting material, and was based on previously reported literature procedures[126–129] to generate the intermediate **a**. This route contains a considerable number of synthetic steps (6), a low overall yield (~ 9%), and in some cases requires column purification, which makes the synthesis expensive and unsuitable for a large-scale synthesis of BDTD.

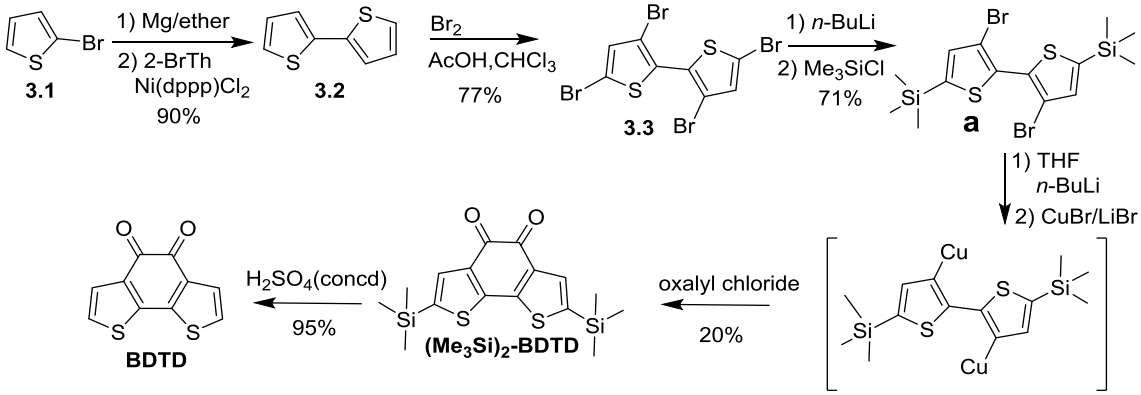

Scheme 1: Multi-step route toward BDTD.

Here, we report an alternate synthetic route toward BDTD, and this approach is presented in Scheme 2. This path uses the inexpensive and commercially available 3-

bromothiophene as starting material. It is highly convenient, since the reaction can be carried out in only two steps, in high yields, and requires no column purification, allowing for multigram synthesis.

The synthesis of the dione **3.5**, which is the key intermediate, was carried out using a modified literature procedure for analogous systems.[130] After **3.5** was isolated, it was subjected to oxidative ring closing using iron(III) chloride or iron(III) bromide in DCM.

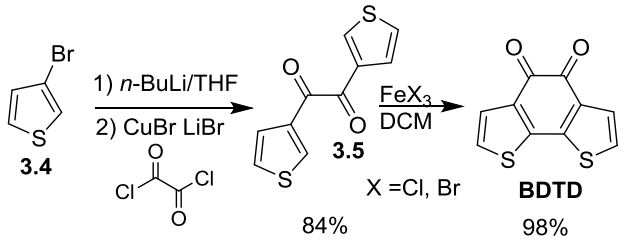

Scheme 2: Short synthesis of BDTD.

Various experiments were carried out to optimize the oxidative ring-closing conditions in DCM—*e.g.* different concentrations, reaction times and temperatures (20, 35 and 40 ˚C). Monitoring of the reaction by TLC for several hours (1 – 24 h) led to the conclusion that the reaction must be carried out at room temperature, for at least two hours, and using three or more equivalents of $FeCl_3$ or $FeBr_3$ to achieve high conversion. If less than 2.5 equivalents of iron chloride were employed full reaction conversion was not observed, even if the reaction was run for more than 24 h. Figure 20 presents the various chemical transformations on BDTD reported recently in our group.[131] Most of these chemical transformations are straightforward and can be done in one or two steps, and without requiring laborious purifications, hence demonstrating the versatility of the aromatic dione BDTD.

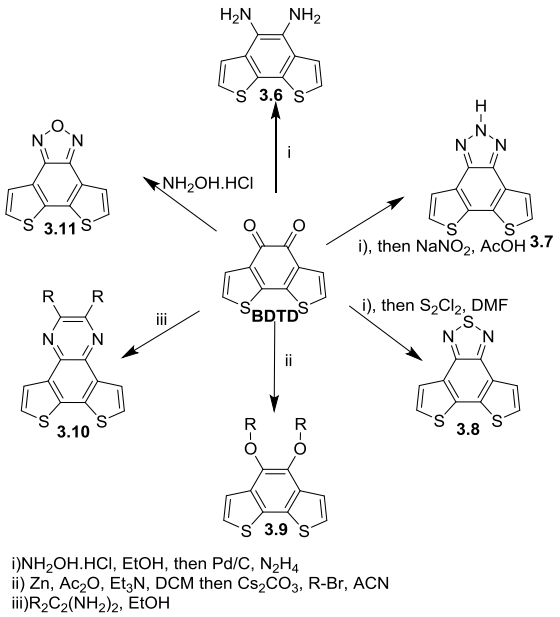

Figure 20: Wheel of possibilities for the transformation of BDTD into useful precursors for organic electronics.

3.1.3 Ring Opening Reaction leading to Ester Derivatives

As seen in the previous paragraphs, creating new synthons is the key for developing new materials that have tunable properties. While studying the conditions for the alkylation of the brominated derivative of BDTD, with the hope of creating a one-pot version of the conditions ii) in Figure 20, an interesting reaction was observed. When employing a base directly on BDTD, the dione moiety ring-opens, and addition of alkyl bromide leads to esters derivatives of dithiophenes. Interestingly, the sought alkylation of BDTD happens simultaneously. As a result, two products can be observed when treating dibromo-benzodithiophene with alkyl bromide in a basic environment, as shown in Scheme 3.

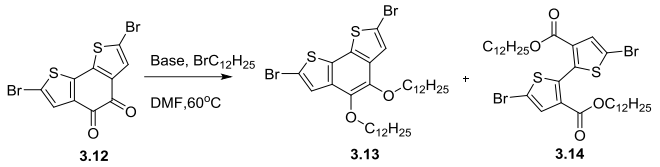

Scheme 3: Two products obtained when treating BDTD with dodecyl bromide in a basic environment.

In order to optimize reaction conditions, BDTD was exposed to a variety of basic conditions, which are summarized in Table 5. Cesium carbonate was found to be the most efficient base, working both at room temperature and upon heating. When employed with the latter conditions, the ring opening was favored, leading to 70% yield of compound **3.14** (Table 1, entry 7). In contrast, at room temperature, compounds **3.13** and **3.14** were produced in more balanced yields of 25% and 32 %, respectively. Potassium carbonate and sodium carbonate both produced compound **3.13** in low yield (9-18% and 18% respectively), and compound **3.14** in moderate yield (42-50% and 54% respectively) (Table 5, entries 2, 3 and 5). If employing these bases at room temperature, compounds **3.13** and **3.14** were obtained in trace amounts (Table 5, entries 1 and 4).

Table 5: Summary of the conditions: base, temperature and yields for the formation of alkylated BDT (3.13) and the ring opening compound (3.14).

Entry	Base	Temp (°C)	**3.13** (%)	**3.14** (%)
1	K_2CO_3	RT	trace	trace
2	K_2CO_3	65	9	42
3	K_2CO_3	reflux	18	50
4	Na_2CO_3	RT	trace	trace
5	Na_2CO_3	60	18	54
6	Cs_2CO_3	RT	25	32
7	Cs_2CO_3	65	9	70
8	NaOH	65	0	0
9	Li_2CO_3	65	0	0

When using other bases, such as lithium carbonate or sodium hydroxide, no products were observed, upon heating or at room temperature, and the starting material was recovered (Table 5, entries 8 and 9).

As compound **3.13** is the minor product of the reaction presented in Table 3, a new route was designed as an attempt to generate it in a more efficient way. Previously, alkylated dibromo-BDT[132] was synthesized in three steps, involving three purifications via column chromatography, a total reaction time of 4 days, and an overall yield varying from 34% to 50%, depending on the alkyl chains (Scheme 4, top). By combining the two first steps, the new proposed route is only composed of 2 reactions, and a total reaction time of a day. The overall yield is of 30% with dodecyl chains. To note, the one-pot reduction and alkylation is similar to the conditions presented above. The difference is the use of zinc powder as a reducing agent. When trying to use these conditions directly on brominated BDTD, the bromide groups are cleaved off.

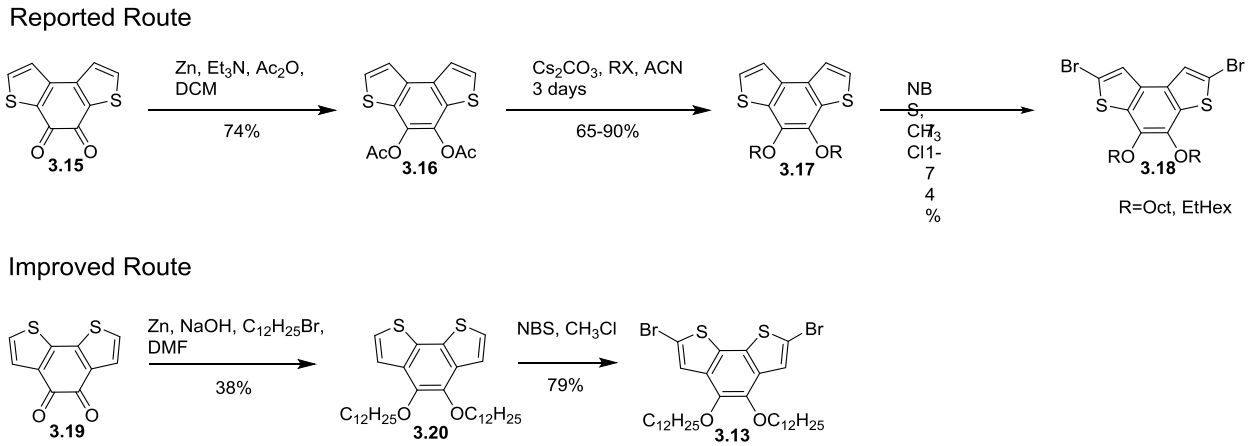

Scheme 4: Reported and improved route for the synthesis of dibromo-bis(dodecyloxy)benzodithiophene.

3.1.4 Synthesis of Four Polymers Based on Dialkyl [2,2'-bithiophene]-3,3'-dicarboxylate and Bis(dodecyloxy)benzodithiophene

Compounds **3.13** or **3.14** can be directly utilized as monomers to produce conjugated polymers. Compound **3.14** is an interesting synthon as it offers an easy synthesis for carboxylate-functionalized polythiophenes, which are employed in dye-sensitized solar cells, in field-effect transistors, and in chemo- and bio-sensors.[133–137]As a proof of concept of the simplicity of derivatizations, four polymerizations were run utilizing Stille or Suzuki coupling, as displayed in Figure 21. The polymers are based on compounds **3.13** (**Th-Th**) and **3.14** (**BDT**) and on thiophene (**Th**) or benzene (**Ph**) units. The Stille couplings were performed in a microwave reactor for 10 hours. The Suzuki couplings were achieved with base free conditions, previously developed by our group.[138]

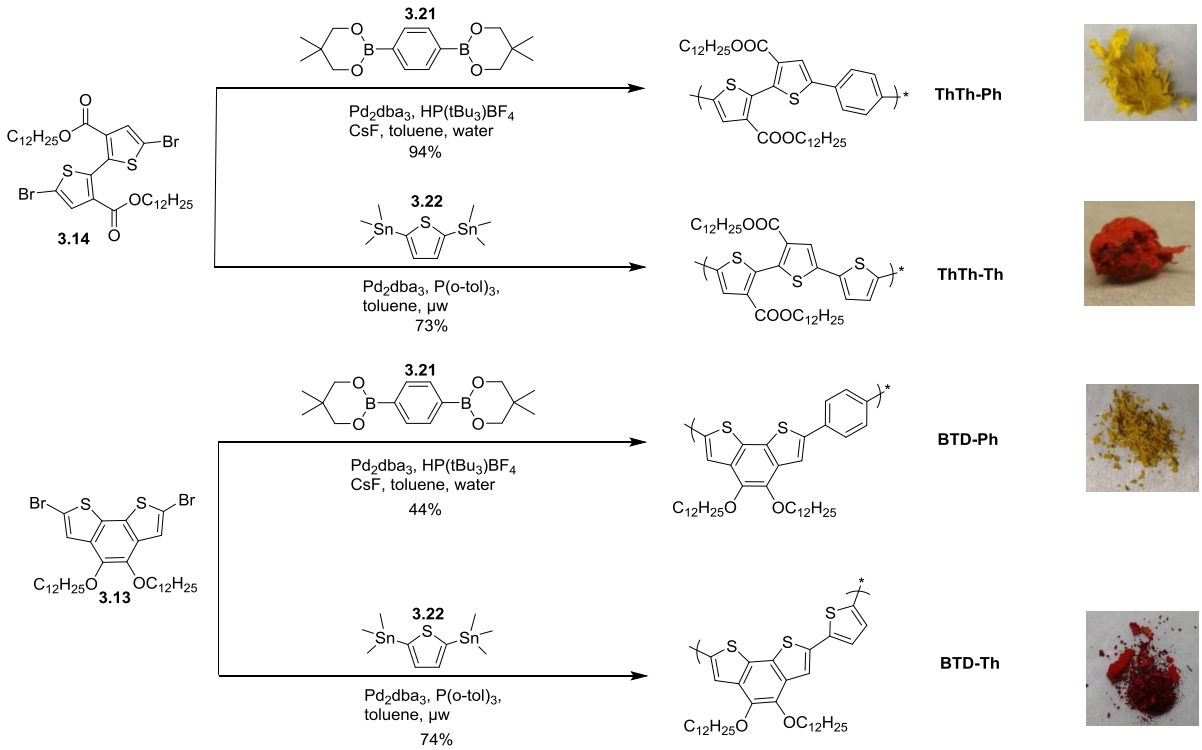

Figure 21: Suzuki and Stille co-polymerizations for the synthesis of ThTh-Ph, ThTh-Th, BDT-Th and BDT-Ph and photography of the polymers obtained.

Yields and molecular weights, shown in Table 6, are good for all polymers, except BDT-Ph. This is probably due to the precipitation of BDT-Ph during the polymerization. Repetition of this polymerization in tetrahydrofuran failed to lead to higher molecular weight polymers. In general, Suzuki polymerizations need more fine tuning of the conditions (bases, ligands and solvent) to achieve high molecular weight when compared with Stille polymerizations.

Table 6: Molecular weights, polydispersity, absorption maxima in solution and film, optical band gap and emission maxima for ThTh-Ph, ThTh-Th, BDT-Th and BDT-Ph

	Yield (%)	Mn^{a} (kDa)	Mw/Mn^{a}	$\lambda_{max}{}^{b}$ (nm)	$\lambda_{max}{}^{c}$ (nm)	$E_{gap}{}^{Opt}$ (eV)	$\lambda_{em}{}^{b}$ (nm)
ThTh-Th	73	19	1.6	425	433	2.44	564
ThTh-Ph	94	39	2.9	385	408	2.70	512
BDT-Th	74	36	1.1	494,532	493,532	2.16	570
BDT-Ph	44	7	1.1	427,449	493	2.31	470

[a]Determined by SEC in THF against polystyrene standard. [b]in DCM solution. [c]Recorded for thin films drop-cast onto glass slides.

The ester-functionalized polymers (ThTh-Ph and ThTh-Th) were submitted to basic hydrolysis. IR spectroscopy showed the conversion of ester moieties to carboxylic acids groups. Unfortunately, the resulting polymers were not soluble in any organic solvents, due to the absence of alkylated chains on the polymeric chains, and could not be well-characterized. Nevertheless, Liu *et al.* [139] exploited favorably this difference from soluble to insoluble property with integrating polycarboxylate thiophenes into dye-sensitized solar cells devices.

3.1.5 Electrochemistry and Optoelectronic Characterization

3.1.5.1 DFT Calculations

In this chapter, DFT and TDDFT computations were performed on tetramer units of the four synthesized polymers, at the B3LYP/6-31G* level of theory. Four repeats units are a suitable compromise between the number of repeat units and the time needed for calculations. Figure 22 illustrates the electronic density of the frontier orbitals for the studied polymers. A side-view of the polymer chains is also presented. A noticeable difference is observed in terms of planarity between the series ThTh and BDT. The BDT family, having a fused system, is more planar and more rod-like than the ThTh family. As a result, the electronic orbital densities are more delocalized along the chains for the BDT family than for the ThTh family, where the orbital densities for both frontier orbitals are unequally distributed on the polymeric chain. When comparing the aromatic linkers (Th or Ph), polymers containing Ph have a deeper HOMO and a more negative LUMO, increasing the overall band gap. The reason is that phenylene groups are less electron rich than thiophene groups.

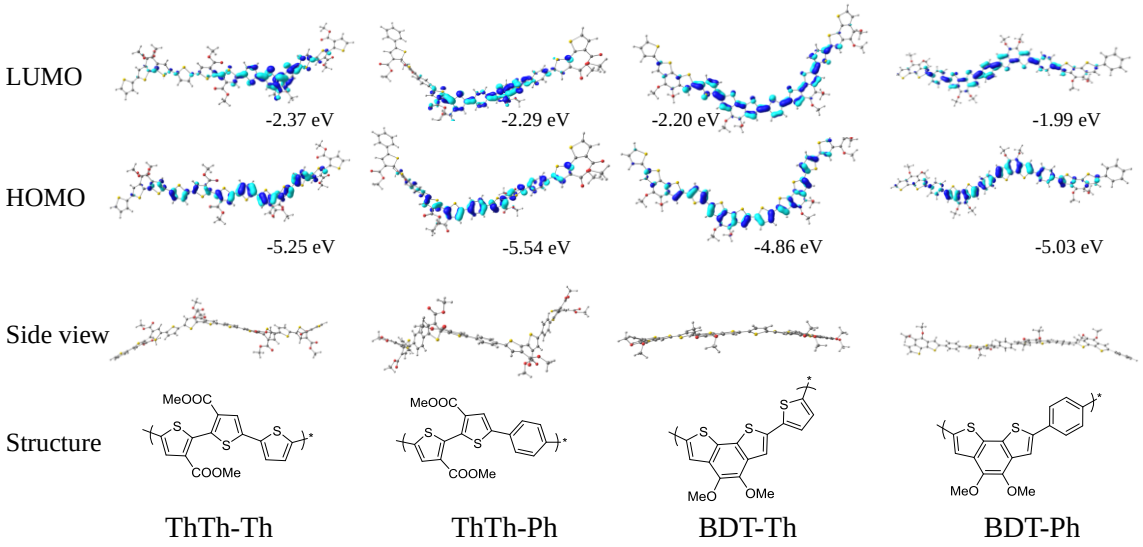

Figure 22: Illustration of frontier orbitals for tetramers of ThTh-Th, ThTh-Ph, BDT-Th and BDT-Ph, and side views and structures of the polymers.

Figure 23 displays the simulated UV-visible absorption spectra. A bathochromic shift is observed from ThTh-Ph (λ_{max}=444 nm) to BDT-Ph (λ_{max}=466 nm), to ThTh-Th (λ_{max}=501 nm) and to BDT-Th (λ_{max}=534 nm). Thiophene units, being a greater donor moiety than phenylene, raise the HOMOs and decrease the bang gap. For all polymers, the maxima peaks are of HOMO→LUMO character only (>95 %.) Interestingly, the oscillator strengths are comparable for ThTh-Th, ThTh-Ph and BDT-Th, but the HOMO→LUMO transition is more intense for BDT-Ph.

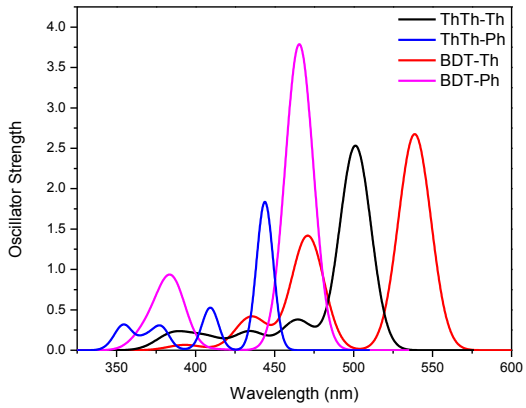

Figure 23: Simulated absorption spectra of the four tetramers ThTh-Th, ThTh-Ph, BDT-Th and BDT-Ph, computed at the B3LYP/6-31G* level.

3.1.5.2 Steady State UV-Vis Absorption

Simple characterizations can be performed to assess fundamental optoelectronic properties of these polymers. Figure 24 illustrates the absorbance spectra of the polymers both in toluene solution and drop-cast as films. In solution, a bathochromic shift is observed from ThTh-Ph (λ_{max}=385 nm) to ThTh-Th (λ_{max}=425 nm) to BDT-Ph (λ_{max}=449 nm) to BDT-Th (λ_{max}=532 nm), which agrees largely with the results obtained by calculations. In films, the absorptions are shifted to longer wavelengths, due to intermolecular aggregation.[140] The maximum absorption peaks are red-shifted from ThTh-Ph to ThTh-Ph to BDT-Ph to BDT-Th. To note, BDT-Ph has a tail on the 600-800 nm region, which is likely due to a film defect.

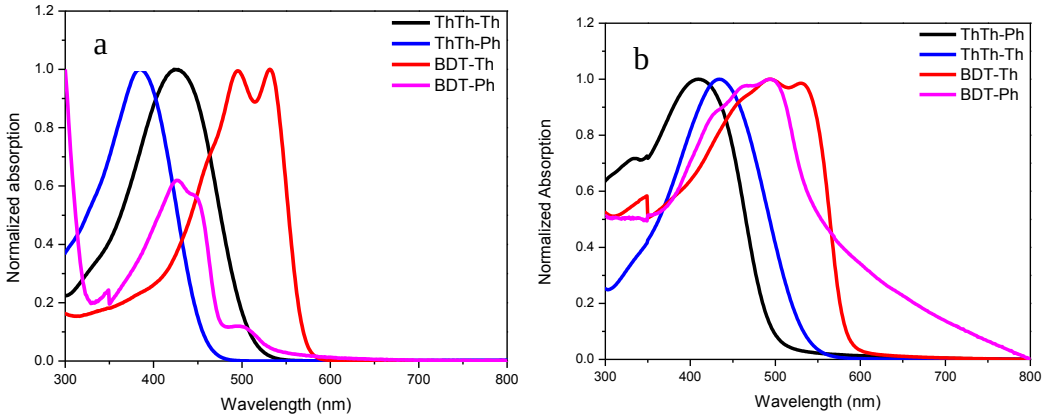

Figure 24: UV-Visible absorbance in (a) toluene and (b) drop-cast as thin films for ThTh-Th, ThTh-Ph, BDT-Th and BDT-Ph

3.1.5.3 Fluorescence and Quantum Yield

The polymers were highly fluorescent in solution under UV-light, so fluorescence spectra were recorded in toluene and are portrayed in Figure 25. The fluorescence spectra denote structureless bands for ThTh-Th and ThTh-Ph. On the contrary, bands are well defined for BDT-Ph and BDT-Th. The profiles of the fluorescence peaks are dependent on the

molecular weights, on the conformation of the polymers, and on the solvent.[141] The absorbance and fluorescence spectra are mirror-like in the ThTh series, and show a broad spectra, that is likely indicative of helical conformations in the chains.[142] In the BTD series, the peaks are defined and the fluorescence spectra contain a shoulder in the longer wavelengths, denoting the formation of excimers. Other experiments, such as a fluorescence based solvent-study of the polymers, circular dichroism or dynamic light scattering would provide more in-depth characterization of the conformation of the four polymers.

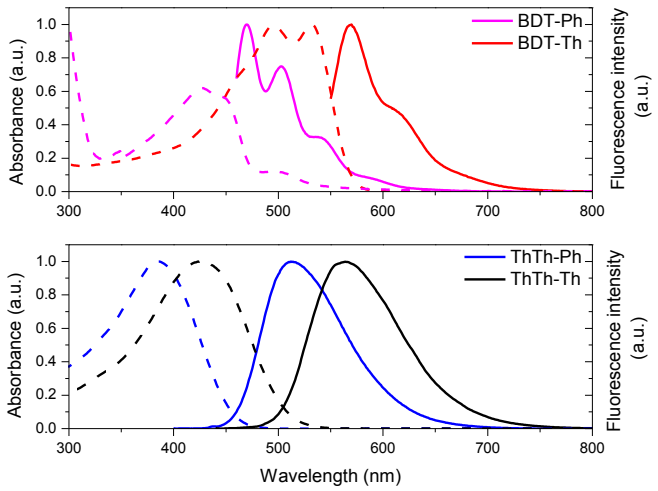

Figure 25: UV-visible spectra (dotted lines) and fluorescence spectra (solid line) in toluene of ThTh-Th, ThTh-Ph, BDT-Th and BDT-Ph

To summarize, we have shown in these sections the straightforward synthetic path toward BDTD, and the different approaches to derivatize this aromatic dione to produce various acceptor and donor molecules by relatively simple synthetic methodologies. A ring opening reaction was discovered and studied to produce ester-functionalized thiophenes. These units can be precursors of a multitude of compounds. As a proof of concept, four

polymers were synthesized, and their spectroscopic properties were investigated. To note, the ester-functionalized bithiophenes synthons could be the starting point to build bisthiophene dicarboximide, which have recently been under the spotlight due to their use in highly efficient solar cells.[143]

3.2 Structure: Property Relationship Study of Isomeric Benzodithiophene-Vinylene Copolymers

3.2.1. Context and Motivation for the Study of Isomeric Polymers

Switchable black-to-transmissive windows, malleable solar cells, and artificial skins are some examples of up-coming technologies that have garnered attention this past decade. These highly engineered materials are based on conjugated materials that, since the mid-1980's, have been extensively studied. Polymeric materials are of interest for their facile tunability and their solution processability. The prospect of printing materials instead of using high temperature ovens, or vacuum chamber makes polymers a front runner in organic electronics.

Interestingly, of the myriad of investigations into these polymers, only a few studies focus on the influence of isomeric systems on the macromolecular properties. For instance, Osaka *et al.*[144] reported the effect of isomeric structures on transistor performances, for polymers based on naphthodithiophenes (NDT). Angular NDT showed higher mobilities than linear NDT, as the former polymers gave highly order structures with a close π-stacking distance. The importance of the backbone curvature was reported by Rieger *et al.*, when looking at copolymers of alkylated dithiophenes and isomeric units

of benzodithiophenes.[145] They related the macroscopic properties (UV-visible spectroscopy, electrochemistry, charge carrier mobilities) to the degree of curvature of the polymers.

Of the conjugated synthons used in organic electronics, benzodithiophene units have been monomers of choice in organic field effect transistors and bulk hetero-junction solar cells, acting as the donor moiety of the p-type polymers. Poly(4,8-bis(octyloxy)-2-vinylbenzo[1,2-b:4,5-b']dithiophene) has been employed in bulk heterojunction solar cells, showing efficiencies up to 2.63%.[146] Other benzodithiophene isomers have been reported in bulk heterojunction solar cells; however, they have not been directly compared.

In these sections, we conduct a fundamental study of the impact of isomerism on optoelectronic properties: spectroscopy, electrochemistry, spectroelectrochemistry and colorimetry. The polymers were constructed from three isomers of benzodithiophene: 2,7-dibromo-4,5-bis(octyloxy)benzo[2,1-b:3,4-b']dithiophene (**BDT-1**), 2,7-dibromo-4,5-bis(octyloxy)benzo[1,2-b:4,3-b']dithiophene (**BDT-2**) and 2,6-dibromo-4,8-bis(octyloxy)benzo[1,2-b:4,5-b']dithiophene (**BDT-3**). This study provides some insights on the importance of fine-tuning structures for colorimetric applications.

3.2.2 Synthesis of the Monomers and Polymers

3.2.2.1 Synthesis of Isomeric Monomers

The three monomers exploited in this study can be synthesized in four to five steps from commercially available 3-bromothiophene. As shown in Scheme 5, the route for the

monomer preparation is straightforward, scalable, and high yielding. The procedures for the monomer synthesis were adapted from reported literature procedures.[147,131,148]

For the first isomer (**BDT-1**), the coupling presented in section 3.1.2 led to compound **3.5**, followed by a ring closing with iron(III) chloride to produce compound **3.19**. The BDTD **3.19** was then reduced and acetylated with zinc and acetic anhydride. Further alkylation with 1-bromooctane led to compound **3.24**. Bromination of **3.24** was done via n-bromosuccinimide leading to the monomer **BDT-1** in good yield. The overall yield for these five steps was 63%.

For the second isomer (**BDT-2**), Grignard homo-coupling of 3-bromothiophene (**3.4**) led to 3, 3'dithiophene (**3.25**). Compound **3.25** was heated at reflux for 10 days with oxalyl chloride in DCM to produce BDTD **3.15** in very good yields. Reducing the reaction time to 9 or 8 days decreased the yields to 89 and 77%, respectively. As pointed out by Turro and coworkers,[149] the use of Lewis acids did not favor the reaction. The ring closing was also successfully run in the microwave reactor: a reaction time of 48 min in a pressured vessel at 83ºC gave a yield of 55%. Compound **3.15** was then reduced, acetylated, alkylated and brominated in a similar fashion than the first isomer. The overall yield for these 5 steps was 37%.

For the last isomer (**BDT-3**), commercially available benzo[1,2-b:4,5-b']dithiophene-4,8-dione **3.27** was reduced and alkylated in a one-spot reaction. Upon bromination, the monomer **BDT-3** was obtained. The overall yield for these two steps was 59%.

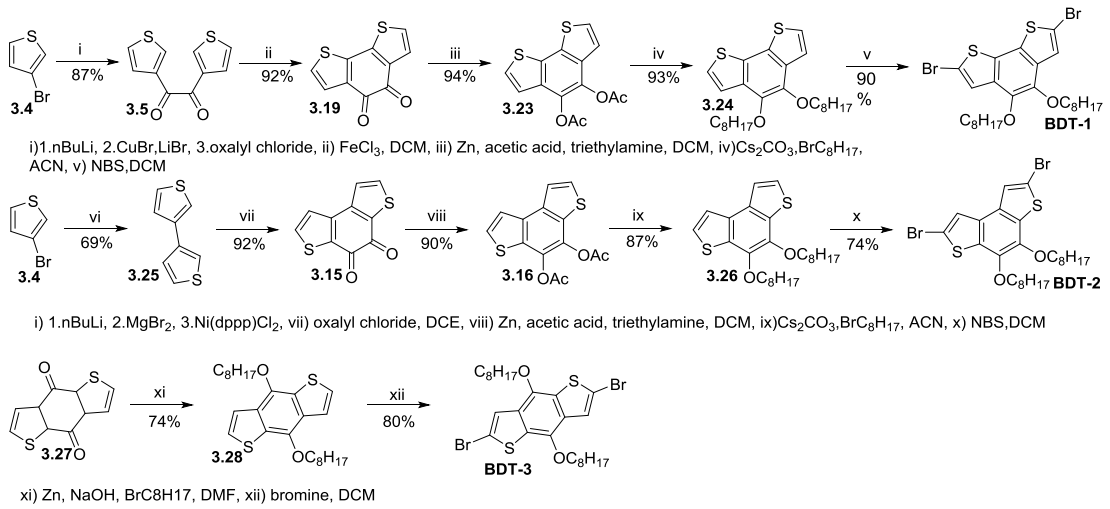

Scheme 5: Synthesis of monomers BDT-1, BDT-2, and BDT-3.

3.2.2.2 Polymerization: Conventional heating *vs.* microwave heating

Three isomeric polymers, based on the previously synthesized BDT units, were obtained via Stille polycondensation. The commercially available (E)-1,2-bis(tributylstannyl)ethene **3.29** monomer was coupled with the corresponding isomers of BDT (**BDT-1**, **BDT-2** and **BDT-3**), as displayed in Scheme 6. Polymerizations were done both under conventional and microwave heating.

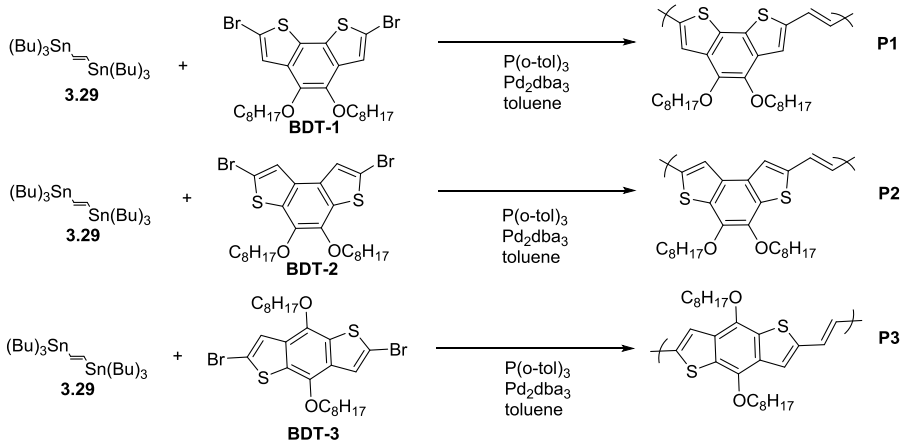

Scheme 6: Synthesis of polymers P1, P2 and P3

As discussed in the introduction, using a microwave reactor reduces the reaction time. Step –polymerizations, such as Suzuki and Stille couplings, are generally run from 36 to 96 hours. All three polymers were heated conventionally for 96 hours or in a microwave reactor for 3 hours. Table 7 summarizes the yields, molecular weight and PDI of the polymers. The results are comparable in terms of yields and molecular weights. The main difference is found in the polydispersity (PDI), with the PDI of the polymer being greater when using the microwave reactor. However, this disparity can be avoided by separating the molecular weights by fractions with a Soxhlet extractor. Lastly, it was found on several occasions that the molarity is an important parameter. If over 0.1 M, the polymerizations "crash out" after 24 hours when heated conventionally, or after 3 hours when in the microwave reactor, resulting in insoluble materials. The polymerizations proceeded well when a concentration of 0.04 M of monomer was employed.

Table 7: Summary of the yields, molecular weights and PDI for P1, P2, and P3, with conventional or microwave heating.

Compd	Microwave or Conventional	Yield (%)	Mn/Mw (kDa)	PDI
P1	C	70	21/64	3.04
P2	C	64	15/34	2.33
P3	C	44	10/20	2.0
P1	M	59	12/63	5.2
P2	M	90	11/31	2.80
P3	M	56	13/22	1.66

3.2.3. Ground State and Excited State Characterizations of the Polymers

3.2.3.1 DFT and TDDFT Calculations

To analyze the geometrical and optoelectronic properties of the newly-made polymers, properties of tetramer units, where octyl groups are replaced by methyl groups, are simulated with DFT and TDDFT computations, at the B3LYP/6-31G* level. In Figure

26, the frontier orbital for all polymers are illustrated. Both HOMOs and LUMOs are delocalized along the whole polymer backbone, which is quite different from common D-A copolymers, in which electrons are usually localized on the donor or the acceptor moieties.

The values for the HOMOs levels are similar for the three polymers. There is a minor variation in the LUMO levels. P2 has the most destabilized LUMO, due to the presence of orbital density on the oxygen atoms, and to a geometric effect, discussed below.

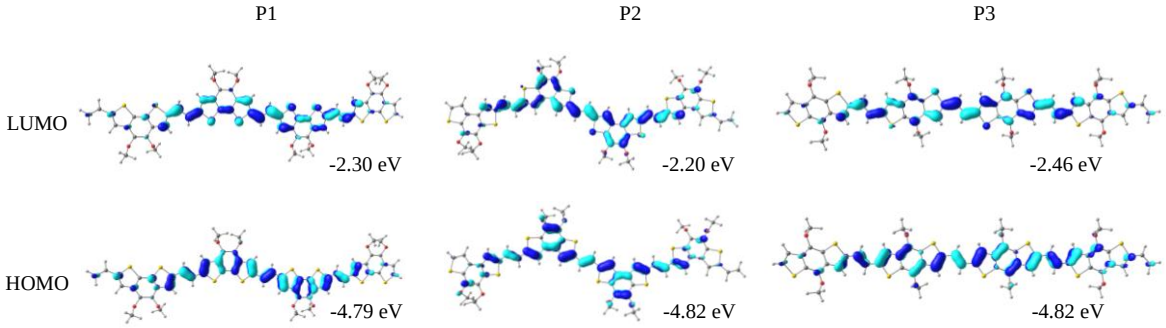

Figure 26: Frontier orbital representations for P1, P2 and P3, computed at the B3LYP/6-31G* level.

Looking at the geometry of the chains, due to the different angles induced by the BDT monomers, the three polymers have different degrees of curvature, which is represented by contour lines in Figure 27.[150] P3, composed of the "flat" monomer BDT-3, can be represented as a straight chain, rod-like. P1 and P2 have stronger curvatures, as both BDT-1 and BDT-2 monomers induce a change in the chain angle.

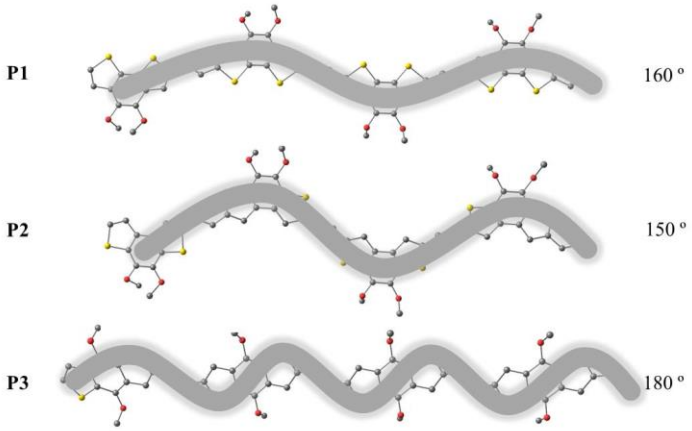

Figure 27: Geometry of the polymers: contour lines obtained after DFT calculations, and the corresponding monomer angle (angle introduced by the corresponding benzodithiophene into a linear polymer chain).

Figure 28 represents the simulated absorption spectra, obtained by TDDFT, at the B3LYP/6-31G* level. The theory predicts bathochromic shifts from P2 to P1 to P3, and similar oscillator strength for all three polymers. The order of the transitions follows the predicted energy gaps from Figure 26, which increases from P2 to P1 to P3 due to the stabilization of the LUMOs levels from P2 to P1 to P3. The main transitions at ≈525-600 nm correspond to solely (>97%) HOMO → LUMO transitions.

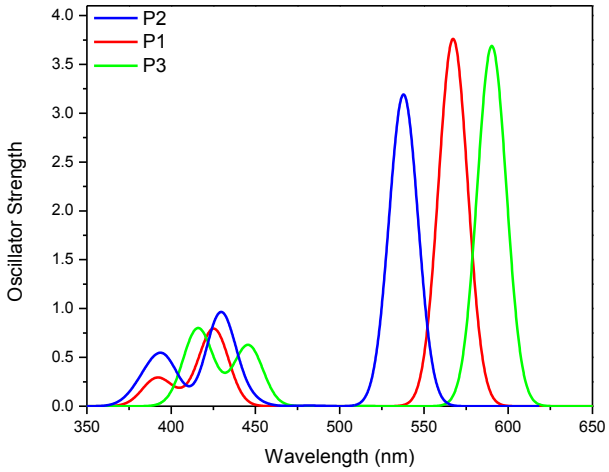

Figure 28: Simulated absorption spectra for tetramers of P1, P2 and P3. Calculations were done on the B3LYP/6-31G* level, in vacuum.

3.2.3.2 UV-visible Spectroscopy

Figure 29 displays the experimental absorption spectra, both in toluene solutions and in thin films of the three polymers. In solution, the trends are the same as those obtained with TDDFT computations: a bathochromic shift is seen from P2 (λ_{max}=447 nm) to P1 (λ_{max}=471 nm) to P3 (λ_{max}=508 nm). The same variation is observed for solution fluorescence (Figure 5a), where fine structural emission bands are observed, and are red-shifted from P2 to P1 to P3. This bathochromic shift can be explained by electronic and geometric effects. For the geometric influence, the polymer with the higher degree of curvature, or the stronger conformational energy, has the shorter overall conjugation length, and hence the larger optical gap.[150] The electronic effect will be probed by electrochemistry experiments in the subsequent section.

In films, all polymers aggregate and the resulting absorption spectra show broader and more red-shifted bands as compared to solution.[151] The spectral differences while evaluating the three polymers is more delicate, with P2 still having the shortest maximum wavelength, and P1 and P3 maxima being close. Interestingly, a fine structural absorption band can be seen for P3, which is likely due to fine-structure building in this polymer.[151]

These polymers were highly fluorescent under UV-light, so quantum yields were taken in solution with rhodamine B as the actionometer. The fluorescence maxima wavelengths are summarized in Table 8, and the average quantum yields are 0.26 for P1, 0.20 for P2 and 0.35 for P3. These values are similar to those obtained for P_3HT polymer in solution.[152] Thin films of polymers show weak fluorescence, and were not quantified.

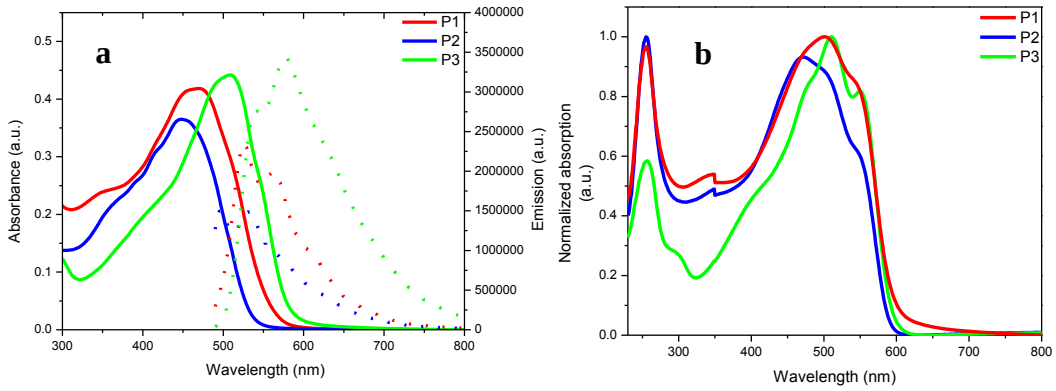

Figure 29: Absorption and emission Spectra of polymers P1, P2 and P3, (a) in toluene solution and (b) drop-cast as films.

3.2.3.3. Redox Properties

Thin films of polymers were drop-cast onto a platinum button electrode from toluene solutions, and electrochemically cycled in a 0.1M $TBAPF_6$ in acetonitrile until stable and reproducible voltammograms were obtained. CV and DPV are presented in Figure 30. The onsets of oxidation for the polymers in DPV are of 0.30 V for P1, 0.48 V for P2 and 0.42 V for P3 *vs.* Fc/Fc^+. The stabilization of P2 and P3 on oxidation may be due to the oxygen atoms: the delocalization of electrons goes through the oxygen atoms for P2 and P3, whereas for P1 the delocalization does not pass by the oxygen atoms. The resulting HOMO/ LUMO values for the polymers, based on DPV, are P1: -5.42 eV / -3.02 eV, P2: -5.60 eV/ -3.06 eV, and P3: -5.54 eV / -3.12 eV. The LUMOs for all three polymers vary within 0.1 V, and for the HOMO, there is a greater voltage difference: from 0.1 to 0.2 V, which is the opposite of the trend observed by computations. It is likely that the morphology of the polymers in thin films is responsible for this difference.

It is interesting to note that the band gap values obtained by electrochemistry share the same trend as the optical band gap obtained by UV-visible spectroscopy (Table 6). The

difference between the electrochemical band gaps and optical band gaps can be explained by a difference in morphology (films in electrolytes to polymers dissolved in solution are compared), as well as by a difference in electronics: in electrochemistry, the actual removal or addition of an electron is probed, whereas in spectroscopy, an electron is excited from the ground state to the excited state.[153]

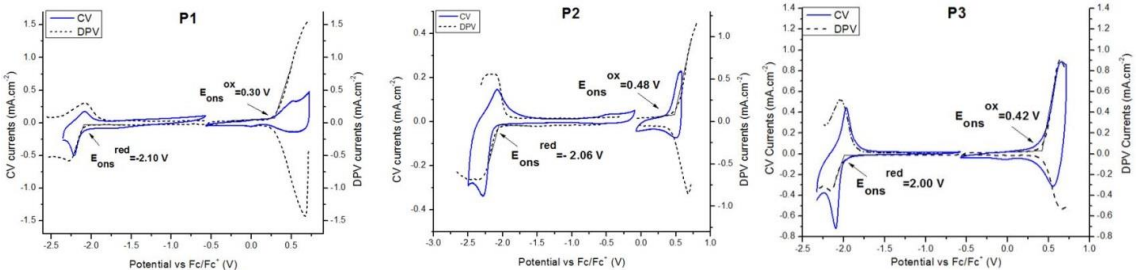

Figure 30: CV and DPV of P1, P2 and P3 films on Pt-button electrode, recorded at 100 mV/s scan rate in a 0.1 M $TBAPF_6$ ACN solution.

Table 8: Photophysical and electrochemical data for P1, P2 and P3.

						electrochemistry[c]				
	UV-vis-NIR			Fluorescence		CV		DPV		
	λ_{max} [a] (nm)	λ_{max} [b] (nm)	E_{gap}^{opt} (eV)	λ_{max} [a] (nm)	quantum yields[d]	$E_{1/2}^{ox}$ (V)	$E_{1/2}^{red}$ (V)	E_{on}^{ox}(V)/ HOMO(eV)	E_{on}^{red}(V)/ LUMO(eV)	Egap (eV)
P1	471	501	2.06	527	0.26	0.47	-2.15	0.30/-5.42	-2.10/-3.02	2.40
P2	447	471	2.10	497	0.20	0.53	-2.19	0.48/-5.60	-2.06/-3.06	2.54
P3	508	511	2.06	541	0.35	0.59	-2.03	0.42/-5.54	-2.00/-3.12	2.42

[a]In toluene solution. [b]Recorded for thin film sprayed on glass slide. [c]Recorded for thin films drop-casted from chloroform onto Pt button electrodes. [d]Recorded in toluene solution with Rhodamin B as the actionometer.

3.2.4 Spectroelectrochemistry and Colorimetry of the Polymers

3.2.3.1 Spectroelectrochemistry

Thin films of the polymer were spray-cast onto phosphonic acid-treated ITO, from 5 $mg.mL^{-1}$ toluene solution and subjected to spectroelectrochemical analysis. Figure 31

shows the spectroelectrochemical response in terms of absorbance as a function of the applied potential. All three spectra show sharp absorption bands in the neutral state. For P1 and P3, the absorption peaks decrease in intensity from the pristine state to the first applied potential (-0.5 V), denoting a change of absorption when placing the film in the electrolyte solution. For all three polymers, upon oxidation, the intensity of absorption in the visible spectrum is reduced, while the absorption in the NIR increases. This indicates the creation of lower energy polaron and bipolaron charge carriers at the expense of the π to π* transition. Interestingly, if the potential is not kept applied, all polymers return to their colorful (electronically neutral) state, ranging from a second to minute timescale.

We do not observe the depletion of the polaronic absorption with a concurrent increase of the bipolaronic absorption, meaning that the polymers are not fully oxidized at 0.8 to 1 V. However, an increase in voltage makes the films unstable and non-reversible. Moreover, the optical change decreases monotonically for P1 and P2, but irregularly in P3. We speculate that this irregularity is due to the morphology of the P3 chains, which can less easily accommodate the "twistons" that are formed, due to its more rigid structure.[154]

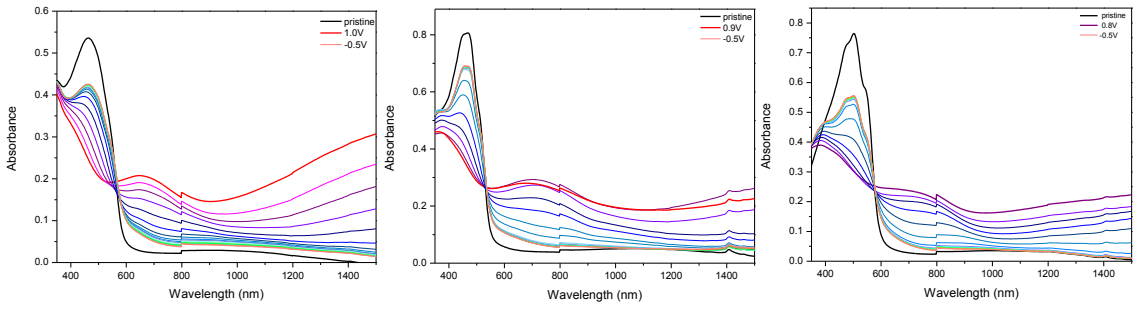

Figure 31: Spectroelectrochemical analysis of P1 (left), P2 (middle) and P3 (right). The voltage increases by 100 mV from the two boundaries voltages displayed in the legend. A thin film was spray-cast from a 5 mg·mL^{-1} solution in toluene, and electrochemical oxidation was carried out in 0.1 M $TBAPF_6$/PC solution, using Ag/Ag^+ reference electrode and a Pt wire counter electrode. The applied potential was increase in 100mV steps from -500 mV to 900 mV vs Fc/Fc^+.

3.2.3.2 Colorimetry and Photography

In order to evaluate the colors of the polymers films as the human eye perceive them, the L*a*b* color coordinates for polymer films were measured as a function of different electrochemical doping. The a* and b* values for each voltage steps are shown in Figure 32, and the neutral and fully oxidized states as displayed in the insets. Here we notice as well the difference between the pristine state and films at -0.5 V, a change that decreases the saturation of the color. As seen in the photograph, each polymer has a different shade of orange-red. P2 appears have a greater yellow component; P1 has similar positive values of a* and b*, so it looks orange; while P3, with a greater a* value, is redder. At intermediate doping levels, the polaronic transitions for P1 and P2 result in negative a* values. At full stable oxidation, the a* values are near zero while the b* values stay negative, hence the faintly green residual color visible in the photograph for P1 and P2. For P3, the polymer does not reach its full oxidation, hence switching from a coquelicot color to a pale orange-brown state, as seen in the photograph.

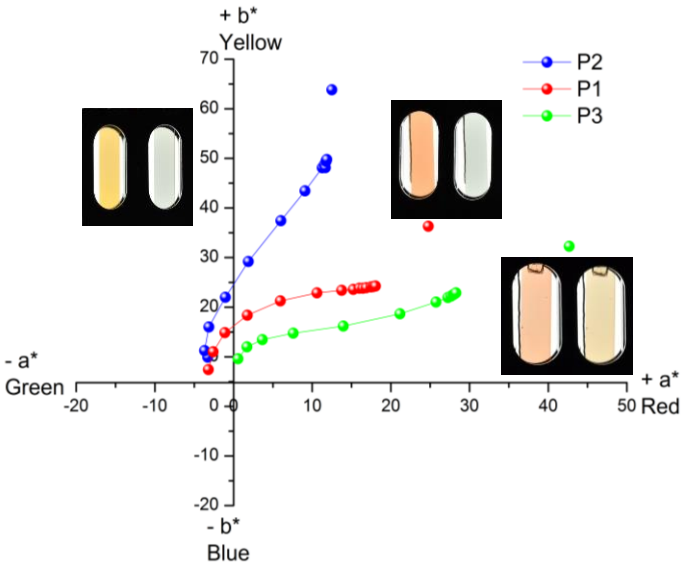

Figure 32: Colorimetric a*b* (CIE 1976 L*a*b*) color coordinates of thin films of P1, P2 and P3, taken as a function of level of electrochemical oxidation (-500 to 800 mV *vs.*

Fc/Fc^+, 100 mV steps), with inset photographs of the three films studied in their neutral (-500 mV) and oxidized (800 mV) states.

In conclusion, we have achieved in this study the synthesis of three isomeric units of benzodithiophene as well as their co-polymerization by conventional and microwave heating. The spectroscopic studies reveal a change of properties as a function of the isomer. Computational and electrochemical analyses prove that this difference is due to a combination of geometric and electronic parameters. Geometrically, the bathochromic shift in solution from P2 to P1 to P3 is related to the degree of curvature of the polymers. Electronically, the involvement of the oxygen atoms influence the oxidation potential, hence the band gap. For all three polymers, the spectroelectrochemical studies show a similar profile with the disappearance of the visible absorption spectra upon oxidation, and the building of polaronic and bipolaronic peaks. Macroscopically, we observe for P1 and P2 a clear color change from orange to color-neutral when increasing the applied potential. For P3, the color change goes from red to brown, suggesting that the full oxidation level is not reached, or the morphology of the polymer is not able to delocalize the polarons as well as in the two other isomeric polymers. This study investigates a complete spectroscopic structure:property relationship, and highlights that employing isomeric polymers can be useful for macroscopically fine-tuning the colors of the overall materials.

3.3 Experimental Details

1,2-di(thiophen-3-yl)ethane-1,2-dione. A solution of 3-lithiumthiophene, labeled as Solution A, was prepared as follows: 100 mL of 2.5 molar *n*-butyllithium (0.250 mol) in hexanes was added *via* cannula to 250 mL of anhydrous THF, previously cooled to -78

°C. The mixture was stirred for 10 minutes, and then 23.4 mL of 3-bromothiophene (40.76 g, 0.250 mol) was added dropwise. The mixture was stirred for ~150 minutes, keeping the temperature at -78 °C. Meanwhile, a solution, labeled as Solution B, was prepared as follows: In a 3000-mL round bottom flask (equipped with stir bar and a septum), containing 1750 mL of anhydrous THF, was added LiBr (21.7 g, 0.250 mol, 1 equiv.) and CuBr (35.9 g, 0.250 mol, 1 equiv.), the CuBr and LiBr mixture was stirred until all the salts dissolved, then this mixture was cooled to -40 °C or to lower temperatures. Solution C: 9.66 mL of oxalyl chloride (14.3 g, 0.113 mol, 0.45 equiv.) was dissolved in 250 mL of anhydrous THF in a 500-mL round bottom flask (previously equipped with a septum) and cooled to -40 °C or to lower temperatures. Solution A was added *via* cannula to Solution B, and the mixture was strongly stirred for ~5 minutes; then the Solution C was slowly added *via* cannula. The mixture was kept in the cold bath for 2 hours, allowed to warm up to room temperature, and quenched with 100 mL of saturated NH_4Cl(aq). THF was removed by rotary evaporation, and ~400 mL of ethyl acetate was added to the resulting mixture, which was then transferred to a separatory funnel and washed with saturated NH_4Cl(aq.) (3x, 150 mL), water (2x, 100 mL), and brine (1x, 100mL). Hexanes (300 mL) was added to the organic mixture, and the mixture was dried with Na_2SO_4, and then filtered through a short path of silica (the silica was flushed with hexanes:diethyl ether 1:1 to recover the entire product). The organic solvents were completely removed by rotary evaporation, and then the resulting yellow solid was strongly stirred in ~80 mL of a mixture 1:10 of diethyl ether:pentane (or 1:10 diethyl ether:hexanes), until all the solid chunks turned into a small powder. The resulting fine solid was filtered in a Buchner funnel, washed with cold pentane, and then

air-dried. The organic solvent of the remaining filtrate was removed by rotary evaporation and the procedure (diethyl ether:pentane treatment) was repeated with the resulting solid, but using smaller amounts of the solvent mixture (this procedure was repeated three times total). The resulting solids were collected and subjected to vacuum to remove solvent traces. Alternatively, the crude solid can be purified by column chromatography (silica, and 1:3 of diethyl ether:hexanes). A pale yellow solid was isolated, 21.022 g, 84.1%yield. ^{1}H NMR (500 MHz, CD_2Cl_2): δ_H 8.43 – 8.30 (m, 2H), 7.78 – 7.66 (m, 2H), 7.48 – 7.35 (m, 2H). ^{13}C NMR (125 MHz, CD_2Cl_2): δ_C 185.9, 137.8, 137.6, 127.7, 127.1. HRMS (ESI-TOF,$[M+Na]^+$) *m/z* calcd. for $C_{10}H_6O_2S_2$ 244.9701, found 244.9696.

Benzo[1,2-b:6,5-b']dithiophene-4,5-dione (BDTD). To a 500-mL Erlenmeyer flask, equipped with a stir bar and an inlet adapter and containing 250 mL of DCM, was added anhydrous $FeCl_3$ (19.5 g, 120 mmol, 3 equiv). The mixture was stirred for a few seconds, and then the diketone **2** (8.89 g, 40 mmol, 1 equiv.) was added in one portion. A silicon-oil bubbler was connected to the inlet adapter, and the reaction mixture was stirred for 2 h at room temperature. The mixture was quenched with ~100 mL of chilled water and stirred for 5 minutes more. Afterwards, DCM was removed by rotary evaporation. The resulting solid was filtered and washed with plenty of deionized water and stirred in 200 mL of water until a fine powder was formed. The solution was then filtered and washed again with plenty of water. The resulting solid was air-dried for 10 minutes, washed with 200 mL of diethyl ether and dried under vacuum. The resulting solid can be recrystallized from acetonitrile or an extra purification can be carried out as follows: the black solid was added to ~200 mL of DCM, stirred for 10 minutes, and then 100 mL of

silica was added. The mixture was stirred until the solid was dispersed on the silica, and then the entire mixture was transferred to a chromatographic column containing a short path of silica. The column was then flushed with a mixture of diethyl ether:DCM [1:3] until all the black-purple solid was recovered; the solvent can be roto-evaporated and recycled into the column, a green stain remains on the silica after the product was recovered. After removal of the organic solvent, the resulting solid was stirred in hot ether for 15 minutes, vacuum-filtered, and then air-dried. The resulting black solid was dried under vacuum, 8.63 g, 97.8% yield. ^{1}H NMR (500 MHz, CD_2Cl_2, 38 °C): δ_H 7.47 (d, 2H, J = 5.2 Hz), 7.26 (d, 2H, J = 5.2 Hz). ^{13}C NMR (125 MHz, CD_2Cl_2, 38 °C): δ_C 175.3, 144.5, 135.9, 128.1, 126.5. HRMS (DART, $[M+H]^+$) *m/z* calcd. for $C_{10}H_4S_2O_2$ 220.9726, found 220.9726.UV-Vis: λ/nm(ε): 271 (15006), 280 (13540), 320 (6733), 488 (2134), 526 (1842).

Benzo[1,2-b:6,5-b']dithiophene-4,5-dione dioxime. To a 25-mL round-bottom flask, containing a stir bar, and under argon atmosphere, was added BDTD (0.1 g, 0.45 mmol, 1 equiv), hydroxylamine hydrochloride (0.079 g, 1.14 mmol, 2.5 equiv), and 10 mL of 200-proof ethanol. The flask was equipped with a condenser and the mixture was warmed to reflux (75 – 80 °C), and stirred for 24 hours. The ethanol was removed by rotary evaporation, and the resulting solid was purified by column chromatography (silica, ethyl ether:hexanes, gradient 1:2 to 1:0) to yield a bright orange solid, 0.084 g (74%). ^{1}H NMR (500 MHz, DMSO-d_6): δ_H 14.71 (s, 0.6H), 13.07 (s, 0.6H), 12.36 (s, 0.9H) , 8.20 (d, 0.7H, J = 5.2 Hz), 8.03 (d, 1H, J = 5.2 Hz), 7.62 (dd, 1.3H, J = 5.3 Hz, J = 9.2 Hz), 7.55 (d, 1H, J = 5.2 Hz), 7.49 (d, 0.7H, J = 5.2 Hz). ^{13}C NMR (125 MHz, DMSO-d_6): δ_C

134.6, 130.4, 130.1, 127.3, 126.4, 124.0, 123.9. HRMS (ESI, $[M-H]^-$) *m/z* calcd. For $C_{10}H_6N_2O_2S_2$ 248.9798 , found 248.9805.

Benzo[1,2-b:6,5-b']dithiophene-4,5-diamine. To a 250-mL round-bottom flask, containing a stir bar, and under argon atmosphere, was added BDTD (2 g, 9.1 mmol, 1 equiv), hydroxylamine hydrochloride (1.6 g, 2.5 equiv), and 100 mL of 200-proof ethanol. The flask was equipped with a condenser and the mixture was warmed to reflux (75 – 80 °C), and stirred for 20 hours. The reaction mixture was cooled to room temperature, and 200 mg of 10% of Pd on activated carbon (Pd/C) was added. An addition funnel containing a solution of hydrazine monohydrate (15 mL of $N_2H_4 \cdot H_2O$ in 25 mL of EtOH) was placed on top of the condenser. The reaction mixture was warmed up to 65 °C, and then the hydrazine solution was added dropwise for ~1h. The reaction temperature was increased to 85 °C, and then the mixture was stirred for 48 hours. The mixture was allowed to cool to ~60 °C and filtered (by gravity filtration, and the filter was washed with ethanol to recover the entire product). The solvent was removed by rotary evaporation, and the resulting solid was dispersed in water, filtered, washed with plenty water and cold ethanol. The resulting yellow solid was air-dried for 1 minute, placed under vacuum and stored cold and under argon. In the event that the product had dissolved when washing with ethanol, it was recovered by removing the organic solvent from the filtrate and by repeating the filtration procedure. A bright yellow solid was isolated, 1.409 g, 70% yield. ^{1}H NMR (300 MHz, CD_2Cl_2): δ_H 7.35 (q, 4H, J = 5.5 Hz), 3.85 – 3.52 (s, br, 4H). ^{13}C NMR (75 MHz, $CDCl_3$): δ_C 130.8, 125.9, 125.6, 124.1, 120.9. HRMS (APCI, $[M+H^+]$) *m/z* calcd. for $C_{10}H_8N_2S_2$ 221.0202, found 221.0200.

Dithieno[3',2':3,4;2'',3'':5,6]benzo[1,2-c][1,2,5]thiadiazole. To a 25-mL round-bottom flask, equipped with a stir bar, a septum and a bubbler, and containing argon atmosphere, was added DMF (2 mL) and sulfur monochloride (0.6 mL, 0.98 g, 7.3 mmol, 4 equiv). The flask was cooled to 0 °C, then the mixture was stirred, and benzo[1,2-b:6,5-b']dithiophene-4,5-diamine (previously dissolved in 2 mL of anhydrous DMF) was added dropwise *via* syringe. The mixture was allowed to warm to room temperature and stirred for 2 hours. The reaction mixture was quenched with 15 mL of water, stirred for 5 minutes, vacuum-filtered, and air-dried for 5 minutes. The resulting sticky solid was extracted with dichloromethane (DCM) by grinding it with a spatula. The resulting DCM solution was filtered to remove sulfur byproduct. Then silica (~40 mL) was added to the DCM solution, and then the DCM was removed by rotary evaporation. The resulting silica was transferred to a filtration funnel (vacuum) containing a short path of silica, then sand was placed on top of the silica. The silica was flushed with hot hexanes (~250 mL). TLC was taken frequently from the hexanes fractions to confirm that all the sulfur byproduct had been eluted, and then a new filtration flask was placed under the funnel. The silica was flushed with a mixture 2:1 DCM:hexanes until all the yellow product had come out. The solvent was removed by rotary evaporation and the resulting solid was recrystallized from hot ethanol (~50 mL). The fine yellow needles were collected by filtration, washed with ethanol, air-dried, and put under vacuum, 0.370g, 82% yield. ^{1}H NMR (500 MHz, $CDCl_3$): δ_H 8.00 (d, 2H, J = 5.3 Hz), 7.51 (d, 2H, J = 5.3 Hz). ^{13}C NMR (125 MHz, $CDCl_3$): δ_C 150.8, 135.8, 129.3, 125.3, 124.4. HRMS (APCI, $[M+H]^+$) *m/z* calcd. for $C_{10}H_4N_2S_3$ 248.9609, found 248.9616.

2H-dithieno[3',2':3,4;2'',3'':5,6]benzo[1,2-d][1,2,3]triazole. Benzo[1,2-b:6,5-b']dithiophene-4,5-diamine (0.22g, 1 mmol, 1 equiv) was dissolved in 16 mL of glacial acetic acid, and cooled to 15 °C. A solution of $NaNO_2$ (0.21 g, 3 mmol, 3 equiv) in 6 mL of water was added dropwise, and then the mixture was stirred for 10 minutes. The resulting solid was filtered, washed with water, and air dried; 0.17 g of a yellow solid was obtained, 75% yield. ^{1}H NMR (500 MHz, DMSO, 90 °C): δ_H 16.4 – 15.8 (br, 1H), 7.97 (d, 2H, J = 5.3 Hz), 7.91 (d, 2H, J = 5.3 Hz). ^{13}C NMR (125 MHz, DMSO, 120 °C): δ_C 130.7, 125.9, 125.6, 121.4, 121.2. HRMS (APCI, $[M+H]^+$) *m/z* calcd. for $C_{10}H_5N_3S_2$ 231.9998, found 232.0003.UV-VIS: λ/nm(ε): 248 (11044), 268 (7056), 304 (12379), 312 (11013), 327 (6840), 408 (1629).

Tetrathieno[3,2-a:2',3'-c:3'',2''-h:2''',3'''-j]phenazine. To a 125 mL round bottom flask was added BDTD (0.21 g, 0.9 mmol, 1 equiv), Benzo[1,2-b:6,5-b']dithiophene-4,5-diamine (0.21 g, 0.9 mmol, 1 equiv), 60 mL of 200 proof ethanol and 1 ml of acetic acid. The mixture was refluxed for 2 hours. After cooling to room temperature, the resulting solids were filtrated, washed with ethanol and air dried. 0.325 g (88%) of a green solid was obtained. ^{1}H NMR ($CDCl_3$, TFA): δ_H 8.70 (d, 4H, J = 5.4 Hz), 7.84 (d, 4H, J = 5.6 Hz). ^{13}C NMR ($CDCl_3$, CF_3COOH): δ_C 124.40, 124.19, 123.47, 104.99. HRMS (EI, $[M+H]^+$) *m/z* calcd for $C_{20}H_8N_2S_4$: 404.9643, found 404.9660 UV-VIS: λ/nm(ε): 262 (18038), 269 (18484), 304 (26180), 312 (24834), 413 (8967), 440 (10464).

Benzo[1,2-b:6,5-b']dithiophene-4,5-diyl diacetate. To a 500-mL round bottom flask equipped with a stir bar was added BDTD (1.82g, 8.27 mmoles, 1 equiv), zinc powder (5.4 g, 82.7 mmol, 10 equiv) and 50 mL of dichloromethane. Acetic anhydride (7.8 mL, 82.7 mmol, 10 equiv) and triethylamine (17.3 mL, 12.4 mmol, 15 equiv) were added

quickly. The mixture was stirred overnight at room temperature. The solution was filtered through celite, and extracted successively with water, 1M HCl solution, water, $NaHCO_3$ saturated and water. The organic phase was dried with magnesium sulfate and the solution was concentrated under vacuum; 2.3 (91%) of white solid was obtained. ^1H NMR (300 MHz, CD_2Cl_2): δ_H 7.51 (d, 2H, J = 5.3 Hz), 7.32 (d, 2H J = 5.5 Hz), 2.41(s, 6H). ^{13}C NMR (75 MHz, $CDCl_3$): δ_C 20.46, 121.15, 125.89, 131.77, 134.29, 168.16. HRMS (EI, $[M+Na]^+$) *m/z* calcd for $C_{14}H_{10}O_4S_2$ 328.9913, found 328.9923.

4,5-bis(octyloxy)benzo[1,2-b:6,5-b']dithiophene To a 10- mL round bottom flask equipped with a stir bar was added the previous compound, (0.463 g, 1.37mmol, 1 equiv), cesium carbonate (2.42 g, 6.8 mmol, 5 equiv), octylbromide (1.20 mL, 6.8 mmol, 5 equiv) and 50 mL of acetonitrile. The mixture was refluxed for 3 days. After cooling to room temperature, acetonitrile was evaporated and the resulting paste was dilute in dichloromethane and extracted successively with a solution of 1 M HCl, brine (2x) and dried with magnesium sulfate. The solution was concentrated and purify by column chromatography using hexane as the eluent; 0.532 g (87%) of a colorless oil was obtained. ^1H NMR (300 MHz, $CDCl_3$): δ_H 7.53 (d, 2H, J = 5.3 Hz), 7.35 (d, 2H J = 5.3 Hz), 4.23 (t,4H, J = 6.5 Hz), 1.89 (q, 4 H, J = 6.5 Hz), 1.56 (q, 4 H, J = 8.2 Hz), 1. 33 (m, 16H), 0.94 (t, 6H, J = 6.5 Hz). ^{13}C NMR (75 MHz, $CDCl_3$): δ_C 14.37, 22.94, 26.47, 29.59, 29.75, 30.72, 32.12, 74.60, 122.26, 124.33, 129.40, 134.58, 143.68. HRMS (EI, $[M+H]^+$) *m/z c*alcd for $C_{28}H_{38}O_2S_2$ 447.2386, found 447.2385. UV-Vis: λ/nm(ε): 252 (25076), 255 (24963), 303 (12188), 314 (11686), 343 (3133).

Dithieno[3',2':3,4;2'',3'':5,6]benzo[1,2-c]furazan. To a 150-mL glass pressure vessel, equipped with a stir bar, was added the diketone BDTD (0.78g, 3.5 mmol, 1 equiv),

hydroxylamine hydrochloride (0.61g, 8.8 mmol, 2.5 equiv), and 70 mL of ethanol (200 proof). The vessel was equipped with its respective Teflon cap, and the mixture was stirred at 85 °C for 24 hours. The temperature was then increased to 140 °C, and the reaction mixture was stirred for 48 – 60 hours. The mixture was cooled to room temperature and transferred to a round bottom flask. The solvent was removed by rotary evaporation, and the resulting solid was washed with water. The solid was then purified by column chromatography (silica, 1:5 ethyl acetate:hexanes). The resulting solid was stirred in a mixture of hot diethyl ether:hexanes 1:1 for 10 minutes. The mixture was cooled to room temperature, filtered, washed with the ethyl ether:hexanes (1:1 mixture), and air-dried. The remaining filtrate was roto-evaporated, and the procedure was repeated with the remaining solid (two times). The solids were collected and dried under vacuum. A yellow solid was received, 0.49 g (60% yield). Alternatively, this compound can be made in a 100-mL round-bottom flask, equipped with a condenser, at 85°C for 10 days. ^{1}H NMR (300 MHz, $CDCl_3$): δ_H 7.91 (d, 2H, J = 5.3 Hz), 7.56 (d, 2H, J = 5.3 Hz). ^{13}C NMR (75 MHz, $CDCl_3$): δ_C 146.0, 137.3, 126.5, 124.3, 122.7. HRMS (EI, $[M]^+$) *m/z* calcd. for $C_{10}H_4N_2OS_2$ 231.9765, found 231.9762. UV-Vis: λ/nm(ε): 269 (21838), 287 (17653), 299 (19073), 312 (17560), 360 (11708).

General procedure for the Ring Opening.

Each reaction was done in duplicate, and the yields are the average yield obtained.

In a dry round bottom flask, 2,7-dibromobenzo[1,2-b:6,5-b']dithiophene-4,5-dione (1 equiv.), base (2.5 equiv.), dodecyl bromide (3 equiv.) and DMF (10 mL/mmol of reactant) were added. The reaction was stirred overnight, for 12 hours, with or without

heat. After cooling down, the mixture was extracted with ether, washed three times with brine, and the organic phase was dried with magnesium sulfate. The solution was concentrated under reduced pressure. The resulting oils were purified with a silica column, with hexanes as eluant. The first spot gave the compound 1, and the second spot, fluorescent, provided the compound 2. The fractions were concentrated under reduced pressure.

Compound 3.13. ^{1}H NMR (300 MHz, $CDCl_3$): δ_H 7.44 (2H, s), 4.11 (4H, t, J=6.5), 1.80 (4H, q, J=7 Hz), 1.49 (4H, br), 1.27 (32 H, br) 0.88 (6H, t, J=7 Hz). ^{13}C NMR (75 MHz, $CDCl_3$): δ_C : 142.76, 134.13, 128.98, 124.65, 112.79, 74.39, 31.92, 30.32, 29.69, 29.65, 29.63, 29.46, 29.37, 26.08, 22.69, 14.12. HRMS (APCI) Calculated for $C_{34}H_{52}Br_2O_2S_2$ [$M+H^+$]: 717.1833, found m/z: 717.1841.

Compound 3.14. ^{1}H NMR (300 MHz, $CDCl_3$): δ_H 7.48 (2H, s), 4.10 (4H, t, J=6.5), 1.50 (4H, t, J=7 Hz), 1.26 (36H, br), 0.88 (6H, t, J=7 Hz). ^{13}C NMR (75 MHz, $CDCl_3$): δ_C 161.30, 139.39, 132.71, 131.89, 113.23, 62.25, 31.92, 29.66, 29.64, 29.54, 29.36, 29.30, 28.45, 25.97, 22.69, 14.13. HRMS (APCI) Calculated for $C_{35}H_{52}Br_2O_4S_2$ [$M+H^+$]: 749.1732, found m/z: 749.1744.

Procedure for Stille Polymerization for BDT-Th and ThTh-Th

To an oven-dried microwave vial (12 mL) equipped with a stir bar, the dibromoderivative (1 equiv.) (compound **1** or **2**, 1 equiv.), 2,5-bis(trimethylstannyl)thiophene (1 equiv.) tris(dibenzylideneacetone) dipalladium(0) catalyst (4% equiv.) and tri(o-tolyl)phosphine ligand (12% equiv.) and dried, undegassed toluene (8 mL) were added. The reaction was placed in the microwave, at 150 ^{o}C for 10 hours. After allowing to cool to room

temperature, the mixture was precipitated into methanol, and stir for 15 min. The solids were filtered and washed with plenty of methanol. The solids were submitted to Soxhlet extraction, successively with methanol, hexanes and dichloromethane. The methanol and hexanes yields little to no solids. The DCM fraction was concentrated under reduced pressure, diluted with a minimal amount of dichloromethane, and precipitated into methanol. All characterizations were done for the polymers from the dichloromethane fraction.

Poly (didodecyl [2,2':5',2''-terthiophene]-3,3'-dicarboxylate) ThTh-Th Orange solids. 73% yield ^{1}H NMR (300 MHz, $CDCl_3$): δ_H 7.62 (2H, s), 7.15 (2H, s), 4.13 (4H, t, J=6 Hz), 1.20 (40H, br), 0.86 (6H, t, J= 6.2 Hz).

Procedure for Suzuki Polymerization for BDT-Ph and ThTh-Ph

The solvents were freeze-pump-thaw three times. Compound **1** or **2** (1 equiv.), 1,4-bis(5,5-dimethyl-1,3,2-dioxaborinan-2-yl)benzene (1 eq.), cesium fluoride (6 eq.), tris(dibenzylideneacetone) dipalladium(0) catalyst (2% equiv.) and tri(t-butyl)phosphonium tetrafluoroborate (6% equiv.) were added to a 10 mL schlenk tube. The flask was purged with argon four times. To this flask, 3 mL of THF and 1 mL of water were added (12 mL per mmol of monomer). The reaction refluxed for 2 days. The polymer solution was precipitated into methanol and submitted to soxhlet extraction with methanol, hexanes and dichloromethane, successively. The methanol and hexanes yields little to no solids. The DCM fraction was concentrated under reduced pressure, diluted with a minimal amount of dichloromethane, and precipitated into methanol. All characterizations were done for the polymers from the dichloromethane fraction.

Poly (didodecyl 5-phenyl-[2,2'-bithiophene]-3,3'-dicarboxylate) ThTh-Ph

^{1}H NMR (300 MHz, $CDCl_3$): δ_H : 7.81 (2H, s), 7.67 (4H, s), 4.13 (4H,t, J=5.8 Hz), 1.22 (40H, br), 0.86 (6H, t, J= 6.5 Hz).

Procedure for polymerization via conventional heating for isomeric polymers P1, P2 and P3.

Solvents were degassed via the freeze-pump-thaw method 4 times prior to reaction. (E)-1,2-bis(tributylstannyl)ethane (1 equiv.), dibromobenzodithiophene-dione monomer (1 equiv.), P(*o*-tol)$_3$ (0.03 equiv.), and Pd_2dba_3 (0.01 equiv.) were added to a previously dried Schenk tube. The mixture was placed under vacuum for 2 hours, was backfilled with argon gas, and the vacuum-purge cycle was repeated three times. Toluene (quantity adjusted to have a 0.04M per monomer) was then added, and the mixture was stirred at 90°C for 4 days. The reaction was cooled down to room temperature, and the mixture was drop-wisely precipitated into methanol. The mixture was filtered into a 25X80mm cellulose thimble and washed 3times with methanol (30 mL). The resulting solids were purified by soxhlet extractions: methanol (one day), hexanes (one day), and toluene (one day). The toluene fraction was concentrated in vacuuo, and precipitated into methanol. The resulting precipitate was filtered on a nylon filter membrane, and the polymer was collected and dried under high vacuum.

General procedure for polymerization via microwave heating for isomeric polymers

(*E*)-1,2-bis(tributylstannyl)ethane (1 equiv.), dibromobenzodithiophene-dione monomer (1 equiv.), P(*o*-tol)$_3$ (0.03 equiv.), Pd_2dba_3 (0.01 equiv.) and toluene (quantity adjusted to have a 0.04M per monomer) were added to a microwave vessel. The vessel was placed in the microwave for 3 hours at 160^{o}C. The mixture was allowed to cool to room

temperature and precipitated into methanol. After that, the same work-up was done as for the conventionally heated polymer.

CHAPTER 4.

QUADRUPOLAR (DONOR)$_2$-ACCEPTOR ACID CHROMOPHORES FOR DSSCS: INFLUENCE OF THE ACCEPTOR CORE.

4.1 Design rationale of (Donor)$_2$-Acceptor Sensitizers and Preliminary Study

4.1.1 Design Rationale

As described in Chapter 1, dye-sensitized solar cells (DSSCs) are photovoltaic devices that have been found to be highly efficient for solar conversion.[155,156] Dyes originally consisted of compounds containing metal coordination complexes, mainly based on ruthenium.[43,156] While these dyes are efficient, they have a limited absorption in the long wavelength region of the visible spectrum, can be difficult to purify and can have limited tunability.[49] To resolve these issues, organic dyes have been designed and are showing efficiency comparable to inorganic dyes.[48,49,157] In addition, both types of dyes can also be used together as co-sensitizers to generate high efficiency devices, up to 12.3 %.[54]

Most organic dyes tend to follow the same D-π-A architecture, where the donor (D) acts as a chromophore and is linked to the metal oxide bound acceptor (A) via a π-conjugated bridge (π).[47] While many of the studies focus on varying the nature of the sensitizer to enhance the efficiency of the devices, others vary the arrangement of the architecture. For instance, Fischer *et al*[158] reported on D-π-A dyes where the π bridge is composed of linear or branched oligothiophenes. They found a difference in performance depending on the configuration of the dye: the linear oligothiophenes are more efficient than the branched, due to an increase of dye loading on the TiO_2 surface. However, the branched oligothiophenes were more stable over time, making these dyes more interesting overall.

This report suggests that isomerism is a parameter to consider while designing dyes. Another interesting approach, described by Ning *et al*[73] employed starbust shaped dyes, a DD-π-A structure. They describe that adding donors on both sides of the π-A synthon permits the absorption of less energetic photons, but fails to enhance the efficiency of the devices, because of the mismatched frontier orbital level or unfavorable absorption into TiO_2.

The first study on a quadrupolar D_2A sensitizer was reported by Patel *et al*.[159] The donor moieties were thiophene and the acceptor unit was benzo(triazole- thiadiazole) (BTzTD), a novel structural synthon allying both the strength of the 2,1,3-benzothiadiazole (BTD) unit and the alkylation moiety of the 2H-benzo[d]-[1,2,3]triazole (BTz). Unfortunately, the LUMO levels of the sensitizers and the level of the TiO_2 CB were comparable, and when employing these dyes in DSSC devices, the optimized IPCE and the J-V figures of merits were low. To improve this system, we developed D_2A systems where the acceptor unit (A) is an internally fused donor-acceptor molecule, as illustrated in Figure 33. Changing the core from a pure acceptor to a fused donor-acceptor system creates a conjugated donor system along the molecule (represented in blue in Figure 33) and keeps the LUMO level high enough for electron injection into TiO_2.

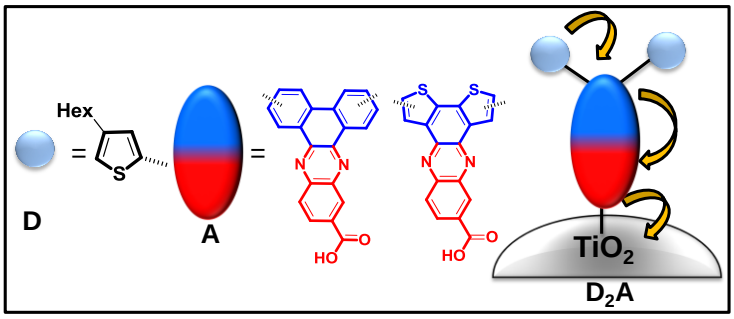

Figure 33: Representation of the donor unit (D) and acceptor core (A) illustrating the use of dithienophenazine (DTP) and dibenzophenazine (DBP) as internally fused donor-acceptor core molecules.

This chapter focuses on the conception and development of these quadrupolar dyes, and investigates the influence of the acceptor core as well as the effect of using structural isomers. Using a combination of computational, electrochemical, and spectroscopic methods, we prove that the optical and electronic properties vary with the nature of the core, and with the isomerism. Moreover, we evaluate the photophysical properties of the excited states. After integrating the sensitizers in DSSCs, we demonstrate that the dyes are successful in generating charge carriers. Most interestingly, the nature of the core affects the open circuit voltage while the isomerism seems to weakly affect the short circuit current density.

4.2.2 Model Systems

In a preliminary study, we synthesized three molecules based on dibenzo[a,c]phenazine-11-carboxylic acid (DBP*a*), dithieno[2,3-a:3',2'-c]phenazine-9-carboxylic acid (DTPl*a*) and dithieno[3,2-a:2',3'-c]phenazine-9-carboxylic acid (DTPb*a*) (Figure 34). The goal of this study is to briefly screen the cores, to ensure that their properties are suitable for use as sensitizers.

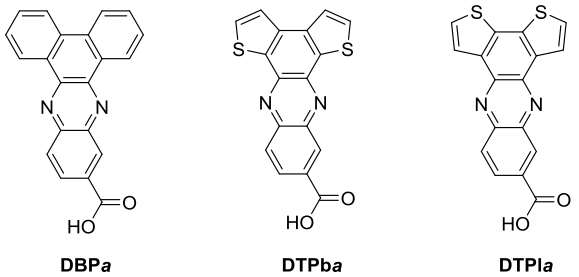

Figure 34: Structures of dibenzo[a,c]phenazine-11-carboxylic acid (**DBP*a***) and of the two isomers of dithieno[a-c]phenazine-9-carboxylic acid (**DTPb*a*** and **DTPl*a***).

The synthesis is a quantitative condensation between diaminobenzocarboxylic acid and the corresponding aryl-dione, as shown in Scheme 7.

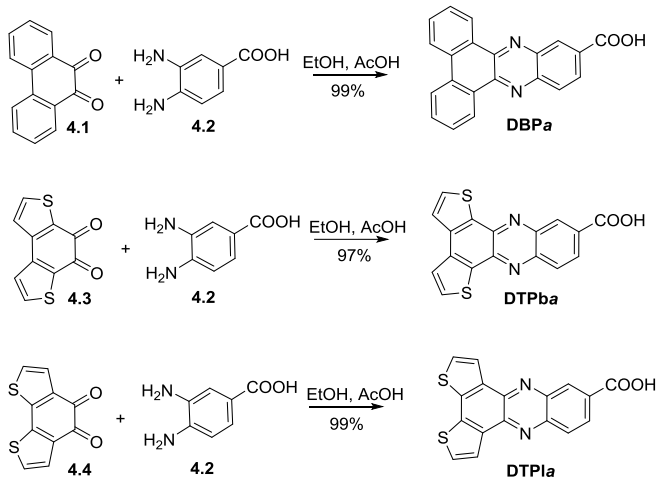

Scheme 7: Synthesis of dibenzo[a,c]phenazine-11-carboxylic acid and of the two isomers of dithieno[a-c]phenazine-9-carboxylic acid.

Diaminobenzocarboxylic acid is commercially available, and the corresponding aryl-diones were synthesized as described in the literature.[131,132,160] Purification was performed by removing the excess diaminobenzocarboxylic acid with ethanol washes. However, the products have limited solubility in common organic solvents. A study on similar compounds indicates that molecules with a phenazine carboxylic acid moiety can aggregate in a three centered H-bonding.[161] We speculate that the limited solubility observed for our compounds is due to this aggregation.

The UV-visible spectra for these compounds are presented in Figure 35. The absorption profiles are similar for DBP*a* and DTPl*a*, with maxima at 380 nm and 402 nm for DBP*a* and at 397 nm for DTPl*a*. DTPb*a* exhibits the most red-shifted transitions of the set of compounds, with two maxima absorption peaks of 409 nm and 433 nm. As the absorption of these molecules is below 450 nm, only photons with an energy greater than 2.8 eV will be absorbed, which will greatly limit the device efficiencies if these molecules were to be integrated into DSSCs. The electrochemistry (Figure 35, right) depicts one electron single reduction potential at -1.6 V for DBP*a* and DTPl*a* and -1.3 V for DTPb*a*.

Correspondingly, the LUMOs are at -3.52 eV for DBP*a* and DTPl*a* and at -3.82 eV for DTPb*a*, showing proper energies to fulfill the electron injection into the TiO_2 CB. Oxidations peaks were not observed in the electrochemical window of benzonitrile.

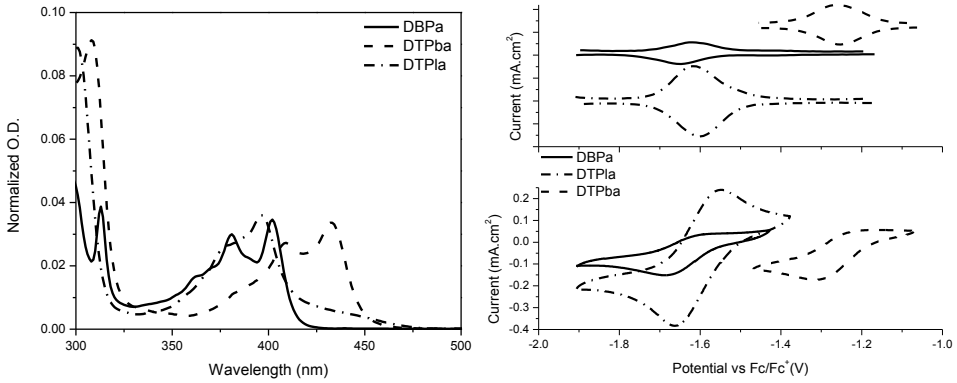

Figure 35: UV-visible absorption spectra (left) and electrochemistry voltamograms in benzonitrile solution (right) of dibenzo[a,c]phenazine-11-carboxylic acid DBP*a* (—) and of the two isomers of dithieno[a-c]phenazine-9-carboxylic acid DTPb*a* (----) and DTPl*a* (-·-·-·).

From this preliminary study on these three cores, we learned that:

- The different isomers of dithienophenazine lead to different opto-electronic properties: DTPb*a* has a deeper LUMO level and a red-shifted absorption compared to DTPl*a*.
- The LUMO energy levels of the compounds are appropriate for electron injection into the TiO_2 CB.
- The maxima of the light absorption are below 450 nm, and should be improved before integrating these compounds in devices.

To increase the range of photons absorbed, we chose to append donating moieties on each side of the fused donor-acceptor cores. The representation of this concept is depicted in Figure 36.

The external donors, grafted on different sites of the core, lead to positional isomeric dyes: linear (L) where the conjugation is along the donor moieties, and branched (B) where the conjugation extends all the way through the acceptor. The different conjugation modes are illustrated in red in Figure 36.

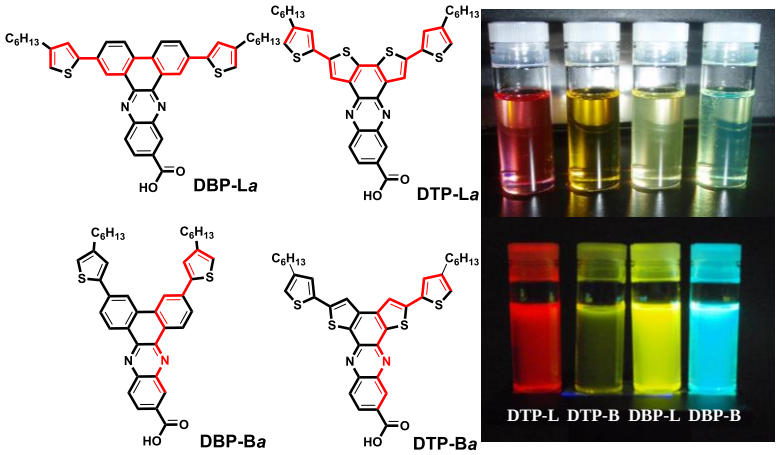

Figure 36: Molecular structures of DBP-L*a*, DBP-B, DTP-L*a*, and DTP-B*a* (left), with photography depicting solutions of the compounds (top right) and under UV-light irradiation (bottom right).

4.2. Direct Synthesis *vs*. Indirect Synthesis via Esterification

4.2.1 Direct Synthesis with Carboxylic Acids Groups

Synthesis of the sensitizers can be achieved in a few steps from starting materials. For the synthesis of the DBP series, as presented in Scheme 8, 2,7-dibromophenanthrene-9,10 dione or 3,6-dibromophenanthrene-9,10 dione were condensed with diaminobenzoic acid to afford the corresponding compounds in excellent yields (95-98%). These dibromo-intermediates were coupled with 4-hexyl-2-trimethylstannyl-thiophene via Stille coupling to afford DBP-L*a* and DBP-B*a* in moderate yields (56% and 54%, respectively).

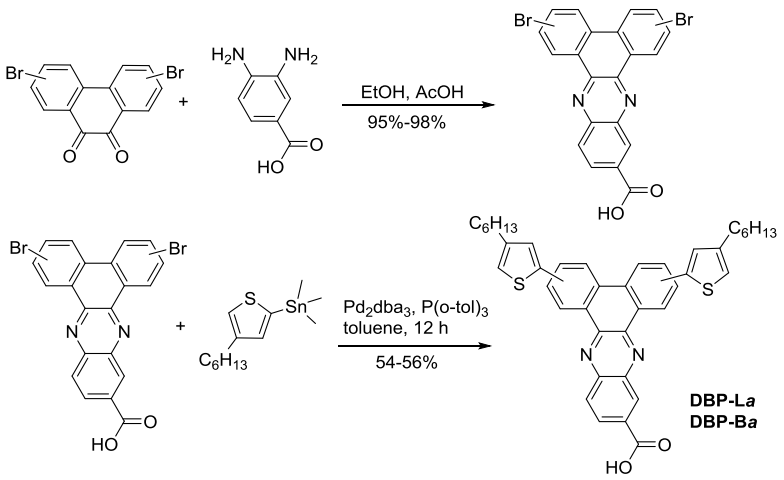

Scheme 8: Direct synthesis of DBP-L*a* and DBP-B*a*.

Unfortunately, all these targets have poor solubility in common organic solvents. Similarly to the preliminary studies, we conjecture that the molecules aggregate in a three centered H-bonding fashion. With the lack of solubility, these molecules are difficult to characterize and to purify. The molecules cannot be distilled (too high molecular weight), recrystallized (no good systems were found despite multiple attempts), or purified using traditional column chromatography techniques (the carboxylic acids remained at the baseline). Other techniques, such as precipitation using different solvents (methanol, acetone), and advanced column chromatography techniques (C-18 silica, alumina, triethylamine washed silica) were attempted and gave promising results. However, the lack of solubility was still a major problem.

4.2.2 Indirect Synthesis through Esterification

To prevent aggregation and to ease purification, the first reagent bearing a carboxylic acid group, 3,4-diaminobenzoic acid was esterified. The synthesis of several alkyl esters of diaminobenzoic acid was attempted: ethyl, butyl, octyl, and methyl. The most successful attempt was obtained with ethanol to produce the ethyl ester.[162] This "trick"

added two more steps: the esterification of the diaminobenzoic acid and the hydrolysis of the final target, and they are presented in Scheme 9, in blue boxes.

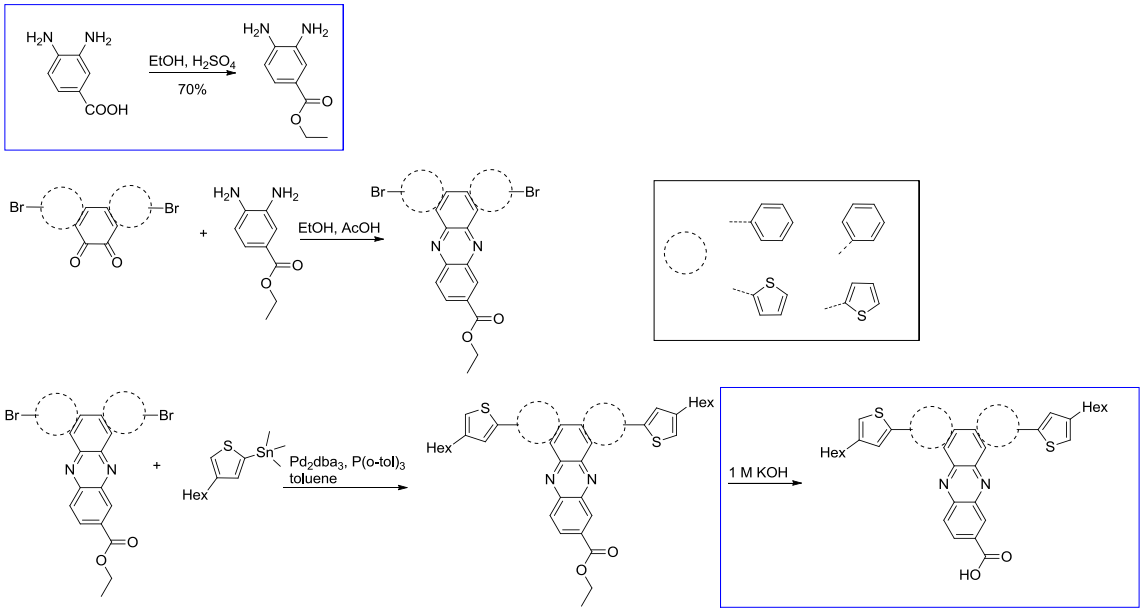

Scheme 9: Indirect synthesis for the D_2A sensitizers.

For the synthesis of DBP-L and DBP-B, 2,7-dibromophenanthrene-9,10 dione **4.5** (or 3,6-dibromophenanthrene-9,10 dione **4.8**) was condensed with ethyl 3,4-diaminobenzoate **4.6** to afford the corresponding compounds **4.7** and **4.9** (96% and 91%, respectively). These dibromo-derivatives were coupled with 4-hexyl-2-trimethylstannyl-thiophene via Stille coupling to afford DBP-L in moderate yields (41% and 66%, respectively). The cross-couplings were performed in 2 h in a microwave reactor. To enhance the purity of the compounds, columns were done *in duplicate*. As a result, some product was lost, explaining the moderate yields.

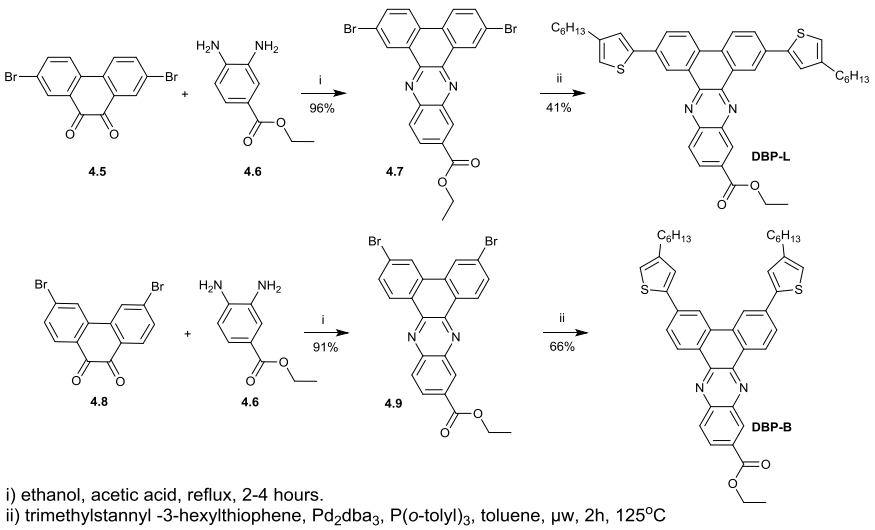

i) ethanol, acetic acid, reflux, 2-4 hours.
ii) trimethylstannyl -3-hexylthiophene, Pd_2dba_3, P(*o*-tolyl)$_3$, toluene, μw, 2h, 125^{o}C

Scheme 10: Synthetic routes to compounds DBP-L and DBP-B.

Similarly, the synthesis of DTP-L and DTP-B proceeded via a condensation of **4.10** or **4.12** with ethyl 3,4-diaminobenzoate **4.6** followed by Stille coupling with 4-hexyl-2-trimethylstannyl-thiophene (Scheme 11). The yields were moderate (95% and 98% respectively for the first step and 61% and 62% respectively for the second step). As previously, duplicate columns were run to ensure purity, leading to the moderate yields.

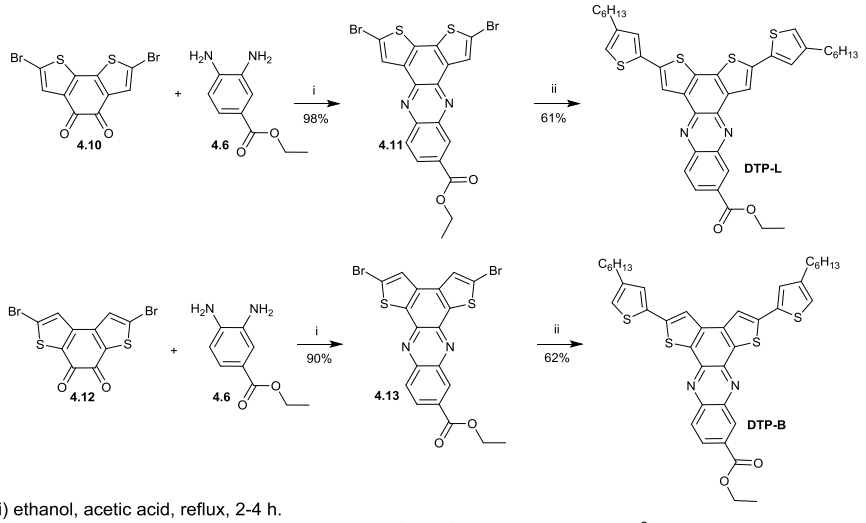

i) ethanol, acetic acid, reflux, 2-4 h.
ii) trimethylstannyl -3-hexylthiophene, Pd_2dba_3, P(o-tolyl)$_3$, toluene, μw, 2h, 125^{o}C

Scheme 11: Synthetic routes to compounds DTP-L, and DTP-B.

To yield the carboxylic acids, the esters were hydrolyzed using a 5M solution of KOH in water, at 150 ºC for 10 minutes, using microwave-assisted heating. The obtained dyes were pure, and did not need to be purified before adsorption onto TiO_2.

4.3 Ground State Characterizations

4.3.1 Density Functional Theory Computations

To gain preliminary insights into the geometrical and electronic properties of the DBP and DTP family of sensitizers, DFT calculations were carried out. As described in Chapter 2, section 2.1.3, hexyl substituents on the thiophene were omitted to simplify the calculations. Illustration of the frontier orbitals for compounds DBP-L, DBP-B, DTP-L and DTP-B are presented in Figure 37. For all compounds, the LUMO is a π^* orbital delocalized across the quinoxaline moiety and the calculated values are all above the experimental TiO_2 CB, predicting feasible electron injection. For the HOMOs, a minimal change in the structure produces a noticeable overall change: the wave function is delocalized along the thiophene donor framework for the linear isomers L and delocalized through the entire molecule for the branched isomers B.

When comparing the DBPs with the DTPs, the nature of the core does not influence the orbital density: both families have a similar electronic density centered on the acceptor core. For the HOMOs, more electron density is observed on the nitrogen of the core of DTP-L compared to DBP-L, but the electrons density is mainly delocalized on the donors. There is a greater difference when comparing DTP-B and DBP-B: for the thiophenes core, the electrons are unsymmetrically distributed along the molecules, and for DBP-B, a quinoidal-like delocalization is observed.

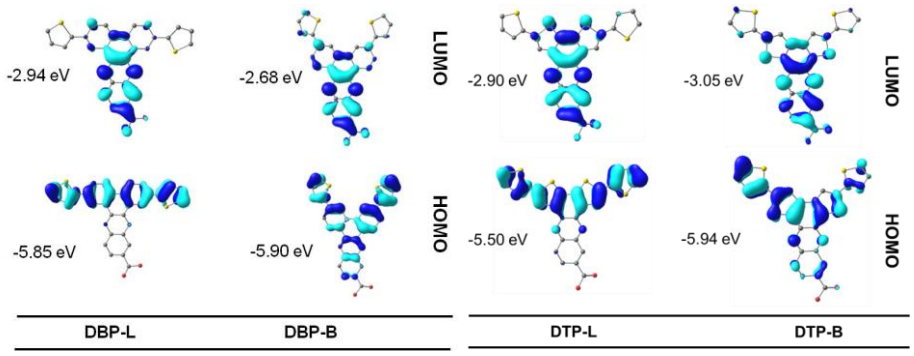

Figure 37: Illustration of the frontier orbitals for DBP-L, DBP-B, DTP-L and DTP-B. Computations were carried out in the gas phase using the B3LYP/6-31G(d) level.

To characterize the nature of the vertical optical transitions, we performed TDDFT calculations in the gas phase, at the B3LYP/6-31G* level. The properties of the excited states determined via TDDFT agree well with the empirical results, particularly concerning the simulated and empirical UV-visible profiles (details are presented in the next section), which are depicted in Figure 38.

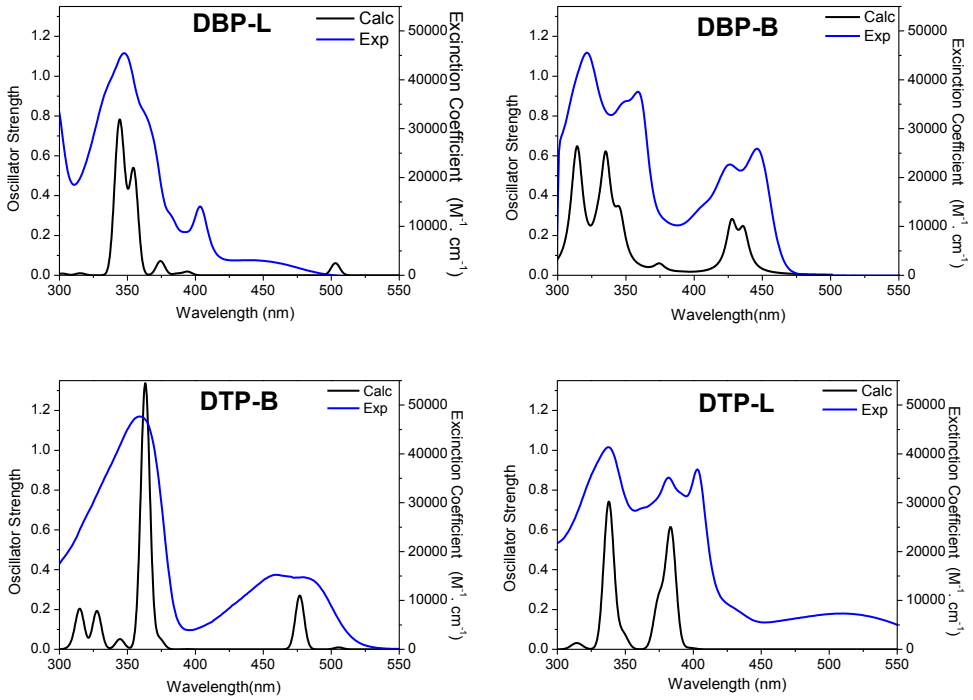

Figure 38: UV-visible absorption spectra in toluene (blue) and simulated absorption spectra determined by TD-DFT at the B3LYP/6-31G* level of theory (black) of DBP-L, DBP-B, DTP-L and DTP-B.

Quantitative data, portraying the strong correlation between the theoretical and experimental results are summarized in Table 9. Column 3 represents the energies associated with the peak transitions observed in toluene and column 4 summarizes their associated energies, obtained by TDDFT. These experimental and calculated values are close (with differences varying between 0.04 eV to 0.2 eV), validating the parameters used for the calculations. For all dyes, the weak low energy transitions are predominantly HOMO→LUMO transitions. Trends also agree when comparing extinction coefficients (Table 7, column 2) and oscillator strength (Table 7, column 5), and the most intense transitions correspond to HOMO→LUMO +2 for DBP-L, HOMO -1→LUMO +1 for DBP-B, and HOMO→LUMO +1 for the DTPs series.

Table 9: Summary of UV-Vis absorption spectra (λ_{max},ε), energy gap (E_{opt}) and TDDFT determination of the optical transitions (E_{calc}), the oscillator strengths (f) and the main electronic configurations involved in the description of the respective excited states for DBP-L, DBP-B, DTP-L and DTP-B.

compd	λ_{max} ($\varepsilon*10^3(M^{-1}\cdot cm^{-1})$)[a]	E_{opt},[a] (eV)	E_{calc},[b] (eV)	f[b]	Electronic configurations[b]
DBP-L	449 (3.0),	2.42	2.46	0.06	95% H→L
	404 (14.1),	3.06	3.14	0.02	82% H-1→L
	348 (45.4)	3.56	3.58	0.34	60% H→L +2
DBP-B	437 (25.9),	2.66	2.86	0.17	69%H→L 21% H-1→L
	344 (37.5)	3.60	3.72	0.48	48% H-1→L+1
DTP-L	518 (7.3),	2.10	2.14	0.10	90% H→L,
	403 (36.9)	3.10	3.23	0.60	70% H→L+1
DTP-B	485 (14.4),	2.37	2.45	0.01	90% H→L
	459 (15.3),	2.70	2.60	0.27	82% H-1→L
	360 (47.6)	3.44	3.40	0.79	63% H→L+1

a: measured in toluene, b: calculated via TD-DFT

4.3.2 Electrochemical Properties

Because of the poor solubility of the dyes in PC and ACN, CV and DPV measurements were carried out in benzonitrile, which conveniently has a wide electrochemical window. As the solubility of the dyes was still limited in benzonitrile, the observed currents are small in the DPV (Figure 39a) and CV (Figure 39b) experiments. While all of the dyes presented reversible reductions, they exhibited irreversible oxidations, as the evolution of the cation radical lead to dimerization or oligomerization processes.[163] Reduction potentials are in the same range, from -1.8 V to -1.4 V *vs.* Fc/Fc^{+}. The electron affinities of the B series are 0.2 eV lower than their isomers L, following the trend of LUMO energies from our DFT calculations. When comparing the cores, DTP has a higher reduction potential than DBP.

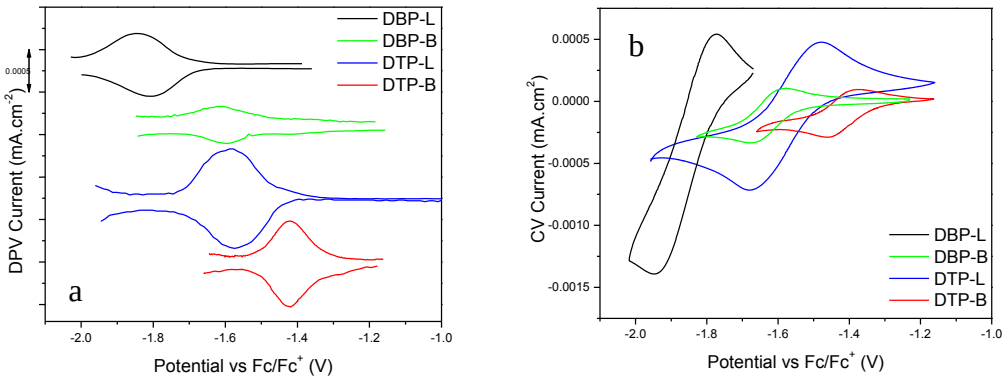

Figure 39: (a) Differential pulse voltammogram and (b) cyclic voltammogram for compounds DBP-L (black), DBP-B (green), DTP-L (blue) and DTP-B (red).

Table 10 summarizes the quantified levels for the HOMOs and LUMOs, as well as their comparison with the simulated values. Due to the irreversibility of the oxidation, the HOMO values were calculated by subtracting the optical energy gap, obtained via UV-visible spectroscopy, from the reduction potential, obtained by electrochemistry. As

pointed out by Brédas,[153] this approximation ignores the exciton binding energy built into the optical gap, so the quantitative levels bear a margin of error.

The LUMO levels are higher than the TiO_2 CB (≈-4.00 eV), and the HOMO levels are deeper than the redox potential of the iodide/triiodide couple (-4.85 eV), indicating the thermodynamic plausibility for electron transfer to the metal oxide and regeneration of the neutral species of the dye.

Table 10: Electrochemical and computational data for compounds DBP L, DBP-B, DTP L and DTP-B

Compd	E_{gap}^{opt} (eV)[a]	$E_{½}^{red}$ (V)[b]	$LUMO_{exp}$ (eV)[b]	$HOMO_{exp}$ (eV)[c]	$HOMO_{calcd}$ (eV)[d]	$LUMO_{calcd}$ (eV)[d]
DBP-L	2.92	-1.80	-3.30	-6.22	-5.55	-3.00
DBP-B	2.69	-1.62	-3.54	-6.23	-5.77	-2.57
DTP-L	2.11	-1.59	-3.53	-5.63	-5.85	-2.94
DTP-B	2.36	-1.53	-3.70	-6.06	-5.94	-3.01

[a]values are determined from UV-Vis spectroscopy in toluene, the onset of absorption defines the energy gap level. [b]values are obtained by DPV in benzonitrile solution; [c]values are obtained by DFT computations. [d]values are calculated using the onset of absorption(a) added to the LUMO (b)

4.3.3 Absorption and Emission Properties

UV-visible spectra in toluene show strong and well defined bands at 290-350 nm and 400-440 nm for DBPs and at 340-400 nm and 480-520 nm for DTPs. (Figure 40). Higher energy bands are attributed to π-π* transitions and lower energy bands correspond to intramolecular charge transfer. For the DTP-B compounds, the absorption peak coalesces at 480 nm. This is similarly observed by Meyer et al[164] and corresponds to two transitions: HOMO-1→LUMO and HOMO→LUMO. When comparing isomers, extinction coefficients in the charge transfer region are higher for the B compounds. This can be correlated to the better overlap of the frontier orbitals. When comparing cores, the DTPs are red-shifted compared to DBPs, due to the stronger donating ability of the thiophene unit. As a result, this simple benzene to thiophene alteration permits the

absorption of less energetic (by 0.3 eV) photons. Extinction coefficients are nearly twice the values reported by Patel et al[159] in similar D_2A system composed of thiophene-benzo(triazole-thiadiazole)-thiophene, suggesting the fused donor-acceptor system is a better candidate for light absorption, compared to systems linked via single bonds.

All compounds displayed fluorescence, with a maximum emission at 432 nm (DBP-B, quantum yield: 0.29), 500 nm (DTP-B, quantum yield: 0.04), 540 nm (DBP-L, quantum yield: 0.16) and 630 nm (DTP-L, quantum yield: 0.16) (Figure 40). These results correlate well with the colors and fluorescence intensities observed in the picture of the dyes under UV light in Figure 36. Interestingly, DTP-B has the lowest fluorescence quantum yield of the series of sensitizers, highlighting the efficiency of the non-radiative process compared to the radiative process in this compound. A previous study[165] revealed a competition between inter system crossing and internal conversion in DBP systems. As this is likely to be the case in our family of compounds, we carried out studies of transient absorption and oxygen sensitization experiments to evaluate the nature of the excited state deactivation. This will be discussed in the subsequent sections.

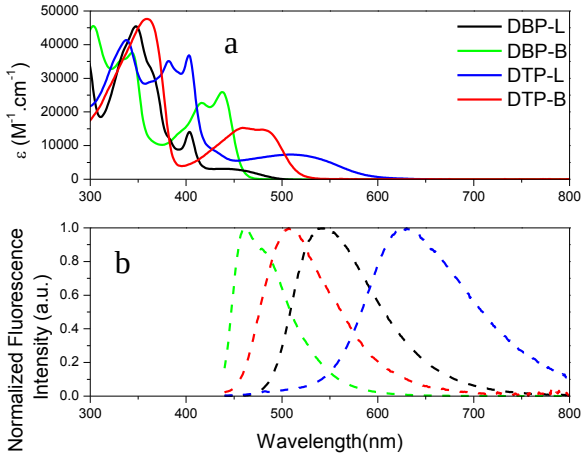

Figure 40: (a) Absorption and (b) normalized emission spectra of compounds DBP-L (black), DBP-B (green), DTP-L(blue), and DTP-B (red) in toluene.

4.4 Excited State Characterizations

To gain insight into the optical properties of the DBP and DTP series, photophysical studies were carried out, and the results are summarized in Table 9. Fluorescence decays for the dyes were measured in toluene solutions, and in each case the decays were monoexponential. There are several trends that can be observed in the data. First, in general all of the dyes exhibit moderately efficient fluorescence with quantum yields in excess of 10%, except for DTP-B. In addition, it can be seen that all of the compounds undergo relatively efficient intersystem crossing to the triplet state, as reflected by the large singlet oxygen quantum yields (Φ_Δ). The only exception is DTP-L, which has a comparatively lower Φ_Δ, likely reflecting a lower triplet yield. Third, the L isomers have longer fluorescence lifetimes than the B isomers; this trend is similar to that observed in previous studies on DBP derivatives.[166] The radiative and non-radiative decay rates (k_r and k_{nr}, respectively) were computed using the fluorescence quantum yield and lifetime values and the data are compiled in the table. In general, the radiative rates vary from 10^7 – 10^8 s^{-1}, which is consistent with the charge-transfer nature of the lowest singlet states. The non-radiative decay rates (k_{nr}) are a composite of intersystem crossing and internal conversion, and there are no systematic trends that can be inferred among the series. The one outstanding feature is the relatively high k_{nr} value (>10^9 s^{-1}) DTP-B, which reflects its low fluorescence quantum yield (0.04).

Table 11: Photophysical data for compounds DBP L, DBP-B, DTP L and DTP-B.

Compd	λ_{max} [a] (nm)	λ_{em} [a] (nm)	Stokes Shift (eV) [a]	Φ_f [b]	τ_f [c] /10^{-9} s	τ_t [c] / 10^{-6} s	k_f [c] / $10^6 s^{-1}$	k_{nr} [c] / 10^6 s^{-1}	k_t [c] / 10^6 s^{-} $_1$	Φ_Δ [d]
DBP-L	401, 449	545	0.49	0.16	14	6.6	11	42	0.16	0.58
DBP-B	344, 437	462	0.15	0.29	1.6	5.9	140	340	0.17	0.41
DTP-L	403, 510	628	0.46	0.16	9.4	5	100	150	0.22	0.15
DTP-B	362, 464, 485	545	0.29	0.04	0.7	4.7	28	2300	0.21	0.51

[a] in toluene solution; [b] measured using coumarin 6 in ethanol (Φ_f =0.78) as the actionometer; [c] measured in a solution of toluene; [d] measured using terthiophene in oxygen saturated $CDCl_3$ (Φ_Δ =0.70) using as the actionometer.

In thiophene containing conjugated oligomers, photoexcitation produces a singlet excited state which undergoes moderately efficient intersystem crossing to generate a long-lived triplet excited state.[159,167,168] Consistent with this general behaviour, the singlet oxygen yield measurements indicate that intersystem crossing is efficient in the DPB and DTP compounds. Thus, in order to probe the triplet excited state further, nanosecond transient absorption (TA) studies were carried out in degassed solutions of the compounds in toluene solution, and the resulting difference absorption spectra are shown in Figure 41. All of the compounds exhibit TA extending through the visible region (λ_{ex} = 355 nm), with pronounced ground state bleaching evident for the "branched" set, DBP-B and DTB-B. The comparatively long transient lifetimes (4-7 μs) and observation of oxygen-induced quenching suggest that the TA signal is due to the triplet-triplet absorption. Note that the amplitude of the TA signal observed for DTP-L is considerably weaker compared to that observed for the other compounds. This is consistent with the singlet oxygen yield measurements, which imply that the triplet yield is low for this compound. Taken together, the TA and singlet oxygen yield results imply that intersystem crossing is the predominant non-radiative decay pathway active in this series of compounds.

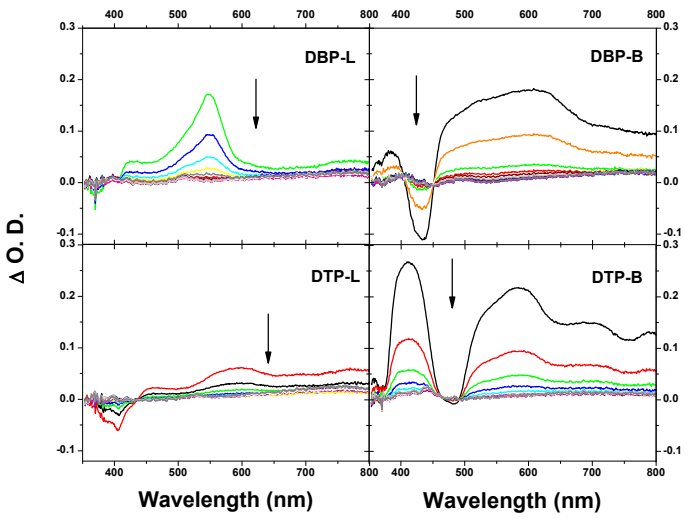

Figure 41: Transient absorption difference spectra of (a) DBP-L, (b) DBP-B, (c) DTP-L, and (d) DTP-B in toluene at room temperature (initial delay = 70 ns, subquent spectra are at delay increments of 4 μs). Arrows show direction of change with increasing delay time. The spectra were obtained with the excitation wavelength of 355 nm and with a laser energy of 6-7 mJ per pulse. (The excitation energy and ground state absorption were matched at 355 nm for all samples).

4.5 Integration of the Sensitizer into Devices and their Properties

Carboxylic acid derivatives DBP-L*a*, DBP-B*a*, DTP-L*a* and DTP-B*a* were adsorbed onto mesoporous TiO_2 films from DMF solution at a concentration of 10^{-4} M. To allow for the comparison of the cell performance with the different sensitizers, one set of conditions (solvent, electrolyte and additives) was tested. In this fundamental study, we did not seek to optimize the conditions by meticulously exploring the effects of solvent, electrolyte and additive on the cell performance, and thus, cell results should be viewed as being "unoptimized." Standard deviations for the devices parameters, presented in Table 12 in the subsequent sections, show the reproducibility of our measurements.

4.5.1 Variation of IPCE

IPCE responses were recorded for all dyes in devices, as illustrated in Figure 42. As seen in the introduction, IPCE curves illustrate how efficiently the cell transforms photons into electrons. All sensitizers are able to transform photons into charge carriers; however, this process works moderately. Indeed, IPCE for DBP-L, DTP-L and DTP-B are under 40 %, and DBP-B has the highest IPCE of 50% at 425 nm. It is interesting to note that the IPCE tracks the absorption spectrum of the sensitizers as observed by solution UV-visible spectroscopy. Then, similarly to what have been observed previously, the DTP series are red shifted compared with the DBP family. Moreover, the B sensitizers have a higher IPCE than the corresponding L derivatives.

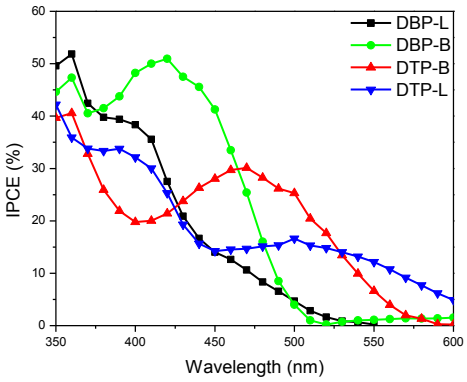

Figure 42: Photocurrent of DSSCs made from DBP-L, DBP-B, DTP-L, and DTP-B.

4.5.2 J-V Curves and Overall Power Conversion Efficiencies

For the current-voltage response shown in Figure 43, two effects can be seen. The first one is the effect of the nature of the core on the V_{oc}. DTPs series have V_{oc} of ~420 mV and DBPs series have a V_{oc} of ~500 mV. As seen in Chapter 1, a raise in V_{oc} can be attributed to a shift of the TiO_2 CB, to the surface blocking caused by a different dye loading, or to a different electrolyte-dye interaction.[48] In our case, given the similar structure of the dyes and the uniform conditions used, we speculate that the variation in

the V_{oc} is most likely due to the shift of the TiO_2 CB. This is supported by numerous empirical and theoretical studies that relate the sensitizer structure with the TiO_2 CB shift.[58,169–173] These studies report that a sensitizer with stronger donor units improve both the electrostatic and charge transfer effect on the TiO_2 surface, hence raising the TiO_2 CB and ultimately, the V_{oc}. In our study, we show that the nature of the acceptor unit matters. In these D_2A sensitizers, the acceptor DTP core is a more electron-rich system; however, the resulting Voc is smaller than with the DBP core.

When examining the short circuit current (J_{sc}), linear systems L exhibit lower values than the branched systems B. This slight increase can be correlated with the IPCE data, where the B systems have a higher overall IPCE than the L systems. B systems have a greater overlapping of electronic density, smaller injection barrier (0.2 eV lower), a lower fluorescence yield, and a larger triplet yield than the L systems. These characteristics can favorably shift the J_{sc}.

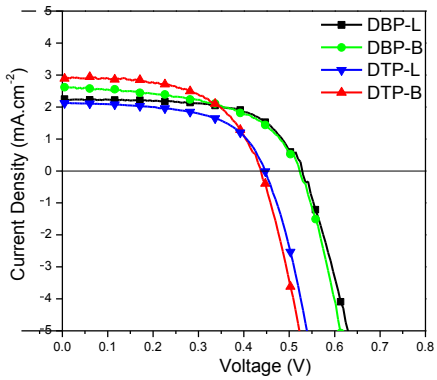

Figure 43: J-V response of cells made from DBP-L, DBP-B, DTP-L and DTP-B.

Table 12 represents the values for the figures of merit of the photovoltaic curves. The V_{oc} is at ~500 mV for the DBP series and ~420 mV for the DTP series. These values are slightly less than the maximum value of 700 mV for a cell with an iodine/triiodide redox couple. The fill factors range from 0.5 to 0.6, which are average numbers for DSSCs.

The main factor limiting the cell performance is the short circuit current of 2-3 $mA \cdot cm^{-2}$. Because of these low current density values, the overall PCE is low, from 0.56% for DTP-L to 0.74% for DBP-L. To increase the overall efficiencies, several solutions include the optimization of the cells by adding a co-adsorbant to reduce back electron transfer, or the modification of the dyes to extend the absorption into the IR region.

Table 12: Open circuit voltage (V_{oc}), short circuit current (J_{sc}), fill factor (FF), and power conversion efficiency (PCE) for the studied sensitizers, for three or more devices for DBP-L, DBP-B, DTP-L and DTP-B.

Compd	V_{oc} (V)	J_{sc} ($mA \cdot cm^{-2}$)	FF	PCE (%)
DBP-L	0.52 ±0.01	2.2 ±0.2	0.62 ±0.02	0.73 ±0.02
DBP-B	0.49 ±0.02	2.6 ±0.1	0.53 ±0.03	0.66 ±0.02
DTP-L	0.43 ±0.02	2.2 ±0.2	0.54 ±0.04	0.53 ±0.05
DTP-B	0.4 ±0.01	2.9 ±0.03	0.53 ±0.07	0.66 ±0.06
N3	0.7	11.4	0.4	3.29

In conclusion, a thorough study of quadrupolar D_2A sensitizers has been carried out, both in solution and upon integration into DSSCs. The nature of the acceptor moiety was changed from dithienophenazine to dibenzophenazine. This slight change induces a noticeable change in the solution optoelectronic properties. The nature of the core impacts the photophysical and photoelectrochemical properties: in solution, the DTPs have a smaller energy gap, a higher HOMO, and greater fluorescence and non-radiative rate constants. When integrated into DSSCs, the Voc is ~ 100mV greater for the DBPs, and this change is likely due to a rising of the TiO_2 CB. Interestingly, when comparing isomeric sensitizers, they also present different optoelectronic properties: the branched dyes have a higher overlapping of the frontier orbital density, a smaller injection barrier for injection into TiO_2 and a greater intersystem crossing access. Upon integration into DSSCs, the IPCE curves differ, and this change can be directly correlated to the overlap of the frontier orbital density, overall influencing the Jsc. The FF are independent of the

isomer used. We have shown in this study that the fine tuning of sensitizers is important for the fundamental understanding of the properties, and the photovoltaic results.

4.6 Experimental

General procedure for condensation of diketones and diaminobenzoate.

To a round-bottom flask, equipped with a stir bar and a condenser, was added the diketone (1 equiv.), ethyl 3,4-diaminobenzoate (1.2 equiv.), ethanol 200 proof (150 mL/g of diketone) and 1 mL of acetic acid. The resulting mixture was brought to reflux for 2 hours, and allowed to cool to room temperature. The resulting solids were filtered, rinsed with plenty of methanol, and air dried to give the corresponding products.

Dithieno[2,3-a:3',2'-c]phenazine-9-carboxylic acid. Orange solid (99%). ^{1}H NMR (300 MHz, DMSO) δ_H 8.75 (1H, s), 8.32 (2H, s), 8.26 (2H, t, J=6.05 Hz), 8.11 (2H, d, J=5.03 Hz). HRMS (EI) Calculated for $C_{17}H_8N_2O_2S_2$ $[M]^+$: 337.0100, found m/z: 337.01169.

Ethyl 3,6-dibromodibenzo[a,c]phenazine-11-carboxylate Yellow solid (91% yield) mp 256-258 ºC IR (υ, cm^{-1}) 2914, 1703, 1417, 1288, 1195, 833, 758, 653. ^{1}H NMR (300 MHz, $CDCl_3$) δ_H 9.16 (2H, dd, J=8.50 Hz J=1.76 Hz), 8.97 (2H, s), 8.53 (2H, s), 8.45 (1H, dd, J=8.80 Hz, J=1.47 Hz), 8.31 (1H, d, J=8.80 Hz), 7.85 (2H, d, J=7.62 Hz), 4.54 (2H, q, J=7.33 Hz), 1.53 (3H, t, J=3.5 Hz) HRMS (ESI-TOF) Calculated for $C_{23}H_{15}Br_2N_2O_2^+$ $[M+H]^+$: 510.9476, found m/z: 510.9480.

3,6-Dibromodibenzo[a,c]phenazine-11-carboxylic acid Yellow solid (91% yield) mp > 300 ºC. IR (υ, cm^{-1}) 2841 (w), 1695, 1595, 1354, 1269, 1095, 823, 754. ^{1}H

NMR (300 MHz, DMSO, 90 ºC) δ_H 9.12 (2H, d, J=8.6 Hz), 8.95 (2H, s), 8.80 (1H, s), 8.37 (1H, dd, J=8.70 Hz, J=1.9 Hz), 8.34 (1H, dd, J=8.80 Hz, J=0.7 Hz), 7.97 (2H, dd, J=8.8 Hz, J=1.7Hz) HRMS (EI) Calculated for $C_{21}H_{10}Br_2N_2O_2$ $[M]^+$: 479.9109, found m/z: 479.9109.

Ethyl 2,7-dibromodibenzo[a,c]phenazine-11-carboxylate Yellows solid (91% yield) mp 265-268 ºC IR (υ, cm^{-1}) 2989, 1708, 1323, 1269, 1205, 1097, 808, 752 ^{1}H NMR (300 MHz, $CDCl_3$) δ_H 9.44 (2H, s), 9.03 (1H, s), 8.48 (1H, d, J=9 Hz), 8.33 (3H, m), 7.89 (2H, d, J=9 Hz), 4.55 (2H, q, J=7.2 Hz), 1.52 (3H, t, J=7.2 Hz). HRMS (ESI-TOF) Calculated for $C_{23}H_{15}Br_2N_2O_2^+$ $[M+H]^+$: 510.9476, found m/z 510.9484.

2,7-Dibromodibenzo[a,c]phenazine-11-carboxylic acid Yellow solid (98% yield) mp > 300 ºC IR (υ, cm^{-1}) 2981, 1720, 1290, 1253, 1190, 1087, 835, 746, 655 ^{1}H NMR (300 MHz, DMSO, 90 ºC) δ_H 9.34 (2H, s), 8.88(1H, s), 8.69 (1H, s), 8.67 (1H, s), 8.42 (2H, s), 8.04 (2H, dt, J=8.8 Hz, J= 2.5Hz), HRMS (APCI) Calculated for $C_{21}H_{11}Br_2N_2O_2^+$ $[M+H]^+$: 482.9163, found m/z 482.9161.

Ethyl 2,5-dibromodithieno[3,2-a:2',3'-c]phenazine-9-carboxylate Bright orange solid (93% yield) mp 241-244 ºC ^{1}H NMR (300 MHz, $CDCl_3$) δ_H 8.98 (1H, s), 8.43 (1H, dd, J= 9Hz, J=1.7Hz), 8.35 (2H, s), 8.27 (1H, d, J=8.8Hz). HRMS (ESI-TOF) Calculated for $C_{19}H_{11}Br_2N_2O_2S_2^+$ $[M+H]^+$: 522.8603, found m/z: 522.8613.

2,5-Dibromodithieno[3,2-a:2',3'-c]phenazine-9-carboxylic acid Orange solid (92% yield) mp > 300 ºC IR (υ, cm^{-1}) 2852 (w), 1695, 1284, 1193, 837, 769, 655. ^{1}H NMR (300 MHz, DMSO, 90 ºC) δ_H 8.82 (1H, s), 8.41 (1H, m), 8.39 (2H, s), 8.35 (1H, d, J=8Hz) HRMS (APCI) Calculated for $C_{17}H_7Br_2N_2O_2S_2^+$ $[M+H]^+$: 494.8290, found m/z: 494.8307.

Ethyl 2,5-dibromodithieno[2,3-a:3',2'-c]phenazine-9-carboxylate Yellow solid (90% yield) mp > 300 ºC IR (υ, cm^{-1}) 3093, 1707, 1417, 1259, 1085, 916, 746. ^1H NMR (300 MHz, $CDCl_3$) δ_H 8.99 (1H, s), 8.41 (1H, dd, J=1.6 Hz, J=9Hz), 8.27 (1H, d, J=9 Hz), 7.68 (2H, s), 4.50 (2H, q, J=7.3Hz), 1.50 (3H, t, J=7.1 Hz) HRMS (EI) Calculated for $C_{19}H_{10}Br_2N_2O_2S_2$ $[M]^+$: 519.8550, found m/z: 519.8563.

2,5-Dibromodithieno[2,3-a:3',2'-c]phenazine-9-carboxylic acid Yellow solid (95% yield) mp > 300 ºC IR (υ, cm^{-1}) 2829 (w), 1695, 1409, 1280, 916, 765. ^1H NMR (300 MHz, DMSO, 90 ºC) δ_H 8.74 (1H, s), 8.35 (1H, dd, J=1.8 Hz, J=8.8Hz), 8.31 (1H, d, J=8.8 Hz), 8.25 (2H, d, J=1.25). HRMS (EI) Calculated for $C_{17}H_6Br_2N_2O_2S_2$ $[M]^+$:491.8237, found m/z: 491.8233.

General procedure for the Stille coupling. To a flame dried round-bottom flask equipped with a stir bar, the dibromo derivative (1 equiv.), tris(dibenzylideneacetone) dipalladium(0) catalyst (3% equiv.) and tri(*o*-tolyl)phosphine ligand (12% equiv.) were added. The flask was evacuated for 30 min and then refilled with argon. To the flask, toluene (50 mL per g of dibromo derivative) and stannyl derivative (3 equiv.) were added. The reaction was allowed to stir overnight at 90 ºC under an inert atmosphere. The mixture was concentrated under reduced pressure and precipitated into methanol. The solids were filtrated, rinsed with methanol, and passed through a small column of silica pad with hexanes-dichloromethane as eluent. The fraction was concentrated under reduced pressure and precipitated into methanol to give the corresponding products in a solid form.

Ethyl 2,7-bis(4-hexylthiophen-2-yl)dibenzo[a,c]phenazine-11-carboxylate (DBP-L) Yellow solid (41% yield) IR (υ, cm^{-1}) 2922, 2854, 1712, 1456, 1257, 1207, 1091, 825, 723. ^{1}H NMR (300 MHz, $CDCl_3$) δ_H 9.47 (2H, s), 9.05 (1H, s), 8.37 (4H, m), 7.95 (2H, d, J=9Hz), 7.46 (2H, s), 7.00 (2H, s), 4.55 (2H, q, J=7 Hz), 2.71 (4H, t, J=8Hz), 1.74 (4H, m), 1.51 (4H, t, J=7 Hz), 1.38 (10H, m), 0.93 (6H, t, J=7Hz). ^{13}C NMR (75 MHz, Tol-d_8, 70 ºC) δ_C 165.20, 144.43, 143.94, 143.72, 143.63, 143.28, 141.44, 134.52, 134.43, 132.15, 130.90, 130.62, 129.52, 125.33, 123.36, 122.99, 120.18, 60.76, 31.65, 30.58, 30.36, 29.01, 22.53, 13.68. HRMS calculated for $C_{43}H_{45}N_2O_2S_2^+$ $[M+H]^+$: 685.2917, found m/z: 685.2923.

2,7-Bis(4-hexylthiophen-2-yl)dibenzo[a,c]phenazine-11-carboxy-lic acid (DBP-La) Yellow solid (50% yield), ^{1}H NMR (300 MHz, DMSO, 90 ºC) δ_H 9.36 (2H, s), 8.78 (1H, s), 8.63 (2H, m), 8.39 (1H, d, J=11 Hz),8.32 (1H, d, J=11 Hz) 8.08 (2H, s), 7.56 (2H, s), 7.22 (2H, s), 2.67 (4H, m), 1.70 (4H, m), 1.36 (12H, m), 0.89 (6H, t, J=7Hz). HRMS (EI) calculated for $C_{41}H_{41}N_2O_2S_2^+$ $[M+H]^+$: 657.2609, found m/z: 657.2619.

Ethyl 3,6-bis(4-hexylthiophen-2-yl)dibenzo[a,c]phenazine-11-carboxylate (DBP-B) Yellow solid (66% yield) IR (υ, cm^{-1}) 2922, 2848, 1718, 1602, 1359, 1251, 1211, 1085, 825. ^{1}H NMR (300 MHz, $CDCl_3$) δ_H 9.25 (2H, d, J=8.21 Hz), 8.94 (1H, s), 8.62 (2H, s), 8.36 (1H, dd, J=8.8 Hz, J=3 Hz), 8.27 (1H, d, J=9Hz), 7.91 (2H, d, J=9Hz), 7.41 (2H, s), 7.03 (2H, s), 4.5 (2H, q, J=7 Hz), 2.71 (4H, t, J=8Hz), 1.75 (4H, p, J=7 Hz), 1.51 (4H, t, J=7 Hz), 1.38 (10H, m), 0.93 (6H, t, J=7Hz), ^{13}C NMR (75 MHz, Tol–d_8, 70 ºC): δ_C 165.26, 144.35, 143.96, 143.78, 143.38, 142.97, 141.43, 132.70, 132.36, 132.09, 131.41, 129.38, 125.54, 125.44, 120.63,

120.55, 119.64, 60.67, 52.66, 31.65, 30.54, 30.32, 29.00, 22.53, 13.85, 13.67. HRMS (EI) calculated for $C_{43}H_{44}N_2O_2S_2$ $[M]^+$: 684.2844, found m/z: 684.2817.

3,6-Bis(4-hexylthiophen-2-yl)dibenzo[a,c]phenazine-11-carboxy-lic acid (DBP-Ba) Yellow solid (53% yield) ^{1}H NMR (300 MHz, DMSO, 90 ºC) δ_H 9.25 (2H, d, J=8.83 Hz), 8.90 (2H, s), 8.84 (1H, s), 8.36 (2H, s), 8.04 (2H, d, J=9.69Hz), 7.76 (2H, s), 7.27 (2H, s), 2.70 (4H, t, J=7.8Hz), 1.72 (4H, p, J=7 Hz), 1.37 (16H, m), 0.90 (6H, t, J=6.7Hz). HRMS (EI) calculated for $C_{41}H_{40}N_2O_2S_2$ $[M]^+$: 656.2531 found m/z: 656.2515.

Ethyl 2,5-bis(4-hexylthiophen-2-yl)dithieno[3,2-a:2',3'-c]phena-zine-9-carboxylate (DTP-L) Purple solid (61 % yield) IR (υ, cm^{-1}) 2927, 2852, 1716, 1296, 1251, 1190, 1091, 746, 528, 441. ^{1}H NMR (300 MHz, $CDCl_3$) δ_H 8.85 (1H, s), 8.30 (1H, dd, J=8.8 Hz, J=2 Hz), 8.20 (1H, d, J=9Hz), 8.12, (2H, s), 4.50 (2H, q, J=7Hz), 2.61 (4H, t, J=7.5 Hz), 1.68 (4H, p, 4H, J=7Hz), 1.51 (4H, t, J=7 Hz), 1.36 (10H, m), 0.94 (6H, t, J=7Hz). ^{13}C NMR (75 MHz, $CDCl_3$): δ_C 160.07, 144.51, 143.06, 140.65, 140.22, 139.95, 137.31, 137.17, 136.47, 135.25, 135.16, 134.73, 134.05, 132.34, 131.03, 129.55, 128.79, 126.39, 120.55, 120.04, 119.95, 61.69, 31.96, 30.73, 30.57, 29.33, 22.89, 14.63, 14.36. HRMS (ESI-TOF) Calculated for $C_{39}H_{41}N_2O_2S_4^+$ $[M+H]^+$: 697.2045 found m/z: 697.2060.

2,5-Bis(4-hexylthiophen-2-yl)dithieno[3,2-a:2',3'-c]phenazine-9-carboxylic acid (DTP-La) Purple solid (56% yield) IR (υ, cm^{-1}) 2922, 2850, 1577, 1429, 1188, 1096, 818, 435 ^{1}H NMR (300 MHz, CD_2Cl_2+ TFA) δ_H 8.82 (1H, s), 8.38 (1H, d, J=10.1 Hz), 8.24 (1H, d, J=1.6 Hz), 7.83 (2H, d, J=20.26 Hz), 6.90 (4H, s), 2.55

(4H, q, J=7.4Hz), 1.64 (4H, br), 1.39 (12H, br), 0.97 (6H, t, J=6.3 Hz). HRMS (EI) Calculated for $C_{37}H_{36}N_2O_2S_4$ $[M]^+$: 668.1660 found m/z: 668.1660.

Ethyl 2,5-bis(4-hexylthiophen-2-yl)dithieno[2,3-a:3',2'-c]phena-zine-9-carboxylate (DTP-B) Dark orange solid (62 % yield) IR (υ, cm^{-1}) 3088, 2914, 1701, 1413, 1251, 1193, 746, 441. ^1H NMR (300 MHz, $CDCl_3$) δ_H 8.98 (1H, s), 8.39 (1H, dd, J=9 Hz, J=1.9 Hz), 8.27 (1H, d, J=9Hz), 7.73 (2H, s), 7.30 (2H, s), 6.98 (2H, s), 4.51 (2H, q, J=7.1Hz), 2.65 (4H, t, J=7.8 Hz), 1.68 (4H, m), 1.49 (4H, t, J=7 Hz), 1.36 (10H, m), 0.92 (6H, t, J=7Hz). Calculated for $C_{39}H_{40}N_2O_2S_4$ $[M]^+$: 696.1973 found m/z: 696.1968.

2,5-Bis(4-hexylthiophen-2-yl) dithieno[2,3-a:3',2'-c] phenazine -9-carboxylate (DTP-Ba) Dark orange solid (45% yield) IR (υ, cm^{-1}) 2932, 2860, 1688, 1496, 1415, 1386, 810 ^1H NMR (300 MHz, DMSO, 90 ºC) δ_H 8.61 (1H, s), 8.40 (1H, d, J=9 Hz), 8.25 (2H, s), 8.11 (2H, d, J=7.5Hz), 7.50 (2H, s), 7.25 (2H, s), 2.65 (4H, t, J=7.5 Hz), 1.68 (4H, m), 1.35 (10H, m), 0.89 (6H, t, J=7.6Hz) HRMS (EI) Calculated for $C_{37}H_{36}N_2O_2S_4$ $[M]^+$: 668.1660 found m/z: 668.1646.

CHAPTER 5.

QUADRUPOLAR $(DONOR)_2$-ACCEPTOR ACID CHROMOPHORES FOR DSSC: INFLUENCE OF THE NUMBER AND NATURE OF DONOR UNITS.

5.1 Motivation behind Extending the Donor Chain and Varying the Donor Nature

The previous chapter introduced quadrupolar D_2-A molecules and showed their potential as sensitizers for DSSCs. It also discussed the influence of the nature of the core on the V_{oc} of the devices. This chapter pursues the study of these quadrupolar D_2-A dyes by investigating the donor moieties. As shown in Figure 44, two parameters were explored. First, we studied the influence of increasing the number of external donors by grafting on each side of the DTP acceptor cores one, two, or three thiophene units. Lengthening the donor chain should lead to a bathochromic shift in the absorption spectra, hence permitting the absorption of lesser energy photons. Moreover, increasing the number of donor units may reduce back electron transfer by avoiding iodine atoms to get close to the TiO_2 surface.[174,175] As the previous chapter could not give a clear answer on the influence of the isomerism on the photovoltaic properties, both branched and linear isomers were synthesized and integrated into devices, in order to further explore the properties of isomeric systems. The second part of this chapter analyzes the effect of tuning the nature of the donor unit. In a D_2-A system, varying the nature of the donor modifies the HOMO level of the overall molecule while the LUMO remains unchanged. Dyes with a less positive HOMO allow absorption of longer wavelength photons, and thus increase the light harvesting efficiency. Thus, three different donor units were used:

thiophene (Th), 3,4-propylenedioxythiophene (ProDOT) and dithienosilole (DTS) (Figure 44). Our group has extensive experience with ProDOT derivatives, often used as the monomer of choice for electrochromic polymers.[38176] ProDOT is an electron-rich, a stronger donating group than thiophene, and a synthon with good solubility properties attained with the tunable alkyl chains on the propylene bridge. DTS has been employed in high efficiency polymer solar cells,[177,178] as well as in organic dyes for DSSC.[179,180] Utilizing DTS in DSSC permits the tuning of the HOMO values, a panchromatic absorption of the light, and a reduction of the π-π stacking interactions of the dyes without distorting the co-planarity of the π-system, thanks to the tetrahedral silicon center.[7] The resulting molecules will be compared to their thiophene analogues in terms of spectroscopy (UV-visible absorption), rate of relaxation (fluorescence) and HOMO/LUMO energy levels (DFT calculations, electrochemistry). In this second part, the acceptor moiety is dithieno[2,3-a:3',2'-c]phenazine-9-carboxylic acid (branched DTP).

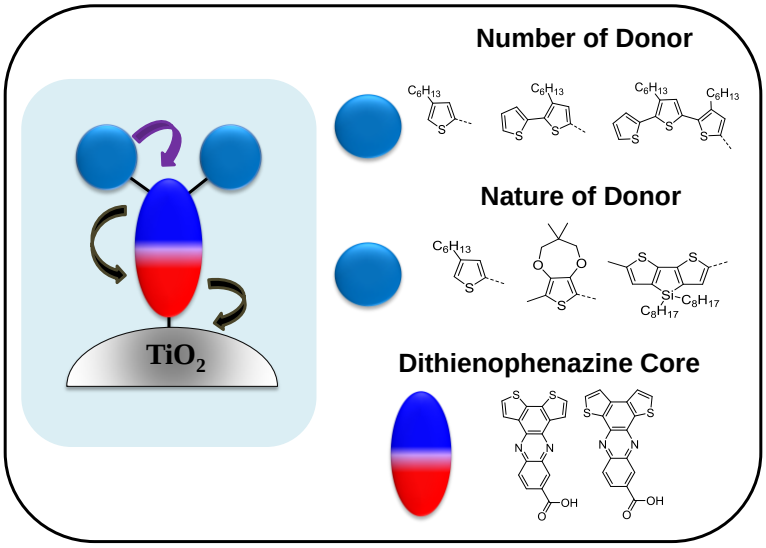

Figure 44: Schematic representation of the synthons employed for studying the influence of the number and nature of the donor units for quadrupolar D_2A sensitizers. The core of these dyes are dithienophenazine moieties**.**

5.2 Synthesis of the Dyes with Increasing Thiophene Units as External Donors

The acceptor cores were first built via condensation between ethyl 3,4-diaminobenzoate and the corresponding dibromobenzodithiophene-4,5-dione, as described in Chapter 4. The external donor chains were built by consecutive stannylation and Stille couplings from 2-methylthiophene **5.3**, also in good yields (42%-95%), as shown in Scheme 12.

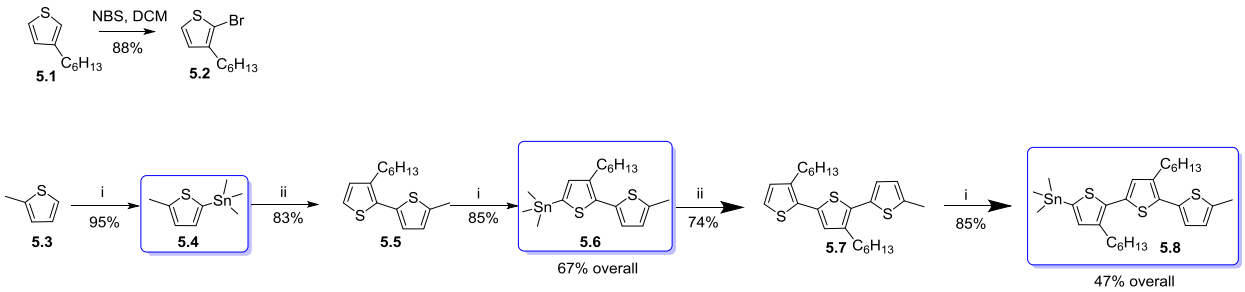

Scheme 12: Synthesis of stannylated thiophene donor moieties.

The target molecules were achieved by Stille coupling between the core **5.9** or **5.10** and the donor blocks **5.4**, **5.6** or **5.8** (in blue rectangle in Scheme 12). Column chromatography *in duplicate* was performed to ensure high purity of the targets DTP-Ln and DTP-Bn, hence lowering the yields in the 20-60% range, as depicted in Scheme 13. Finally, quantitative hydrolyses of the ethyl ester derivatives were performed in basic solution to produce the carboxylic derivatives DTP-Lna and DTP-Bna. Due to solubility considerations, esters derivatives were used for optical and electrochemical characterizations and the carboxylic acids derivatives were used in the DSSC devices. The sensitizers will be differentiated with their number of total thiophene units n (n= 4, 6 or 8), and the mode of conjugation: linear (L) or branched (B). When the carboxylic acids are employed, the suffix "a" will be added to the acronym.

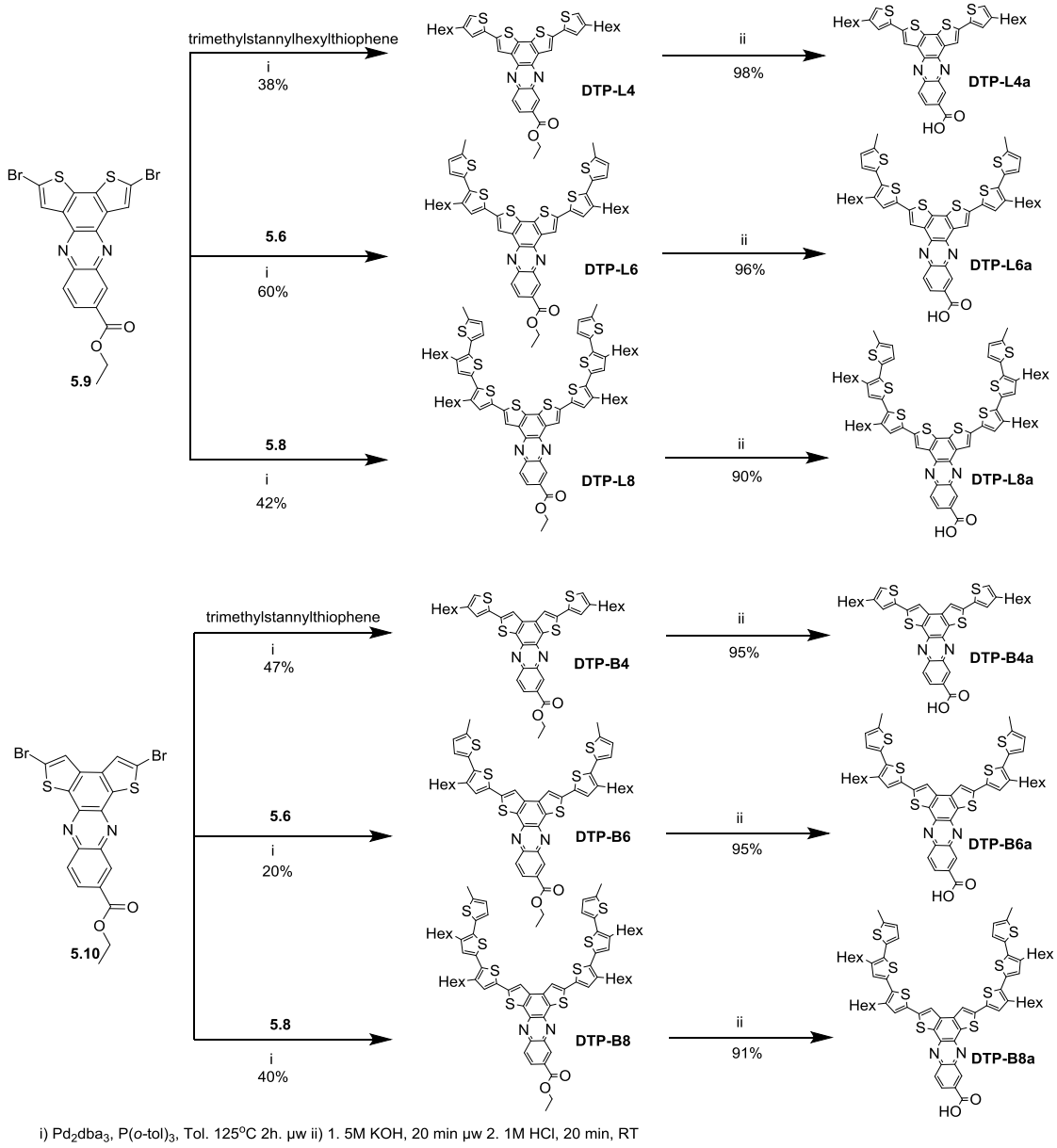

Scheme 13: Synthesis of dyes DTP-L4a, 6a and 8a and DTP-B4a, 6a and 8a. µ

5.3 Ground State and Excited State Characterizations

5.3.1 Density Functional Theory Computations

All molecules were modeled using DFT computations, at the B3LYP/6-31G* level in vacuum. For all sensitizers, the LUMO wave functions are localized on the core acceptor,

independent of the isomer or chain length, as depicted in Figure 45, top molecules. This will most likely facilitate the electron transfer from the excited state to the TiO_2 CB. By contrast, the HOMO densities are dependent on the structural isomer. For the L family, the HOMOs are delocalized only along the thiophene donor framework (Figure 45, bottom left molecules). For the B series, the HOMOs are delocalized within the donor segment and into the acceptor, through the entire molecule for DTP-B4 and DTP-B6 (Figure 45, bottom right molecules). In DTP-B8, the HOMO appears to be delocalized on one branch of the donor framework. However, when comparing the HOMO and HOMO-1 (Figure 46), the two wave functions are symmetrical. Moreover, the energies of the HOMO and HOMO -1 are close: -5.22 eV and -5.26 eV respectively, rendering the two levels quasi-degenerate. The small energy difference is produced by the mono-carboxylic acid group on one side of the phenazine group, causing the molecule to be unsymmetrical. It is important to note that DTP-B8 stills shows some delocalization on the acceptor core, which is absent in DTP-L8.

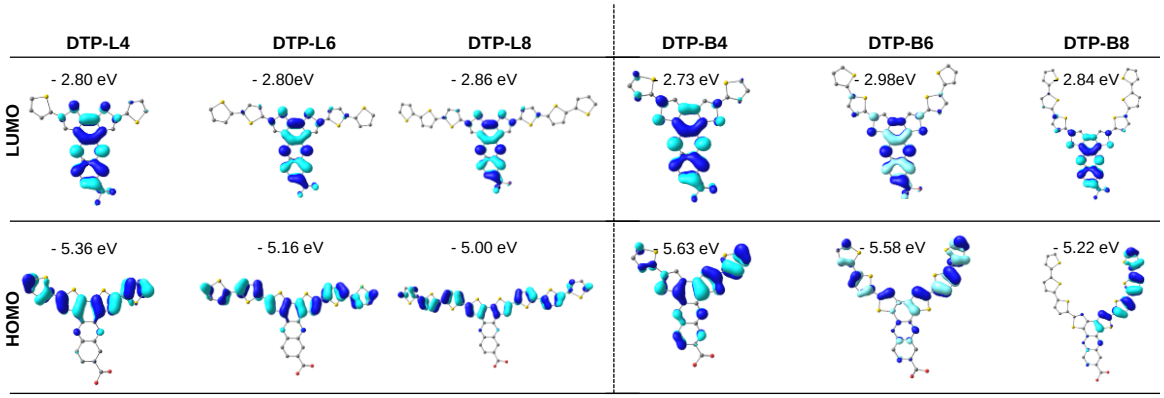

Figure 45: Orbital frontiers of DTP-Ln and DTP-Bn families obtained to the B3LYP/6-31G* level in vacuum.

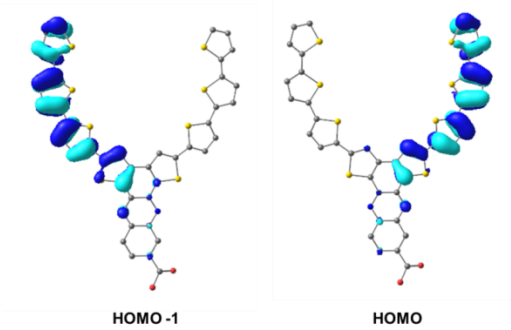

Figure 46: HOMO-1 and HOMO illustration of DTP-B8.

To explore the absorption properties of the molecules, TDDFT calculations provided the simulated absorption spectra as well as the associated transitions (Figure 47 and Table 13). For both families, a red shift in the absorption is predicted with the lengthening of the donor units, as increasing the number of donor groups extends the conjugation and reduces the energy gap (Figure 47a and 47b). For the DTP-L family, the peaks maxima increase from 583 nm to 634 nm to 697 nm for DTP-L4 to DTP-L6 to DTP-L8. For the DTP-B family, the absorption peak maxima are at 506 nm for DTP-B4, 555 nm for DTP-B6, and 603 nm for DTP-B8. When evaluating the isomeric series, the L family is predicted to be red-shifted compared to the B family. This can be related to Figure 45, where the HOMO for the L family is more localized on the thiophene framework, producing a more positive HOMO. When examining the vertical transitions associated with the first excited state, the L series has a single vertical transition, mainly composed of H→L character (Table 13, columns 2, 3 and 4). For the B series, the first excited states are comprised of two transitions (Table 13, columns 5, 6 and 7), that are a combination of H→L and H-1→L.

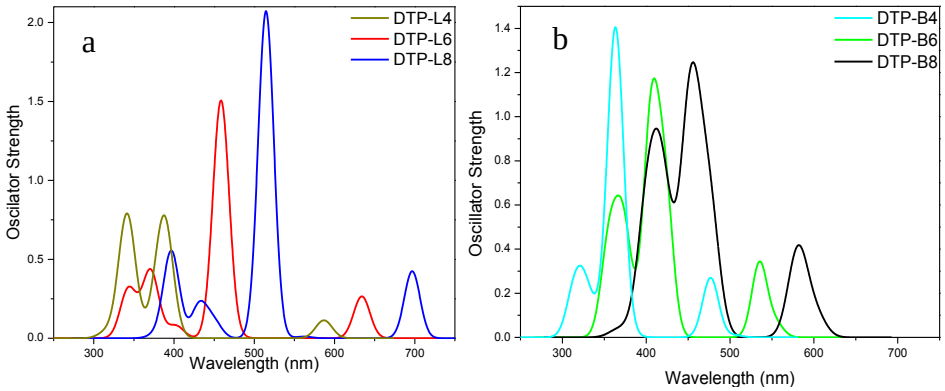

Figure 47: UV-visible spectra of (a) DTP-Ln and (b) DTP-Bn families predicted with TD-DFT, at the B3LYP/6-31G* level of theory.

Table 13: First and second vertical transitions, the oscillator strength and the electronic configurations for DTP-Ln and DTP-Bn compounds.

Compd	**DTP-L4**	**DTP-L6**	**DTP-L8**	**DTP-B4**	**DTP-B6**	**DTP-B8**
Vertical	583	634	697	506	555	603
Transitions				477	535	581
(nm)						
Oscillator	0.06	0.27	0.42	0.01	0.06	0.1
Strength				0.27	0.34	0.4
Electronic	95% H→L	98% H→L	98% H→L	87% H→L	87% H-1→L	60% H→L
Configurations				82% H-1→L	11% H→L	37% H-1→L
					85% H→L	60% H-1→L
					11% H-1→L	37% H→L

5.3.2 Electrochemical Properties

To probe the frontier orbitals energy levels, we used both CV and DPV in DCM solutions (Figure 48 and Figure 49). For DTP-L4 and DTP-B4, the oxidation peaks were irreversible, as the evolution of the cation radical lead to dimerization or oligomerization processes.[181] Thus for those compounds, we approximated the HOMO via the difference between the LUMO, obtained by electrochemistry and the lowest energy of optical transition, obtained by spectroscopy. All other sensitizers, end-capped with methyl groups, exhibit reversible oxidations, and therefore permit a direct measure of the frontier orbital levels. Quantitatively, the reduction potential for the L (Figure 48) (resp. B, Figure

49) series is centered on -1.47 V (resp. - 1.39 V). Oxidation potentials decrease with the increase of thiophene donors, in agreement with the DFT calculations. Consequently, the energy gaps decrease with the lengthening of the conjugated system.

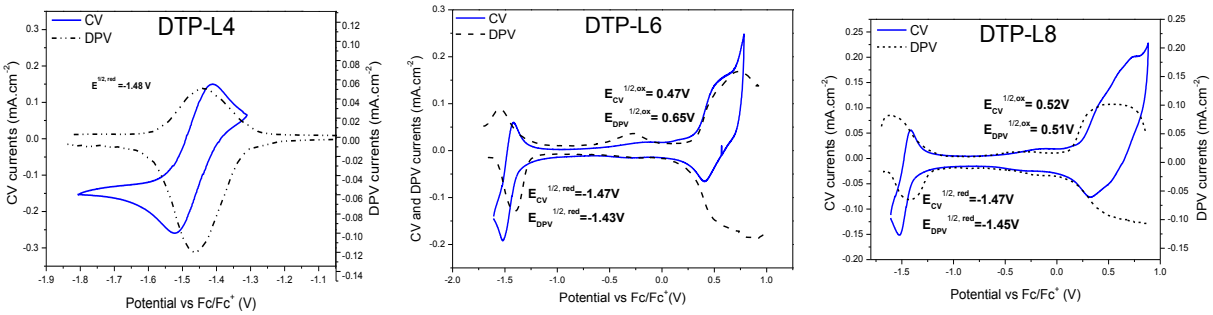

Figure 48: CV and DPV voltammograms for DTP-L4, L6 and L8.

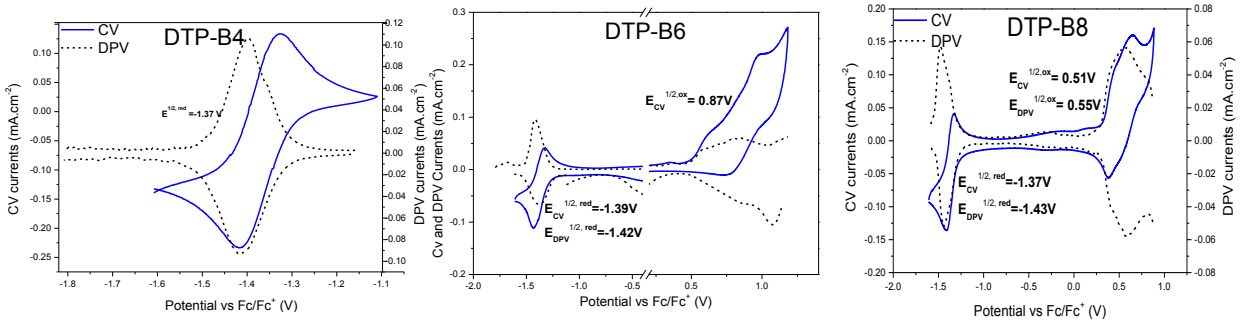

Figure 49: CV and DPV voltammograms for DTP-B4, B6 and B8.

Frontier orbital levels are gathered in Figure 50, and reflect that all dyes are suitable for electron injection onto the TiO_2 CB and dye regeneration with the iodine/triiodide redox couple.[182] Figure 50 also present a graphical illustration of the frontier orbital, which is extremely useful when comparing HOMO and LUMO orbitals at a glance. For example, based on this figure, it is clear that the LUMO values depend on the isomer core, but not on the number of donor units, whereas the HOMO values are dependent of the number of thiophene units and on the isomer. Also, Figure 50 clearly depicts the reduction of the energy gaps for longer isomers DTP-L8 and DTP-B8.

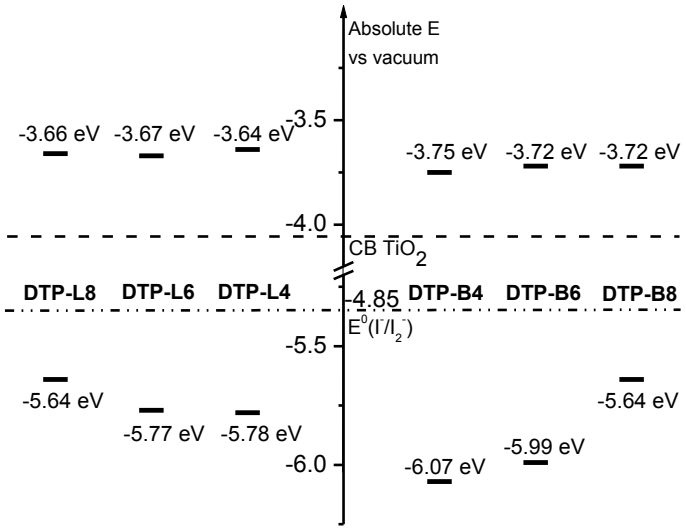

Figure 50: Frontier orbitals for DTP-Ln and DTP-Bn sensitizers obtained by electrochemistry.

5.3.3 Optical Properties

The UV-visible absorption spectra in DCM solution, presented in Figure 51, are consistent with the trends given by DFT calculations and electrochemical studies, and portrays the red shift of the L family, relatively to the B species. Broadened and bathochromic shifted spectra are observed in both series with the lengthening of the conjugated chain. However, the red shift is not linear, and the difference in λ_{max} between DTP-L6 and DTP-L8 is small (5 nm), indicating that the effective conjugation length is of ≈ 6 thiophene units for DTP-L. Hence, having more than six thiophene units on the DTP-L oligomer will not enhance the light absorption of the resulting molecules. Moreover, the spectra exhibit well resolved fine structures, persisting with the building of the donor chain. This is indicative of a rigidification of the conjugated system.[181] Contrastingly, the effective conjugation length is not reached for the B series, and the broad and structureless band reflects the multiple transitions forming the vertical transitions (as shown by TDDFT), and the presence of some conformational disorder in

the conjugated backbone. Extinction coefficients are high, above 50 000 $M^{-1}\cdot cm^{-1}$ for the L family, and above 75 000 $M^{-1}\cdot cm^{-1}$ for the B series, which make these molecules attractive as sensitizers.

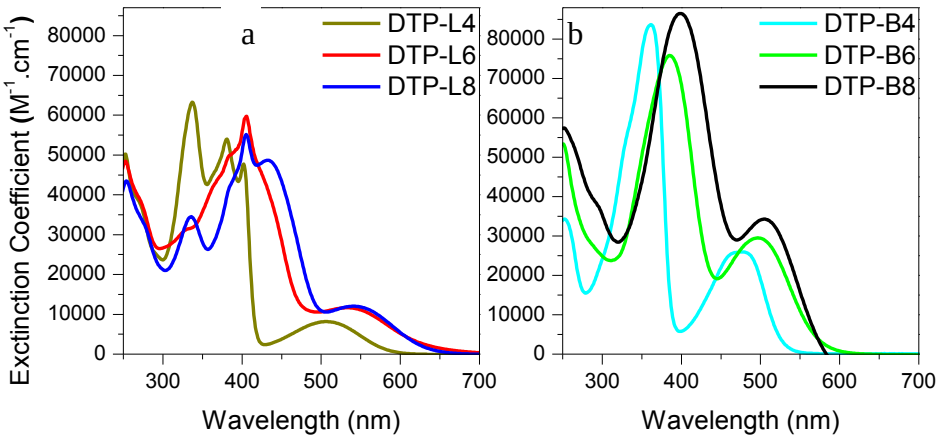

Figure 51: UV-Vis spectra of the (a) DTP-Ln and (b) DTP-Bn series in solution.

5.3.4 Excited States Properties.

In order to probe the properties of the singlet excited states for the oligomers, fluorescence studies were carried out in DCM solution and the results are collected in Table 12. The fluorescence spectra of all oligomers appear as broad, structureless bands (Figure 52). The band maxima for the DTB-B series red-shift with increasing oligomer length: from 580 nm for DTP-B4 to 725 nm for DTP-B6 to 775 nm for DTP-B8. However, the fluorescence maximum is similar for DTP-L6 and DTP-L8 (760 nm and 750 nm, respectively), suggesting that in this series, the conjugation length is limited to ≈6 thiophene repeats. This agrees with the same trend seen in the absorption spectra for the DTP-L series.

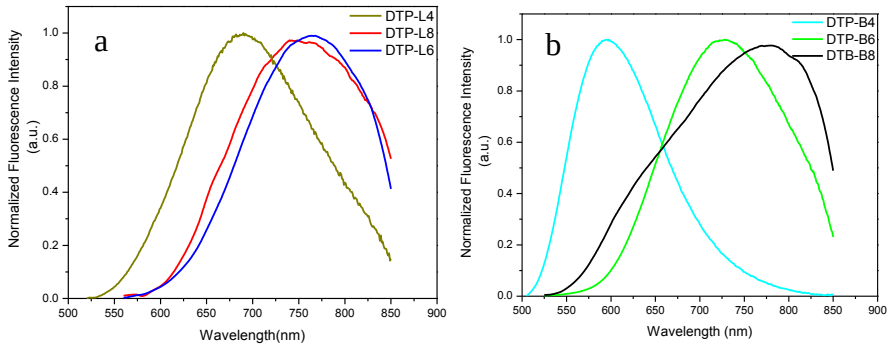

Figure 52: Emission spectra of (a) DTP-Ln and (b) DTP-Bn families in DCM solutions.

The fluorescence quantum yields for the oligomers are comparatively low (Φ_F<0.07), and they generally decrease with the lengthening of the oligomer. More insight into the excited state dynamics is provided by the fluorescence lifetimes and the radiative and non-radiative rates, which are shown in Table 14. For both series, the radiative rates are in the range of 10^7 s^{-1}, which is on the low-side for conjugated organic chromophores;[168,183] the reason for this is likely due to the charge transfer character of the lowest singlet states.

Table 14: Photophysical Data for DTP-Ln and DTP-Bn series[a]

Compd	λ_{max} (nm)	λ_F (nm)	τ_F [b] (ns)	Φ_F [c] (%)	k_r [d] (10^6 s^{-1})	k_{nr} [d] (10^7 s^{-1})
DTP-L4	336, 380, 402, 505	680	10.60	7.4	7.0	8.7
DTP-L6	404, 529	760	3.26	4.7	14.4	29.2
DTP-L8	332, 405, 433, 534	750	1.98	3.5	17.7	48.7
DTP-B4	361, 478	580	0.78	1.3	16.7	126.5
DTP-B6	385, 497	725	0.78	0.8	10.3	127.2
DTP-B8	400, 503	775	0.78	0.5	6.4	127.6

[a]Measurements for DCM solutions at ambient temperature. [b] Emission lifetime measured at fluorescence emission maximum (see left adjacent column). [c] Measured using $Ru(bpy)_3$ (Φ_F = 0.055 in water) as the actinometer. [d] $k_r = \Phi_F/\tau_F$; $k_{nr} = (1-\Phi_F)/\tau_{Fc}$

For the DTP-L set, the lifetimes systematically decrease with the lengthening of the oligomer: from 10.6 ns for DTP-L4 to 3.3 ns for DTP-L6 to 2.0 ns for DTP-L8 (Figure 53). This decrease is due to a combined enhancement in both the radiative non-radiative decay rate along the series. The rise in k_r is likely due to the increased conjugation, and that for k_{nr} may be due to the charge transfer nature of the singlet excited state. By contrast, the lifetimes for all of the DTP-B oligomers are equal (0.8 ns) and comparatively short. This is due to a relatively constant and large non-radiative decay rate ($\approx 10^9$ s^{-1}) for all members of the set. The relatively large non-radiative rates for the oligomers may also be due to the charge transfer character of the singlet excited state.

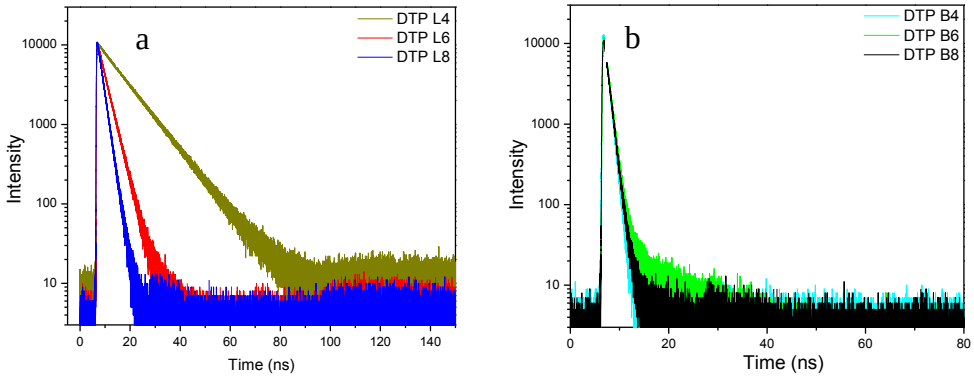

Figure 53: Fluorescence electron lifetime in (a) DTP-Ln and (b) DTP-Bn series.

5.4 Incorporation of the Sensitizer into Devices and their Properties

5.4.1. UV-Visible Absorption

Carboxylic acids derivatives of the oligomers were used for adsorption onto mesoscopic TiO_2 films. Figure 54 shows the UV-visible absorption spectra of the sensitizers adsorbed onto the metal oxide films. All films give rise to relatively strong absorption, with those

for the longer oligomers exhibiting >90% absorption (A > 1.0) for λ < 600 nm. Note that the absorption bands are broadened due to the adsorption onto TiO_2.[184]

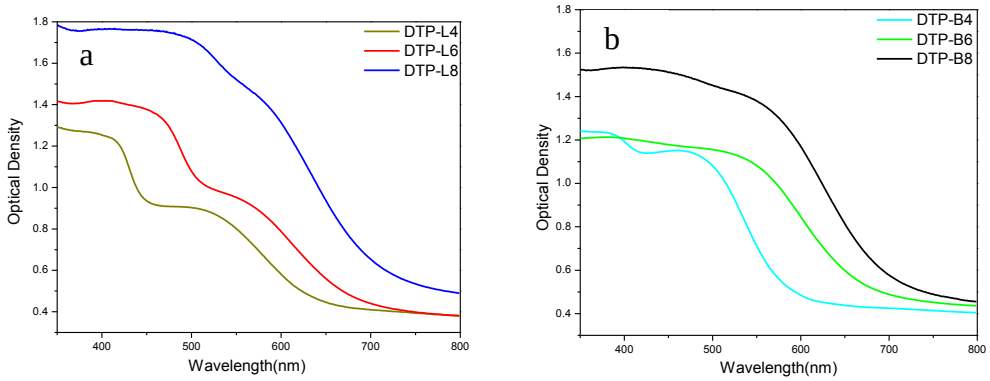

Figure 54: UV-visible spectra of (a) DTP-Ln and (b) DTP-Bn compounds adsorbed on titanium dioxide nanoparticles.

5.4.2 Transient Absorption

To explore the charge injection and recombination properties of the dyes on TiO_2, nanosecond transient absorption (TA) studies were carried out on the dyes adsorbed on TiO_2 film while they are immersed in ACN solution with $LiClO_4$ electrolyte. In this experiment, the sensitizers are photoexcited by a laser pulse. One of the electrons from the sensitizer is excited and gets injected into the metal oxide. The resulting dye cation radical, stabilized by the electrolyte, is probed via spectroscopy, as the cation state of the dye has characteristic absorption bands that differ from the band observed for the dye in its ground state. The electron in the metal oxide band can recombine with the oxidized dye, regenerating the sensitizer in its neutral state. Figure 55 shows the TA signals as a function of the wavelength. The y-axis represents the absorption transients, which are the logarithmic ratio between the light intensity prior to the laser pulse and the light intensity 70 ns after the laser pulse. Figure 55b, representing the branched sensitizers, demonstrates a typical spectrum for the TA experiment: at shorter wavelengths, (< 600

nm), the signal is obscured, due to the strong ground state absorption of the films. Over 600 nm, where the neutral dye is not absorbing anymore, the signals observed arise mainly from the cation radical dyes, and to a lesser extent from the adsorption of the electrons into TiO_2. Figure 55a is more difficult to interpret as the variation in amplitude of the absorption transients is small. This correlates well with the finding of Chapter 4, section 4.4, where DTP-L4 in solution exhibits a weak TA signal. The presence of transient signals throughout the spectra illustrates the strong absorption of the films as well as the appearance of intermediate and cationic species following laser photoexcitation.

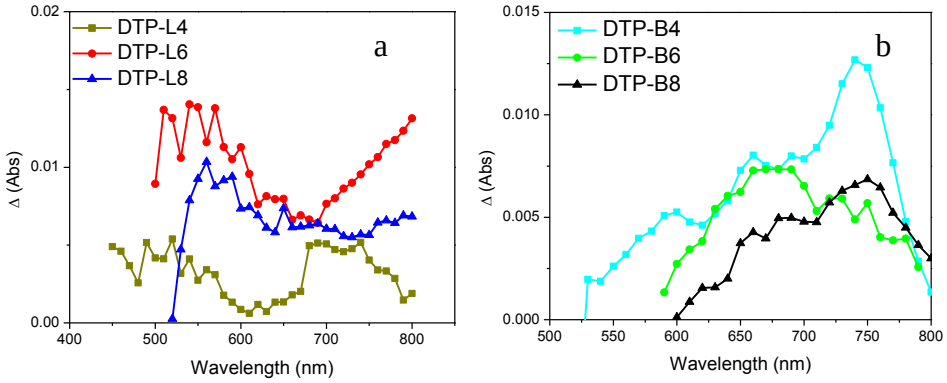

Figure 55: Nanosecond transient absorption spectra of (a) DTP-Ln and (b) DTP-Bn families adsorbed on titanium dioxide nanoparticles.

Charge recombination kinetics were probed in order to determine the timescale of the recombination between the oxidized dye and the electron in the TiO_2 CB, as shown in Figure 56. The data were satisfactorily fitted exponentially which indicates that charge recombination dynamics is homogeneous and dominated by interfacial electron-transfers.[185] The lifetimes were found to be 502, 65 and 10 μs for DTPB-4, DTPB-6 and DTPB-8 respectively, and 134, 30 and 32 μs for DTPL-4, DTPL-6 and DTPL-8 respectively. It is interesting that the charge recombination kinetics for the longer

oligomers is shorter than for the smaller oligomers. This trend has been observed by Yao and co-workers,[186] when studying oligothiophene-perylene bisimide dyads. After a full photophysical study, they assert that, as the size of the oligothiophene increases, so does the density of states. Thus, the electronic coupling between the oligothiophene and the acceptor is enhanced, and thereby produces faster charge separation and charge recombination processes. For the D_2A sensitizers, the appearance of the strong transient absorption and the relatively long lifetimes (slow recombination) suggest that the dyes should function well as sensitizers in a DSSC configuration.

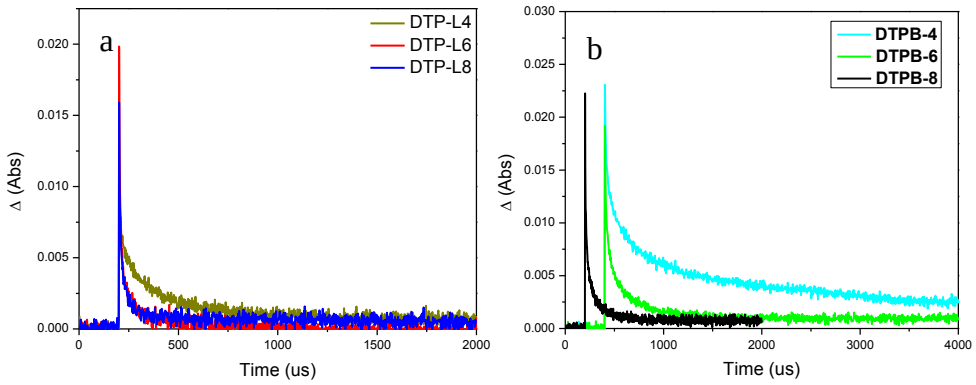

Figure 56: Charge recombination kinetic traces of (a) DTP-Ln and (b) DTP-Bn series adsorbed on titanium dioxide nanoparticles.

5.4.3 Incident Photon-to-Current Efficiency

The dyes were tested in a standard DSSC set-up as a means of carrying out an initial structure : property relationship comparison. We tested only a single DSSC configuration (*e.g.*, solvent, electrolyte, additives), so these device results should be viewed as "unoptimized", therefore they do not show the maximum efficiencies that can be attained. In this study, the results were reproducible and Figure 57 depicts the incident photon-to-current efficiencies for the series of dyes. The IPCE plateaued moderately above 38% from 400 nm to 490 nm for DTP-L8, and above 33% from 420 nm to 540 nm for DTP-

B8, following the trends observed in the UV-visible absorption spectra of the films. A clear improvement is observed with the lengthening of the oligomeric chain: the IPCE response extends into the near IR region for DTP-L6,8 and DTP-B6,8 (λ>700nm) and increase in intensity in the higher energy region. As stated in the introduction, integrating the curve under the IPCE will give an approximation of the current density, and in Table 15, the currents obtained from the IPCE spectra are in good agreement with those measured directly.

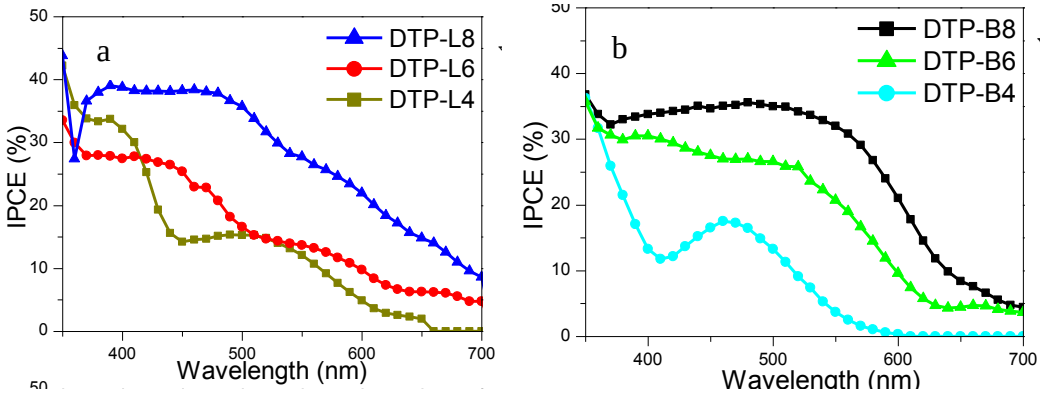

Figure 57: Incident photon-to-current efficiency in the visible region for (a) DTP-Ln series and (b) DTP-Bn series.

5.4.4 J- V Curves and Overall PCE

After measuring IPCE, the current density and voltage responses were recorded and shown in Figure 58. Both V_{oc} and J_{sc} increase with the number of thiophene units. For the current density, this is likely due to the absorption of more photons, as demonstrated with UV-visible absorption and IPCE data. For the open circuit voltage, we infer that the long oligothiophene chain impart dye aggregation and recombination between TiO_2 and the redox couple, hence raising the free electron density. [174,175] Interestingly, V_{oc} values are quasi-independent of the isomer used, indicating that the isomer has a weak to no effects

on the surface charge of TiO_2, or on the balance between electron injection and electron recombination. However, the current densities increase for the branched quadrupolar dyes, and that can be related to the dye harvesting properties that are stronger for the DTP-B series. Interestingly, the photophysical effects seem to be too slow to be noticed, when comparing to the fast femtosecond electron injection to the TiO_2 CB. The maximum power conversion efficiencies for the longest oligomers are of 1.60% for DTP-L8 and 1.78% for DTP-B8. These numbers are to compare with the power conversion efficiency of 3.29% obtained when using the reference N_3 dye.

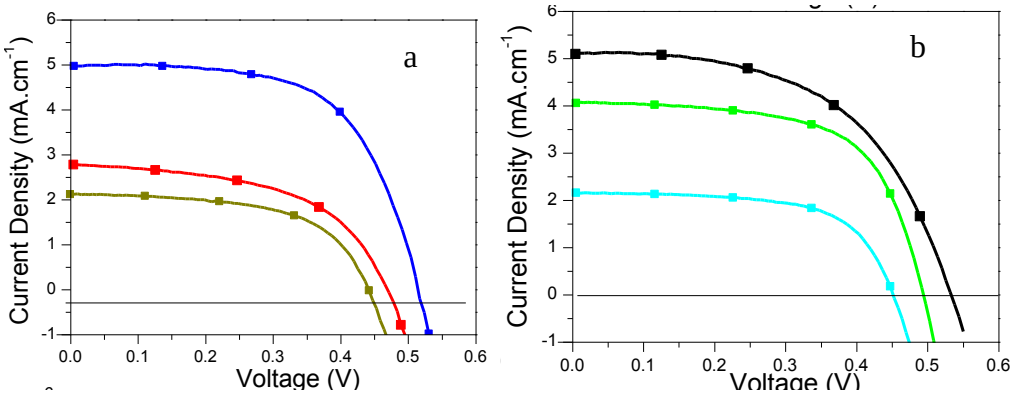

Figure 58: Current density-voltages responses for (a) DTP-Ln series and (b) DTP-Bn series.

Table 15: Summary of Solar Cells Characteristics under 1.5M illumination for DTP-Ln, DTP-Bn and N3.

Compd	J_{sc}^{IPCE} ($mA \cdot cm^{-2}$)	J_{sc} ($mA \cdot cm^{-2}$)	V_{oc} (V)	FF	PCE (%)
DTP-L4	2.12	2.12	0.44	0.58	0.55
DTP-L6	2.76	2.78	0.47	0.53	0.70
DTP-L8	5.16	4.97	0.52	0.62	1.60
DTP-B4	1.33	2.18	0.47	0.66	0.68
DTP-B6	3.40	4.05	0.50	0.63	1.27
DTP-B8	5.16	6.01	0.52	0.57	1.78
N3	n/a	11.41	0.69	0.42	3.29

5.5 Conclusion on the Study of Lengthening the Donor Units

We presented quadrupolar D_2-A molecules with increasing number of thiophene donors. These sensitizers provide two channels for absorbing light and funneling the energy to a single acceptor attached to TiO_2. Lenghtening the oligomeric chain red-shifted the absorption, increasing the light harvesting ability and decreasing the energy gap. The linear isomers present a structure more rigid than the branched isomers, reflecting on the relaxation process of the excited states, with the increase of both radiative and non-radiative rates with the lengthening of the donor chain. These molecules were integrated into DSSCs, and generate working devices. Addition of external donors to the system significantly improves the photovoltaic results, and the increasing trend is linear with the number of donor units added. Optoelectronic and photophysical studies proved that overall IPCE increase is due to the improved LHE and the faster charge separation and charge recombination for the long oligomers. Interestingly, the isomerism affects slightly the photovoltaics properties even though their solution optoelectronic properties differ. The difference in the film lifetimes, on the nanosecond timescale, do not affect the femtosecond electron injection from the sensitizer to the TiO_2 CB [47]. However, the stronger absorption properties of the branched series permit an increase both in IPCE and J-V.

5.6 Synthesis of the Sensitizers with Different External Donors

In the subsequent sections, we will investigate the effect of using different donors appended to the dithienophenazine core. For that, we employed DTP-B4 sensitizers, studied in the first section of this chapter as our reference dye. It will be called consequently Th-DTP. The two other donating units employed are propylene-

dioxythiophene (ProDOT) and dithienosilole (DTS). The units have been known to increase the light harvesting efficiency of the systems by extending the optical absorption to higher wavelength regions.[49] The structures of the sensitizers are shown in Figure 59.

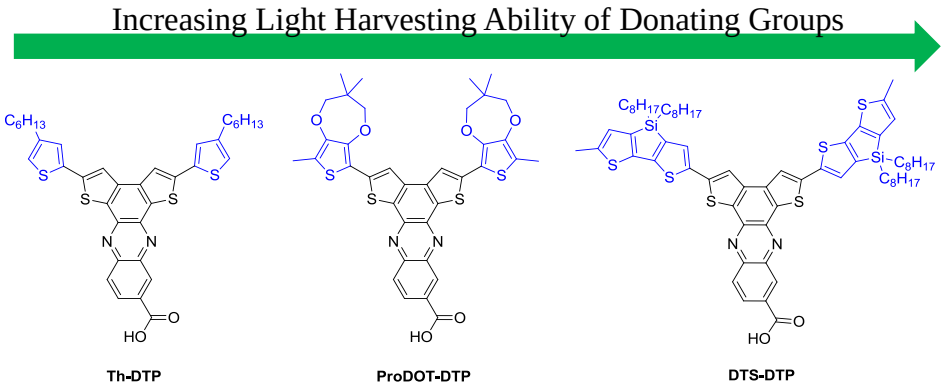

Figure 59: Molecular structure of Th-DTP, ProDOT-DTP and DTS-DTP sensitizers.

The synthesis strategy for the dyes is the same as applied previously. Synthesis of Th-DTP is presented in Chapter 4. For the two others sensitizers, the external donor units were synthesized first, and then attached onto the dithienophenzaine core. The donor units were methylated in one of α-positions, to avoid any irreversibility upon oxidation, effect commonly observed in the dyes presented in Chapter 4. To do so, the precursors **5.11** and **5.14** were treated with one equivalent of n-butyl lithium, and the anion was quenched by iodomethane, as shown in Scheme 14. The purification of the non-methylated, mono-methylated or di-methylated was done with column chromatography for the ProDOT precursor, and via high-performance liquid chromatography for the DTS precursors. The low yield observed with the latter is due to the difficulty in separating the non-methylated DTS from the mo-nomethylated and di-methylated DTS. The intermediates **5.12** and **5.15** were treated a second time with one

equivalent of n-butyl lithium, and quenched this time with trimethylchloride stannanne, to form the stannanes derivatives **5.13** and **5.16** in good yields (94-95%).

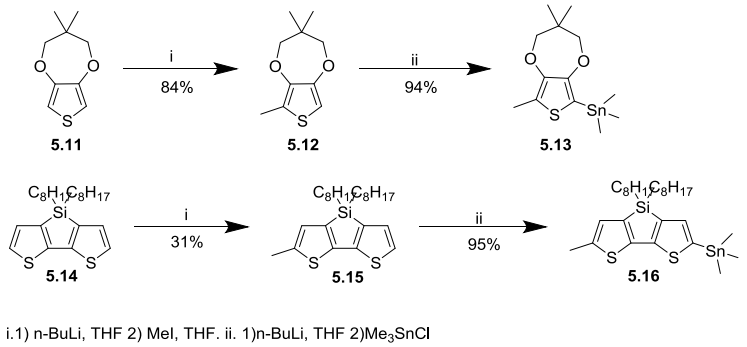

Scheme 14: Synthesis of the external donors unit for ProDOT-DTP and DTS-DTP

The donor units **5.13** and **5.16** were grafted onto the DTP core **5.10** via Stille coupling in the microwave. Purifications were done *in duplicate* by column chromatography to ensure purity of the target molecules ProDOT-DTP and DTS-DTP (Scheme 15). After troubleshooting, the conditions for hydrolysis were determined by dissolving the ethyl esters into dioxane, and were heated in the microwave with the presence of 5 M KOH for 10 min at 150 ^{o}C. The carboxylic acids ProDOT-DTP*a* and DTS-DTP*a* did not need to be purified as the NMR showed a purity >97%.

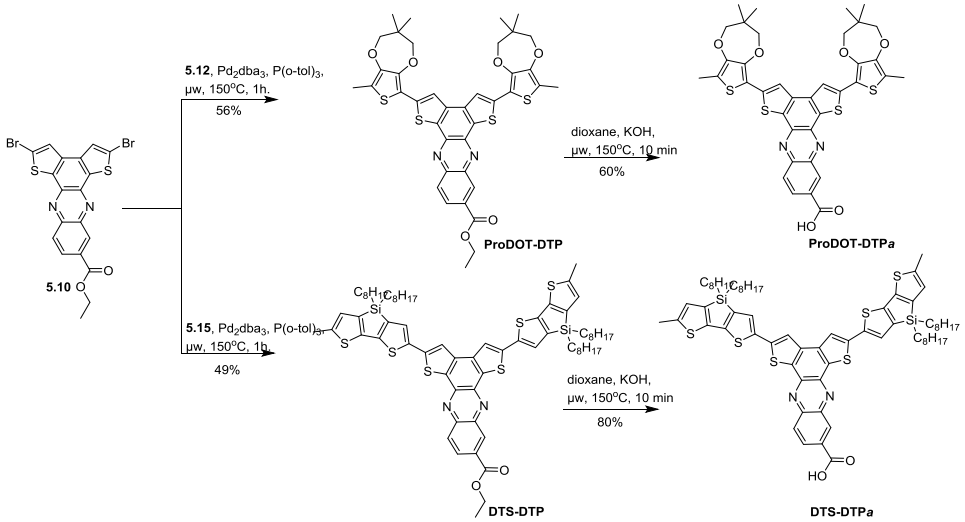

Scheme 15: Synthesis of ProDOT-DTP and DTS-DTP

5.7 Ground State and Excited State Characterizations

5.7.1 Density Functional Theory Computations

All molecules were modeled using DFT computations, at the B3LYP/6-31G** level in vacuum. With no surprise for these types of quadrupolar D_2-A molecules the LUMO wave functions (Figure 60, top molecules) are localized on the acceptor core, independent of donor units. As the molecules are asymmetrical with the presence of one carboxylic acid on the phenazine units, the HOMO and HOMO-1 levels are quasi-symmetrical and quasi-degenerated, with a difference of energy of 0.13 eV for Th-DTP and 0.04 eV for ProDOT-DTP and DTS-DTP (Figure 60). The HOMO and HOMO-1 orbitals densities are delocalized on the entire molecule for Th-DTP, whereas for ProDOT-DTP and DTS-DTP have greater orbital densities on the donating groups. The HOMO values are destabilized from Th-DTP to ProDOT-DTP to DTS-DTP, and the LUMO values, varying from -2.45 eV to -2.73 eV are high enough to predict a facile electron injection into TiO_2.

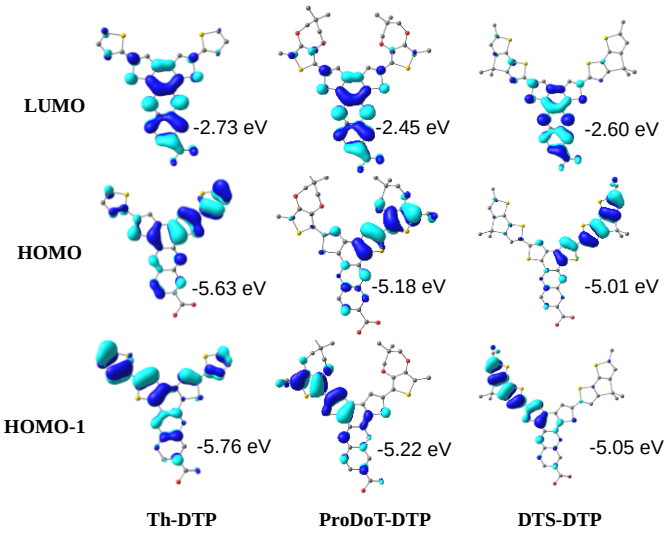

Figure 60: HOMO-1, HOMO and LUMO representation for Th-DTP, ProDOT-DTP and DTS-DTP.

TDDFT computations predict a bathochromic shift from Th-DTP to ProDOT-DTP to DTS-DTP, accordingly to the decrease in the energy gaps. Moreover, the low energy transitions (λ= 476 nm for Th-DTP, λ=509 nm for ProDOT-DTP and λ=575 nm for DTS-DTP) are a mix of HOMO-1 to LUMO and HOMO to LUMO. It is interesting to note that the shape of ProDOT-DTP absorption is nearly a copy of Th-DTP, red-shifted by 70 nm.

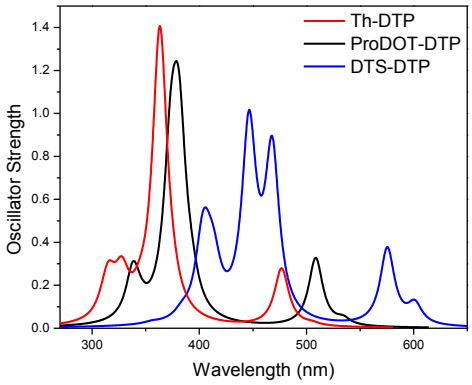

Figure 61: Simulated UV-visible spectra of Th-DTP (red), ProDOT-DTP (black) and DTS-DTP (blue).

5.7.2 Electrochemical properties

The electrochemical properties of Th-DTP have been reported in Chapter 4. CV and DPV for ProDOT-Th and DTS-DTP are shown in Figure 62. The molecules exhibit reversible oxidation and reduction waves. For ProDOT-DTP, one electron reduction wave is observed at -3.58 eV and two reversible oxidation waves are observed at -5.71 eV and at -5.82 eV. Roncali *et al.*[181] similarly reported double oxidation wave for ProDOT derivatives, that corresponds to the cationic and dicationic species. For DTS-DTP, a single oxidation wave at -5.62eV and two reductions waves are seen at respectively -3.32 eV and -3.62 eV.

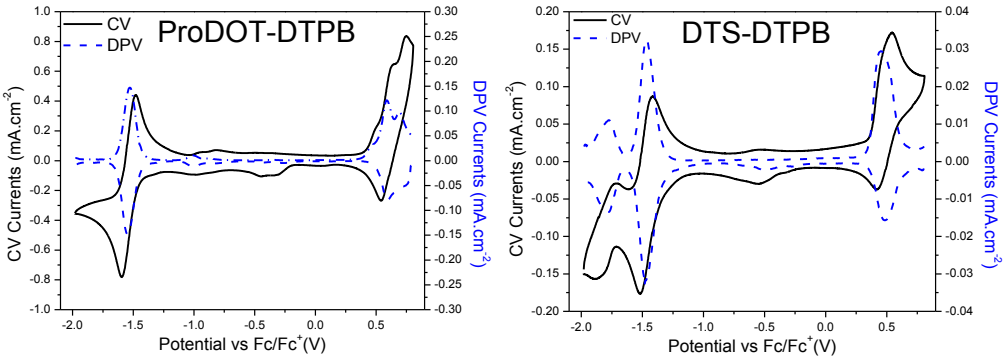

Figure 62: Cyclic voltammogram and differential pulse voltammogram in dichloromethane solution for ProDOT-DTP and DTS-DTP.

Figure 63 shows the frontier orbitals levels of the sensitizers, compared with the TiO_2 CB, and the redox potential of the iodine/triiodide couple. As observed with other D_2-A sensitizers, the LUMO levels for the dyes are above the TiO_2 CB, predicting a thermodynamically feasible electron injection from the excited state of the dye onto the TiO_2 nanoparticles. As predicted by DFT calculations, the HOMO values are destabilized from Th-DTP to ProDOT-DTP to DTS-DTP. Some studies indicate that an offset of at least 0.4 eV of the HOMO of the sensitizers from the redox couple potential is required to regenerate the ground state dye,[67] and this condition is verified here, with the driving force varying from 1.17 eV to 0.77 eV.

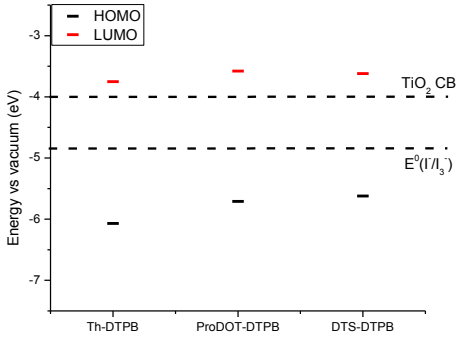

Figure 63: Frontier orbitals for Th-DTP, ProDOT-DTP and DTS-DTP obtained by electrochemistry.

5.7.3 Absorption and Emission Studies

The experimental UV-visible spectra, displayed in Figure 64, match the computational trends obtained with TDDFT. A bathochromic shift is observed in the order of Th-DTP to ProDOT- DTP to DTS-DTP. Between Th-DTP and ProDOT-DTP, the red shift can be explained by the presence of the π-donating oxygen atoms. For DTS-DTP, the overall π system increases (4 more rings), thus explaining that this unit is the most red-shifted. However, when comparing DTS-DTP with a system with the same amount of thiophene rings (*i.e*. DTP-B6 in the beginning of the chapter), DTS-DTP has a bathochromic shift compared to DTP-B6. Thus, the overall bathochromic shift is also caused by the addition of the ring formed with the tetrahedron silicon center. The emission maxima follow the order of the absorption maxima, with a red shift from Th- to ProDOT- to DTS-DTP.

Quantum yields were recorded, using tris(bipyridine)ruthenium (II) chloride as the actionometer, and are low: 1.3 % for Th-DTP, 3.6 % for ProDOT-DTP and 2.11 % for DTS-DTP.

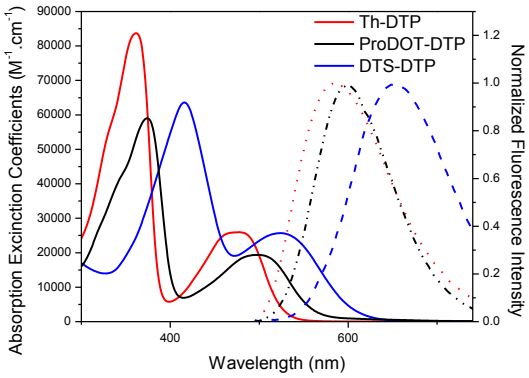

Figure 64: UV-visible (plain lines) and fluorescence (dotted lines) of Th-DTP (red), ProDOT-DTP (black) and DTS-DTP (blue).

Table 14 summarizes the spectroscopic and electrochemical properties, such as the absorption maxima, the energy gaps obtained by the optical onset and electrochemistry,

the frontier orbital values and the quantum yields for the three sensitizers. To note, the energies gaps obtained electrochemically and optically match closely, validating the experiments.

Table 16: Optoelectronic properties for Th-DTP, ProDOT-DTP and DTS-DTP in DCM solution.

Compd	λ_{max} nm ($\varepsilon.10^4$)	E_{gap}^{Opt} (eV)	λ_{em} (nm)	HOMO (eV)	LUMO (eV)	E_{gap}^{CV} (eV)
Th-DTP	361 (8.4), 475 (2.6)	2.34	588	-6.07	-3.75	2.32
ProDOT-DTP	374(5.9), 496 (1.9)	2.19	599	-5.71	-3.58	2.13
DTS-DTP	415 (6.4), 523 (2.6)	2.03	654	-5.62	-3.62	2.00

Further photophysical studies were conducted to characterize the excited states. Time-resolved fluorescence spectroscopy (Figure 65) provides a mono-exponential lifetime of 0.78 ns for Th-DTP. Both ProDOT-DTP and DTS-DTP have double-exponential signals, and their average lifetimes are of 1.3 ns for ProDOT-DTS and 1.18 ns for DTS-DTP. Interestingly, the number of thiophene units has no effect on the electron lifetime, as seen in section 5.3.4. However, changing the nature of the donor unit influences the lifetime. The variation in lifetime is small, and both the radiative and non-radiative decays are within the same order of magnitude.

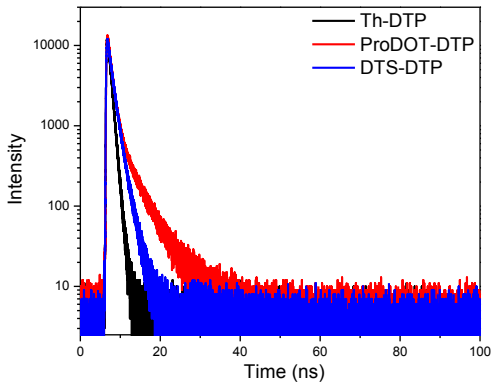

Figure 65: Time-resolved fluorescence spectroscopy of Th-DTP, ProDOT-DTP and DTS-DTP.

Table 15 reviews the absorption and emission data as well as the radiative and non-radiative rate constants. As seen previously, the radiative rate constant for these molecules are on the low-side for conjugated organic chromophores, around 2.10^7 s^{-1}. This is due to the charge transfer character of the lowest singlet state. The non-radiative rate constants are smaller for ProDOT-DTP and DTS-DTP than for Th-DTP, due to the stronger quantum yield.

Table 17: Compilation of photophysical data for Th-DTP, ProDOT-DTP and DTS-DTP.

Compd	λ_{max} (nm)	λ_F (nm)	τ_F [b] (ns)	Φ_F [c] (%)	k_r [d] (10^6 s^{-1})	k_{nr} [d] (10^7 s^{-1})
Th-DTP	361, 475	588	0.78	1.3	16.7	126.5
ProDOT-DTP	374, 496	599	1.31	3.6	27.6	73.8
DTS-DTP	415, 523	654	1.18	2.1	17.9	83.2

5.8 Incorporation of the Sensitizer into Devices and Their Properties

Carboxylic acids derivatives of the oligomers were used for adsorption onto mesoscopic TiO_2 films. The dyes were then tested in a standard DSSC set-up as a means of carrying out a structure : property relationship comparison. As seen in the previous section, we tested a single DSSC configuration (e.g., solvent, electrolyte, and additives).

5.8.1 IPCE

IPCE responses for Th-DTP, ProDOT-DTP, and DTS-DTP are presented in Figure 66. It can be seen that the Th-DTP is more efficient that our previous trials: the IPCE peaks at 30%. This improvement is most likely due to the new TiO_2 paste used for the latter devices. When looking at the two other sensitizers, they surprisingly bear weaker IPCE values, maximizing at 10-15% at 450-500 nm.

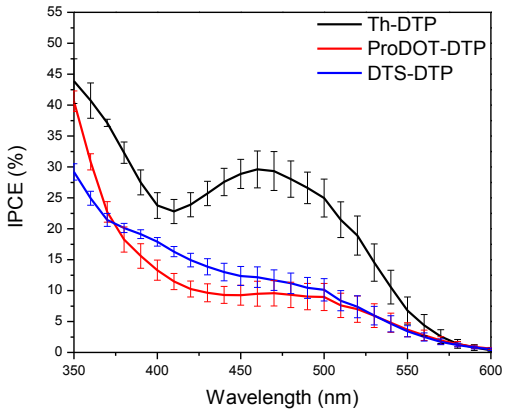

Figure 66: IPCE responses for Th-DTP, ProDOT-DTP and DTS-DTP.

This decrease in IPCE is unexpected, as the frontier orbital levels and the absorption properties were predicting favorable conditions for ProDOT-DTP and DTS-DTP. To understand the cause of the poor IPCE, its different components need to be evaluated. As stated in the introduction,

$$IPCE = APCE \times LHE = \varphi_{inj} \times \eta_{coll} \times \eta_{reg} \times LHE \quad (16)$$

Where APCE is the absorbed photon-to-current conversion efficiency, LHE is the light harvesting efficiency, η_{coll} is the collection efficiency, η_{reg} is the regeneration efficiency and φ_{inj} is the electron injection.

The LHE is the parameter that was designed to be enhanced, and can be calculated via the formula

$$LHE_{\lambda} = 1 - 10^{-A(\lambda)} \quad (13)$$

where A is the absorbance of the dyes adsorbed onto TiO_2 films.

The absorption of the dyes adsorbed onto TiO_2 slides were measured, and the LHE is plotted in Figure 67. This figure illustrates that the intensity of the LHE is similar for Th-DTP and ProDOT-DTP. For DTS-DTP, there is a clear enhancement of the LHE, both in

term of intensity and in the absorption of lesser energy photons, up to 800 nm. Our design meets the expected properties: the light harvesting is enhanced when using DTS-DTP, and it is not the parameter responsible for the low IPCE for ProDOT-DTP and DTS-DTP.

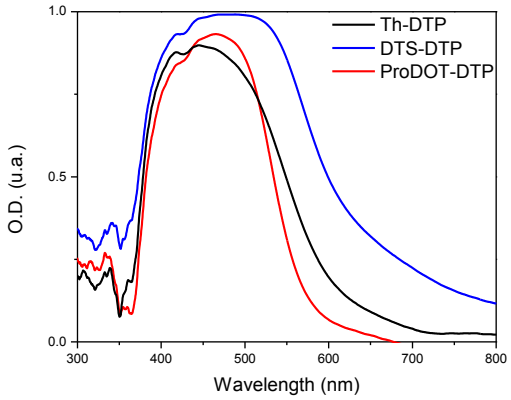

Figure 67: Light harvesting efficiency for Th-DTP, ProDOT-DTP and DTS-DTP.

The next parameter to investigate is the electron injection. The electron injection (φ_{inj}) is related to the driving force ΔG_{inj} of electron injecting from the excited states of dye molecules to the semiconductor substrate.[60] It can be estimated as

$$-\Delta G_{inj} = -e(E^{dye*} - E_{CB}) = -e(E^{dye} - \frac{E_{0-0}}{e} - E_{CB}) \quad (14)$$

Where E^{dye*} represents the oxidation potential of the excited dye, E^{dye} is the redox potential of the ground state of the dyes, $E_{0\text{-}0}$ is the vertical transition energy and E_{CB} is the conduction band edge of the semiconductor.[60] E^{dye} is known through electrochemistry and $E_{0\text{-}0}$ is known through spectroscopic studies (crossing point between the absorption and emission spectra), the values of which can be seen in Table 18. It is difficult to determine exactly E_{CB} as the value is sensitive to the surface condition, the adsorbed dyes and the pH of the solutions. However, the total change is predicted to be less than 0.1 V. According to reference 60, the E_{CB} value is -0.5 V.

Table 18: Oxidation potential, vertical transition energy and driving force for Th-DTP, ProDOT-DTP and DTS-DTP.

Compd	E^{dye} (V)	E_{0-0} (eV)	E^{dye*} (V)	$-\Delta G_{inj}$ (eV)
Th-DTP	0.97	2.41	-1.44	0.94
ProDOT-DTP	0.59	2.32	-1.73	1.23
DTS-DTP	0.50	2.17	-1.67	1.17

The calculated E^{dye*} are of -1.44 V for Th-DTP, -1.73 V for ProDOT-DTP and -1.67 V for DTS-DTP. The obtained negative entropies for electron injection are comprised between 0.9 and 1.2 eV. Katoh *et al.*[60] show that the electron efficiency attain a plateau when $-G_{inj} > 0.5$ eV. Then, the change in IPCE can not be explained by the electron injection.

Then, the most probable influencing factors for the poor IPCE for ProDOT-DTP and DTS-DTP are the collection efficiency η_{coll} and the regeneration efficiency η_{reg}. The underlying limiting processes of the collection efficiency (η_{coll}) are recombination and diffusion, and could be due to the aggregation of the molecules, or the recombination of the electron on the TiO_2 CB with the oxidized dye, or the electrolyte.[59] These factors are difficult to measure, and technical studies, such as transient absorption spectroscopy and electrochemical impedance spectroscopy would need to be performed to quantify the reason behind the low IPCE.

5.8.2 J/V Curves and Overall Power Conversion Efficiency

The photocurrent density-voltage responses of cells made from the three sensitizers in combination with the iodide/triiodide electrolyte were also measured under the irradiance of 100 mV. cm^{-2} simulated under AM1.5 solar simulator, and the detailed cell parameters are shown in Figure 68 and are compiled in Table 19. Th-DTP exhibits a short circuit

photocurrent density (J_{sc}) of 3.27 mA·cm^{-2}, an open-circuit voltage (V_{oc}) of 0.56 V and a fill factor (FF) of 0.62, generating a power conversion efficiency (PCE) of 1.13%.

Both ProDOT-DTP and DTS-DTP sensitizers present a lower J_{sc} of 1.34 and 1.42 mA·cm^{-2} respectively, and a shrunk of the V_{oc} at 0.51 V for ProDOT-DTP and 0.46 V for DTS-DTP. The resulting PCE is reduced to 0.40% for ProDOT-DTP and 0.44% for DTS-DTP.

The lowering J_{sc} is to be correlated with the poor IPCE values obtained for ProDOT-DTP and DTS-DTP. The V_{oc} change is more difficult to explain, but as seen in Chapter 4, the stronger dipole moment of the dyes ProDOT-DTP and DTS-DTP could be responsible of the decrease in open-circuit voltage.

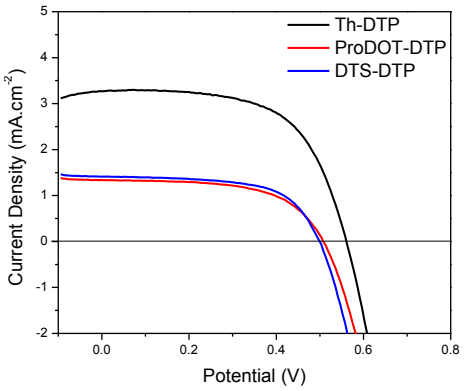

Figure 68: J-V responses for Th-DTP, ProDOT-DTP and DTS-DTP.

Table 19: Summary of solar cells characteristics under 1 sun AM1.5 solar illumination for Th-DTP, ProDOT-DTP and DTS-DTP.

Compd	Voc (V)	Jsc (mA.cm^{-2})	FF	PCE (%)
Th-DTP	0.56 ± 0.01	3.27 ± 0.33	0.62 ± 0.02	1.13 ± 0.07
ProDOT-DTP	0.51 ± 0.01	1.34 ± 0.32	0.59 ± 0.02	0.40 ± 0.11
DTS-DTP	0.46 ± 0.07	1.42 ± 0.30	0.62 ± 0.01	0.44 ± 0.09

In conclusion, varying the nature of the donor units with moieties such as ProDOT and DTS enhances the light harvesting efficiency. However, the IPCE decreases when

comparing Th-DTP to the two new sensitizers. The reasons for the decrease are uncertain and likely a combination of several factors, including the aggregation of the dyes, generating excitons that can be transferred to a surrounding sensitizer, instead of being injected into the TiO_2, or poor charge collection efficiency. Each of these effects can be probed by the use of another redox couple, the addition of co-adsorbants, or more intricate experiments such as transient absorption spectroscopy and impedance spectroscopy.

5.9. Experimental Details

Compound **5.2** (2-bromo-3-hexylthiophene), compound **5.4** and trimethyl(5-methylthiophen-2-yl)stannane were synthesized as reported in literature.

General procedure for Stille Couplings (compounds 5.5and 5.7).

To a flame-dried round-bottom-flask equipped with a stir bar, 2-bromo-3-hexylthiophene (compound **5.2**, 1 equiv.), trimethyltin derivative (trimethyl(5-methylthiophen-2-yl)stannane or compound **5.6**, 1 equiv.) tris(dibenzylideneacetone) dipalladium(0) catalyst (4% equiv.) and tri(o-tolyl)phosphine ligand (12% equiv.) and toluene (50 mL/g of 2-bromo-3-hexylthiophene) were added. The reaction was allowed to stir overnight at 90oC under an inert atmosphere. The mixture was concentrated under reduced pressure and extracted successively with water, a 1M solution of potassium fluoride and water. The organic phase was dried with anhydrous magnesium sulfate, and the solution was concentrated under reduced pressure. The resulting oils were passed through a small column of silica pad with hexanes as eluant. The obtained fractions were concentrated under reduced pressure.

3-Hexyl-5'-methyl-2,2'-bithiophene (**5.5**).Yellow oil (83% yield) ^{1}H NMR (300 MHz, $CDCl_3$) δ_H: 7.14 (1H, d, J=5Hz), 6.92 (2H, m), 6.71 (1H, m), 2.73 (2H, t, J=7Hz), 2.50 (3H, s), 1.62 (2H, quint, J=7Hz), 1.32 (6H, m), 0.89 (3H, t, J=7Hz). ^{13}C NMR (75 MHz, $CDCl_3$) δ_C: 139.90, 139.10, 133.83, 129.80, 125.87, 125.48, 123.22, 31.68, 30.74, 29.23, 29.12, 22.63, 15.29, 14.10. HRMS (ESI-TOF) Calcd for $C_{15}H_{20}S_2$ $[M+H]^+$: 264.1006 found m/z: 264.1003

3,4'-Dihexyl-5''-methyl-2,2':5',2''-terthiophene (**5.7**). Yellow oil (74% yield) ^{1}H NMR (300MHz, $CDCl_3$) δ_H: 7.15 (1H, d, J=4.9Hz), 6.92 (2H, s), 6.91 (1H, s), 6.72 (1H, m) 2.75 (4H,m), 2.51 (3H, s), 1.65 (4H,m), 1.34 (12H, m), 0.89 (6H,m). ^{13}C NMR (75 MHz, $CDCl_3$) δ_C: 139.98, 139.45, 139.20, 133.64, 133.54, 130.88, 130.60, 130.02, 128.53, 125.72, 125.56, 123.42, 31.69, 30.68, 30.61, 29.24, 22.63, 15.32, 14.11. HRMS (ESI-TOF) Calcd for $C_{25}H_{34}S_3$ $[M+H]^+$: 430.1823 found m/z: 430.1815

General procedure for methylation

To a flam-dried round-bottom flask, equipped with a stir bar, compound x or x (1 equiv) and 25 mL of dried THF were placed in a dried-ice/acetone bath for 10 min. n-BuLi (2.5 M in hexanes, 1.05 equiv.) was added carefully and drop-wisely. The resulting mixture was allowed to room temperature for 20 min. The mixture was brought back to -78 C, and iodomethane (1.15 equiv.) was added. The reaction was allowed to room temperature, and stirred for 8 hours, protected from the light. The reaction was quenched by the slow addition of 25 mL of water and the mixture was washed three times with water. The organic phase was dried with anhydrous $MgSO_4$, filtered, and concentrated under reduced pressure. The resulting oil was passed through a small column of silica

pad, with hexanes/dichloromethane (1/1) as eluent for Me_2ProDOT, or separated via HPLC (C_{18} column, ACN/acetone (1/1) as eluent).

3,3,6-trimethyl-3,4-dihydro-2H-thieno[3,4-b][1,4]dioxepine (84% yield) colorless oil ^{1}H NMR (300MHz, $CDCl_3$) δ_H: 6.24 (1H, s),3.71 (4H, d, J=3.2Hz), 2.24 (3H, s), 1.02 (6H, s). ^{13}C NMR (75 MHz, $CDCl_3$) δ_C: 149.75, 118.31, 100.53, 80.12, 39.01, 21.63, 11.65. HRMS Calcd for $C_{10}H_{14}O_2S$ $[M]^+$: 198.0715, found m/z: 198.0712

2-methyl-4,4-dioctyl-4H-silolo[3,2-b:4,5-b']dithiophene. (31% yield) ^{1}H NMR (300 MHz, $CDCl_3$) δ_H: 7.15 (1H, d, J=4.4 Hz), 7.03 (1H, J=4.6 Hz), 6.71 (1H, s), 2.52 (3H, s), 1.22 (28H, m), 0.87 (6H, t, J=6.4 Hz). ^{13}C NMR (75 MHz, $CDCl_3$) δ_C: 149.64, 147.06, 141.94, 140.30, 140.17, 129.53, 127.79, 124.16, 33.20, 31.89, 29.23, 29.19, 24.23, 22.68, 15.35, 14.13, 11.89. HRMS Calcd for $C_{25}H_{40}S_2Si$ $[M]^+$:432.2341, found m/z: 432.2330

General procedure for stannylation

To a dry round bottom flask was added 3-hexyl-5'-methyl-2,2'-bithiophene (resp. 3,4'-dihexyl-5''-methyl-2,2':5',2''-terthiophene) (1 equiv.) and dried tetrahydrofuran (100 mL/g of reactant). The mixture was placed in a dry ice-acetone bath for 10 min, and then n-butyl lithium (1.1 equiv.) was drop-wisely added. The mixture was let warm up at room temperature, stirring. After an hour, the reaction was cooled back down to -78^{o}C, and solid trimethyltin chloride (1.15 equiv.) was added. The mixture was allowed to stir at room temperature overnight, protecting from light. The mixture was concentrated under reduced pressure and extracted twice with water, with a saturated solution of sodium bicarbonate and with brine. The organic phase was dried with anhydrous magnesium sulfate, and the solution was concentrated under reduced pressure. The resulting oils were used without further purifications.

(3-hexyl-5'-methyl-[2,2'-bithiophen]-5-yl)Trimethylstannane (**5.6**) Yellow-brown oil (85% yield) ^{1}H NMR (300MHz, $CDCl_3$) δ_H: 7.00 (1H, t, J=13.5Hz, 6.90 (1H, d, J=3Hz), 6.71 (1H, s), 2.75 (2H, t, J=7Hz), 2.51 (3H, s), 1.65 (2H,m), 1.34 (6H, m), 0.90 (3H,t, J=7Hz), 0.38 (9H, t, J=27Hz). ^{13}C NMR (75 MHz, $CDCl_3$) δ_C: 140.29, 139.63, 138.18, 136.74, 135.71, 134.17, 125.50, 125.38, 31.69, 30.89, 29.40, 29.08, 22.64, 15.31, 14.12, -8.24

(3,4'-dihexyl-5''-methyl-[2,2':5',2''-terthiophen]-5-yl)Trimethylstannane (**5.8**) Brown oil (90% yield, 85% pure) ^{1}H NMR (300 MHz, $CDCl_3$) δ_H: 6.99 (1H,s), 6.91 (3H,m), 6.71 (1H,m) 2.75 (4H,m), 2.51 (3H, s), 1.65 (4H,m), 1.34 (12H, m), 0.90 (6H,m), 0.38 (9H, t, J= 30Hz). ^{13}C NMR (75 MHz, $CDCl_3$) δ_C: 140.58, 139.85, 139.18, 138.39, 136.11, 133.92, 133.71, 130.62, 130.03, 128.54, 128.13, 125.60, 31.69, 30.82, 30.58, 29.24, 22.63, 15.32, 14.11, -8.24.

Trimethyl(3,3,8-trimethyl-3,4-dihydro-2H-thieno[3,4-b][1,4]dioxepin-6-yl)stannane Brown oil. (94% yield) ^{1}H NMR (300MHz, $CDCl_3$) δ_H: 3.67 (4H, d, J=15.5 Hz), 2.24 (3H, s), 1.02 (6H, s), 0.31 (9H, t, J=27.8 Hz). ^{13}C NMR (75 MHz, $CDCl_3$) δ_C: 156.26, 146.97, 124.91, 110.28, 80.24, 38.92, 21.60, 12.02, -8.52.

2-methyl-4,4-dioctyl-6-(trimethylstannyl)-4H-silolo[3,2-b:4,5-b']Dithiophene Brown oil (95% yield). ^{1}H NMR (300 MHz, $CDCl_3$) δ_H: 7.07 (1H, s), 6.69 (1H, s), 2.51 (3H, s), 1.40 (28H, m), 0.87 (6H, t, J=6.4 Hz), 0.38 (9H, t, J=28 Hz). ^{13}C NMR (75 MHz, $CDCl_3$) δ_C: 155.45, 147.19, 141.89, 140.16, 137.56, 136.79, 127.81, 33.23, 31.87, 29.23, 29.16, 24.25, 22.67, 15.37, 14.12, 11.92, -8.11.

General procedure for Stille couplings (compounds DTP-L 4, 6, 8, DTP-B 4, 6, 8 ProDOT-DTP and DTS-DTP)

To a 10 mL microwave vial equipped with a stir bar, the dibromo derivative **9** or **10** (1 equiv.), the corresponding trimethystannyl thiophene (trimethylstannyl hexylthiophene, **6** or **8**) (2.3 equiv.), tris(dibenzylideneacetone) dipalladium(0) catalyst (4% equiv.) and tri(o-tolyl)phosphine ligand (12% equiv.) and 1.5 mL of toluene were added. The reaction was placed in the microwave for 2 hours at 125^{o}C. The mixture was allowed to cool to room temperature and precipitated into methanol. The solids were filtrated, rinsed with methanol, dissolved in dichloromethane and passed through a small column of silica pad with hexanes/ dichloromethane as eluants. The fractions were checked by TLC. In the case they were impure; a preparative TLC was done with hexanes/dichloromethane as eluants. The corresponding fractions were then concentrated under reduced pressure, dissolved with dichloromethane and precipitated into methanol to give the corresponding products in a solid form.

Ethyl 2,5-bis(4-hexylthiophen-2-yl)dithieno[3,2-a:2',3'-c]phenazine-9-carboxylate (**DTP-L4**) Purple solids (61 % yield) IR (2926, 2852, 1716, 1296, 1251, 1190, 1091, 85, 746, 654) ^{1}H NMR (300 MHz, CD_2Cl_2): δ_H: 8.79 (1H, s), 8.30 (1H, dd, J=8.8 Hz, J=2 Hz), 8.16 (1H, d, J=9Hz), 8.12, (2H, s), 7.14 (2H, s), 6.94 (2H, s), 4.50 (2H, q, J=7Hz), 2.61 (4H, t, J=7.5 Hz), 1.68 (4H, p, 4H, J=7Hz), 1.51 (4H, t, J=7 Hz), 1.40 (10H, m), 0.95 (6H, t, J=7Hz). ^{13}C NMR (75 MHz, $CDCl_3$): δ_C: 166.07, 144.50, 143.26, 140.65, 140.22, 139.95, 137.31, 137.17, 136.47, 135.25, 135.16, 134.73, 134.05, 132.34, 131.03, 129.55, 128.79, 126.39, 120.55, 120.04, 119.95, 61.69, 31.95, 30.73, 30.57, 29.32, 22.89, 14.64, 14.36. Calcd for $C_{39}H_{40}N_2O_2S_4$ $[M]^+$: 696.1973 found m/z: 696.1968

Ethyl 2,5-bis(4-hexylthiophen-2-yl)dithieno[2,3-a:3',2'-c]phena-zine-9-carboxylate (**DTP-B4**) Dark orange solids (62 % yield) Low solubility precluded the acquisition of a ^{13}C NMR spectrum. IR (2927, 2850, 1713, 1497, 1418, 1248, 1198, 1090, 808, 746) ^{1}H NMR (300 MHz, CD_2Cl_2): δ_H: 8.28 (1H, s), 7.91 (1H, dd, J=9 Hz, J=2.1 Hz), 7.68 (1H, d, J=8.9Hz), 6.83 (4H, m), 6.77 (2H, s), 4.38 (2H, q, J=7.1Hz), 2.50 (4H, t, J=7.8 Hz), 1.62 (4H, m), 1.40 (15, m), 0.97 (6H, t, J=7Hz). Calcd for $C_{39}H_{40}N_2O_2S_4$ $[M]^+$: 696.1973 found m/z: 696.1968.

Ethyl 2,5-bis(3-hexyl-5'-methyl-[2,2'-bithiophen]-5-yl)dithieno[3,2-a:2',3'-c]phenazine-9-carboxylate (**DTP-L6**). Black purple solids (66 % yield) . IR (2918, 2854, 1714, 1413, 1244, 1188, 1087, 827, 769). ^{1}H NMR (300 MHz, CD_2Cl_2) δ_H: 8.10 (1H, s), 7.75 (1H, d, J=7.9 Hz), 7.58 (1H,d, J=8.6Hz), 7.07 (2H, d, J=38Hz), 6.59 (4H, m), 6.36 (2H, d, J=19 Hz), 4.14 (2H, q, J=6.5 Hz), 2.43 (6H, s), 2.19 (4H, m), 1.35 (23H,m), 0.92 (6H, m). ^{13}C NMR (75 MHz, $CDCl_3$): δ_C: 165.13, 144.22, 139.38, 138.70, 135.88, 134.04, 133.62, 132.99, 132.48, 130.99, 129.94, 128.75, 127.70, 126.55, 125.38, 124.82, 118.34, 61.13, 31.64, 29.86, 29.56, 22.76, 14.90, 13.98. Calcd for $C_{37}H_{22}N_2O_2S_6$ $[M+H]^+$:888.2040, found m/z: 888.1996

Ethyl 2,5-bis(3-hexyl-5'-methyl-[2,2'-bithiophen]-5-yl)dithieno[2,3-a:3',2'-c]phenazine-9-carboxylate (**DTP-B6**) Black orange solids (20 % yield) Low solubility precluded the acquisition of a ^{13}C NMR spectrum. IR (2926, 2852, 1718, 1489, 1418, 1247, 1199, 1089, 806, 764). ^{1}H NMR (300MHz, $CDCl_3$) δ_H: 8.41 (1H, s), 7.96 (1H, d, J=7.7 Hz), 7.82 (1H,d, J=8.7Hz), 6.91 (2H, d, J=7.1Hz), 6.80 (4H, m), 6.67 (2H, s), 4.23 (2H, q, J=7.1 Hz), 2.43 (6H, s), 1.53 (7H,m), 1.31 (16H,m), 0.93 (6H, m). Calcd for $C_{37}H_{22}N_2O_2S_6$ $[M+H]^+$:888.2040, found m/z: 888.1998.

Ethyl 2,5-bis(3,4'-dihexyl-5''-methyl-[2,2':5',2''-terthiophen]-5-yl)dithieno[3,2-a:2',3'-c]phenazine-9-carboxylate (**DTP-L8**). Black purple solids (43 % yield). IR (2926, 2850, 1714, 1456, 1255, 1192, 1092, 826, 476, 653). ^{1}H NMR (300 MHz, CD_2Cl_2) δ_H: 8.17 (1H, s), 7.81 (1H, d, J=7.3 Hz), 7.66 (1H,d, J=8.3Hz), 7.31 (2H, d, J=33.6 Hz), 6.82 (2H, m), 6.62 (4H, m), 6.43 (2H, d, J=8.5 Hz), 4.21 (2H, q, J=7.1 Hz), 2.56 (4H, m), 2.50 (6H, s), 2.29 (4H, m), 1.56 (4H, m) 1.36 (31H,m), 0.96 (12H, m). ^{13}C NMR (75 MHz, $CDCl_3$): δ_C: 165.09, 139.65, 139.25, 138.78, 135.87, 134.20, 133.66, 133.06, 132.68, 130.61, 130.48, 129.92, 127.29, 125.48, 125.15, 31.77, 31.73, 30.38, 29.68, 29.46, 29.33, 22.82, 22.74, 14.98, 13.94. Calcd for $C_{69}H_{76}N_2O_2S_8$ $[M+H]^+$:1220.3673, found m/z: 1220.3676.

Ethyl 2,5-bis(3,4'-dihexyl-5''-methyl-[2,2':5',2''-terthiophen]-5-yl)dithieno[2,3-a:3',2'-c]phenazine-9-carboxylate (**DTP-B8**) Black solids (40 % yield). Low solubility precluded the acquisition of a ^{13}C NMR spectrum. IR (2920, 2860, 1718, 1413, 1247, 1197, 1087, 810, 765, 742). ^{1}H NMR (300MHz, $CDCl_3$) δ_H: 8.02 (1H, s), 7.66 (1H, d, J=7.8 Hz), 7.52 (1H,d, J=8.4Hz), 6.81 (2H, s), 6.69 (2H,s), 6.61 (2H, s), 6.43 (2H, d, J=17 Hz), 6.32 (2H, d, J=6.9 Hz), 4.03 (2H, q, J=7.3 Hz), 2.50 (6H, m), 2.23 (4H, m), 1.56 (4H, m) 1.22 (31H,m), 0.94 (12H, m). Calcd for $C_{69}H_{76}N_2O_2S_8$ $[M+H]^+$:1220.3673, found m/z: 1220.3641.

Ethyl 2,5-bis(3,3,8-trimethyl-3,4-dihydro-2H-thieno[3,4-b][1,4]dioxepin-6-yl)dithieno[2,3-a:3',2'-c]phenazine-9-carboxylate (**ProDOT-DTS**) (56% yield) Red powder. IR (2959, 1717, 1506, 1419, 1391, 1362, 1248, 1196, 1123, 1074, 764. ^{1}H NMR (300MHz, $CDCl_3$) δ_H: 8.95 (1H, s), 8.31 (1H, d, J= 8.9Hz), 8.25 (1H, d, J=8.9 Hz), 7.56, (2H, s), 4.49, (2H, q, J=7.1 Hz), 4.01(4H, s), 3.81 (4H, s), 2.31 (6H, s), 1.48, (3H, t, J=7.2

Hz), 1.14 (12H, s). ^{13}C NMR (75 MHz, $CDCl_3$) δ_C: 165.93, 146.28, 131.67, 128.78, 127.88, 116.38, 112.56, 80.35, 61.69, 23.32, 21.78, 14.59, 11.59. HRMS (MALDI) Calcd for $C_{39}H_{36}N_2O_6S_4$ $[M+H]^+$: 757.1534, found m/z: 757.1574.

Ethyl 2,5-bis(6-methyl-4,4-dioctyl-4H-silolo[3,2-b:4,5-b']dithiophen-2-yl)dithieno[2,3-a:3',2'-c]phenazine-9-carboxylate (**DTS-DTP**) Dark blue solids. IR (2957, 2922, 2820, 1716, 1502, 1419, 1390, 1248, 1126, 1072, 766, 744) ^1H NMR (300MHz, $CDCl_3$) δ_H: 8.80 (1H, s), 8.25 (1H, d, J= 9.0Hz), 8.09 (1H, d, J=9.1 Hz), 7.54, (2H, d, J=4.1 Hz), 7.37 (2H, s), 6.75 (2H, s), 4.47, (2H, q, J=7.2 Hz), 2.54 (6H, s), 1.46 (8H,m), 1.27 (44 H, m), 0.98 (7H, m), 0.88 (12 H, t, J=6.7 Hz). ^{13}C NMR (75 MHz, $CDCl_3$) δ_C: 165.84, 150.61, 146.58, 143.15, 142.87, 141.84, 139.95, 137.58, 137.05, 136.48, 132.63, 131.66, 130.37, 128.96, 128.35, 128.06, 117.49, 61.43, 33.29, 31.91, 29.25, 24.26, 22.74, 15.45, 14.14, 11.82. Calcd for $C_{69}H_{88}N_2O_2S_6Si_2$ [M]+:1224.4709, found m/z 1224.4709..

General procedure for hydrolysis (compounds DTP-L 4a, 6a, 8a and DTP-B 4a, 6a, 8a)

To a 10 mL microwave vial equipped with a stir bar, were added the corresponding ethyl ester dyes (**DTP-L 4, 6, 8 or DTP-B 4, 6, 8**) and 2 mL of a solution of 5 M potassium hydroxide. The reaction was placed in the microwave for 10-20 min at 150^{o}C. The solids were filtered, rinsed with water, suspended and stirred into a solution of 1 M hydrochloric acid for 20 min. The solid were filtered, rinse with water and methanol, and placed under high vacuum. For these compounds, low solubility precluded the acquisition of a ^{13}C NMR spectrum.

2,5-Bis(4-hexylthiophen-2-yl)dithieno[3,2-a:2',3'-c]phenazine-9-carboxylic acid (**DTP-L4*a***) (98% yield) IR (2924, 2853, 1691, 1419, 1294, 1190, 826, 746) ^{1}H NMR (300 MHz, CD_2Cl_2+ TFA): δ_H: 8.82 (1H, s), 8.38 (1H, d, J=10.1 Hz), 8.24 (1H, d, J=1.6 Hz), 7.83 (2H, d, J=20.26 Hz), 6.90 (4H, s), 2.55 (4H, q, J=7.4Hz), 1.64 (4H, br), 1.39 (12H, br), 0.97 (6H, t, J=6.3 Hz). HRMS (EI) Calcd for $C_{37}H_{36}N_2O_2S_4$ $[M]^+$: 668.1660 found m/z: 668.1652.

2,5-Bis(4-hexylthiophen-2-yl)dithieno[2,3-a:3',2'-c]phenazine-9-carboxylate (**DTP-B4*a***) (95% yield) IR (2932, 2860, 1688, 1496, 1415, 1386, 810) ^{1}H NMR (300 MHz, DMSO, 90 ^{o}C): δ_H :8.61 (1H, s), 8.34 (1H, d, J=9 Hz), 8.25 (2H, s), 8.19 (2H, d, J=7.5Hz), 7.50 (2H, s), 7.25 (2H, s), 2.65 (4H, t, J=7.5 Hz), 1.68 (4H, m), 1.35 (10H, m), 0.89 (6H, t, J=7.6Hz) HRMS (EI) Calcd for $C_{37}H_{36}N_2O_2S_4$ $[M]^+$: 668.1660 found m/z: 668.1646

2,5-bis(3-hexyl-5'-methyl-[2,2'-bithiophen]-5-yl)Dithieno[3,2-a:2',3'-c]phenazine-9-carboxylic acid (**DTP-L6*a***) (96% yield) IR (2926, 2850, 1692, 1413, 1296, 1192, 829, 786, 653). ^{1}H NMR (300 MHz, DMSO, 90 ^{o}C): δ_H: 8.77 (1H, s), 8.37 (1H, s), 8.29 (3H,m), 7.35(2H, s), 7.00(2H, s), 6.82 (2H, s), 2.68 (6H, s), 1.67 (4H, m), 1.33 (23H, m), 0.89 (6H, m). Calcd for $C_{47}H_{44}N_2O_2S_6$ $[M+H]^+$:860.1727, found m/z: 860.1687.

2,5-bis(3-hexyl-5'-methyl-[2,2'-bithiophen]-5-yl)Dithieno[2,3-a:3',2'-c]phenazine-9-carboxylic acid (**DTP-B6*a***) (95% yield) IR (2928, 2858, 1699, 1491, 1412, 1202, 1040, 781, 637). ^{1}H NMR (300 MHz, CD_2Cl_2+ TFA): δ_H: 7.97 (1H, s), 7.67 (2H, m), 6.59 (4H, m). 6.38 (2H, s), 6.18 (2H, s), 2.48 (6H, s), 2.16 (4H, br), 1.27 (16 H, br), 0.96 (6H, br) Calcd for $C_{47}H_{44}N_2O_2S_6$ $[M+H]^+$: 860.1727, found m/z: 860.1681.

2,5-bis(3,4'-dihexyl-5''-methyl-[2,2':5',2''-terthiophen]-5-yl)Dithieno[3,2-a:2',3'-c]phenazine-9-carboxylate carboxylic acid (**DTP-L8*a***) (90% yield). IR (2926, 2851, 1699, 1373, 1240, 827, 781, 656). ^{1}H NMR (400 MHz, DMSO, 90 ^{o}C) δ_H: 8.89 (1H, s), 8.42 (2H,s), 8.14 (2H, m), 7.53 (2H, br), 7.01 (4H, m), 6.84 (2H, s), 2.78 (4H, br), 2.68 (6H, s), 1.65 (8H, br), 1.34 (31H,br), 0.90 (12H, br). Calculated for $C_{67}H_{72}N_2O_2S_8$ $[M+H]^+$: 1192.3360, found m/z: 1192.3347.

2,5-bis(3,4'-dihexyl-5''-methyl-[2,2':5',2''-terthiophen]-5-yl)Dithieno[2,3-a:3',2'-c]phenazine-9-carboxylic acid (**DTP-B8*a***) (91% yield). IR (2922, 2855, 1689, 1418, 1204, 1036, 768). ^{1}H NMR (400 MHz, DMSO, 90 ^{o}C) δ_H: 8.48 (1H, s), 8.20 (2H,m), 7.88 (2H, m), 7.26 (2H, s), 6.95 (4H, br), 6.82 (2H, s), 2.66(10H, br), 1.61 (8H, s), 1.33 (31H, br), 0.90 (12H, s). Calcd for $C_{67}H_{72}N_2O_2S_8$ $[M+H]^+$:1192.3360, found m/z:1192.3315.

CHAPTER 6.

CONCLUSION AND OUTLOOK

This thesis presented an improved synthesis of the BDTD unit, the creation of precursors, oligomeric and polymeric materials for π-conjugated materials, and the investigation of D_2-A carboxylic acid chromophores for DSSCs. Figure 69 illustrates a panel of organic electronic applications based from BDT units, highlighting in blue the topics examined in this dissertation, and in red potential applications that can be derived from the present work.

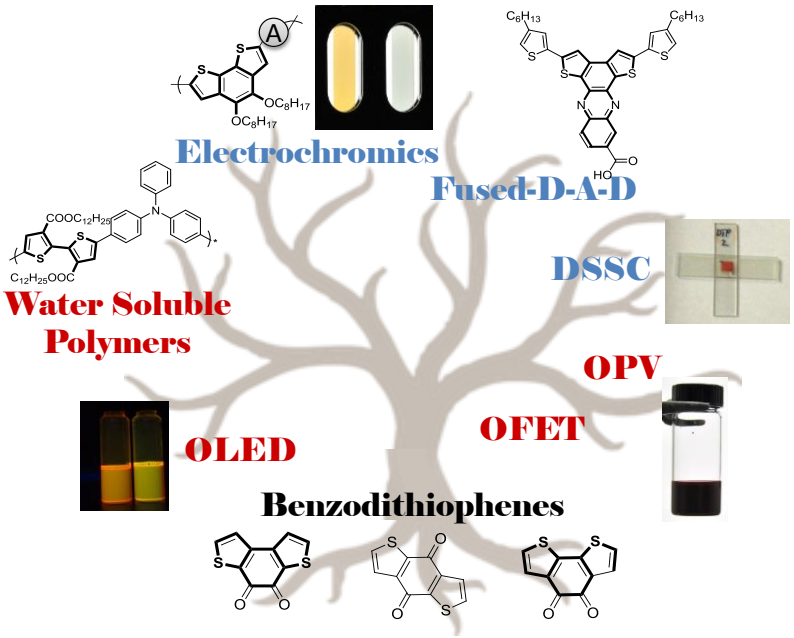

Figure 69: Illustration of diverse applications branching from the BDT core. In blue are topics presented in this thesis, in red are potential applications.

Figure 70 summarizes the derivatization of DBTD to produce various acceptor and donor precursors. Given that the access to novel synthons is vital to generate new π-conjugated materials with improved physical and electronic properties, this contribution helps to the continuous development of the organic electronic field. Moreover, most of these

precursors are fDA systems, which bear advantages in the overall planarization of the molecule and in the deepening of the HOMO level compared with their unfused derivatives. The fDA concept has been so far under-examined, due to the limited number of precursors that were available. This thesis introduces more than six fDA units, giving a lot more freedom and creativity to integrate fDA monomer into small molecules or polymers.

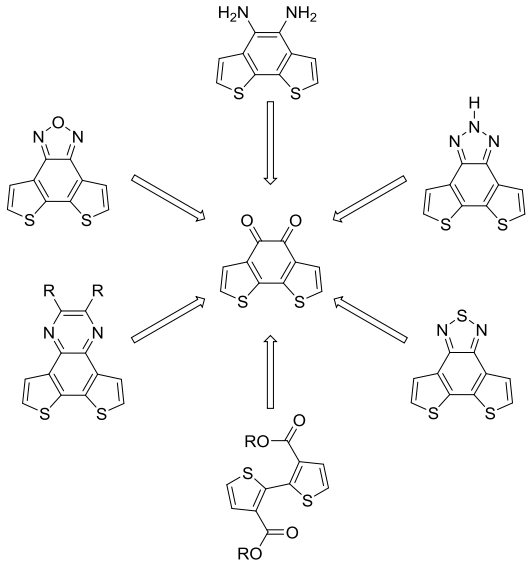

Figure 70: π- Conjugated precursors created via derivatization of BDTD. R groups are alkyl chains.

In this dissertation, the ring opening reaction of BDTD (bottom arrow in Figure 70), leading to the easy synthesis of carboxylated thiophene was discovered. The possibilities of utilization and development of this synthon are boundless. By polymerizing with divers acceptors, conjugated polyelectrolytes could be synthesized, and integrated into chemo- or bio-sensors. By coupling with electrochromic synthons, water soluble electrochromic polymers could be achieved, reliving the manufacturing process of the constraint of expensive and toxic solvents.

A focus was placed on the investigation of the effect of isomerism of the BDT structure on the macroscopic properties of oligomeric and polymeric materials. The fundamental study of three isomeric polymers based on BDT and vinylene reveals that for materials bearing optoelectronic applications, isomerism is an opportunity to fine-tune the properties.

In the two last chapters of this dissertation, a novel DSSC sensitizers architecture, based on D_2-A moieties, was presented. The influence of the nature of the accepting moieties, of the isomerism and of the nature and number of the donating units on optoelectronic and photovoltaic properties were investigated.

The results of this study can be summarized below as well as in Figure 71.

- The proposed D_2-A architecture is able to transform the sunlight energy to electrical energy. By internally fusing the core acceptor, better results were achieved than previous, covalently bound, acceptors.
- Changing the nature of the accepting core to less π-donating units permits to increase the V_{oc}, by positively shifting the level of the TiO_2 conduction band.
- Changing the nature of the donor units increases the light harvesting efficiency and foster the aggregation of the molecules. As the results, the electron regeneration and electron collection are not efficient, and the overall IPCE and J-V response decrease.
- Increasing the number of thiophene donors increases the light absorption, the charge separation, and decreases back electron transfer, leading to an overall, rise of IPCE, J-V and PCE responses.

- Varying the isomers has a great influence on the optoelectronic properties, and a weak influence on the photovoltaics properties. The main change in the devices originates in the better light harvesting ability of the branched isomers, due to the complex nature of the vertical transitions, hence increasing the IPCE, Jsc and PCE values.

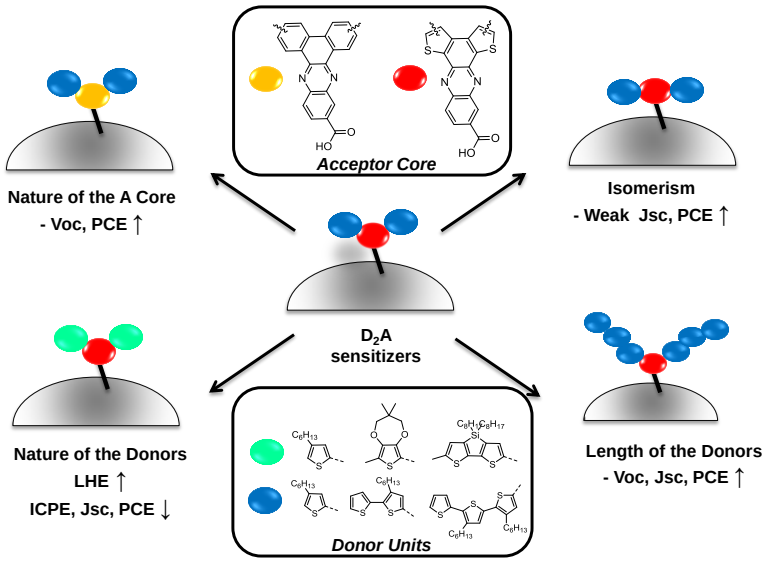

Figure 71: Summary of the effects of the nature of the acceptor core, the isomerism of the structures, and the length and nature of the donor units on the photovoltaic properties.

It is also important to note the differences between the measurements conducted in solutions, and the measurements on the adsorbed dyes. In solution, the properties are a good first guess on the light harvesting abilities, the frontier orbitals level and the photophysical rate constants. Upon adsorption, aggregation of the sensitizers, value of the TiO_2 CB, electron injection and electron recombination, and back electron transfer are examples of parameters influencing the device properties. To obtain an overall picture of the effect of the sensitizers' moieties, more intricate measurements, such as transient absorption or impedance spectroscopy, need to be performed.

With the successful design of an operational family of sensitizers, the path forward is to build on the architecture to create more efficient chromophores. In that goal, an aspect to improve on is to limit any recombination process by separating the electron injection and dye regeneration sites. To do so, dyes with an oligomeric donor backbone (between 5-20 donor units) could be designed. In this case, the LHE and energy gaps will reach a plateau, and the main advantage of this architecture resides in the structural separation of the electron injection site (second cartoon in Figure 72) from the dye regeneration site (fourth cartoon in Figure 72). The aggregation between the donor units should be monitored, and could be minimized by using co-adsorbents, or by using nanostructured TiO_2 rods.

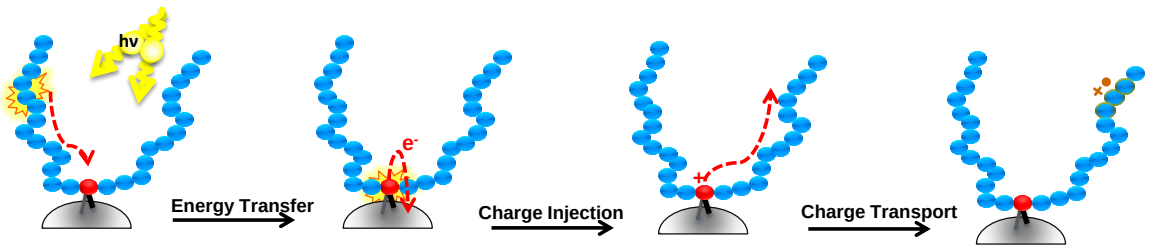

Figure 72: Cartoon illustrating the sequence of events occurring when a D_2-A oligomer is adsorbed at a TiO_2 interface. Light absorption by the donor block is followed by energy transfer to the acceptor moiety which is in close proximity to the metal-oxide interface. Charge injection produces a cation radical (polaron) on the polymer. The polaron diffuses away from the interface by charge transport along the donor block.

REFERENCES

(1) Shakespeare, W. *Hamlet*; 1st ed.; Simon & Schuster; p. 99.

(2) Rao, D. S.; Tilak, B. D. *J. Sci. Ind. Res.* **1685**, *13B*, 829.

(3) Wynberg, H.; Sinnige, H. J. M. *Recl.Trav. Chim. Pays-Bas* **1696**, *88*, 1224.

(4) Natta, G.; Mazzanti, G.; Corradini, P. *Atti accad. nazl. Lincei Rend. Cl. sci. fis. mat. e nat.* **1958**, *25*, 3.

(5) Shirakawa, H.; Louis, E. J.; MacDiarmid, A. G.; Chiang, C. K.; Heeger, A. J. *J. Chem. Soc., Chem. Comm.* **1977**, 578.

(6) Taliani, C.; Danieli, R.; Zamboni, R.; Giro, G.; Sannicolo, F. *Springer Ser. Solid-State Sci.* **1987**, *76*, 326.

(7) Kimura, O. Manufacture of Benzodithiophene Polymers. JP 63122727 A 19880526, 1988.

(8) Kobayashi, K.; Mazaki, Y.; Iwasaki, F. *Synt. Met.* **1988**, *27*, 309.

(9) Fujii, M.; Aso, Y.; Otsubo, T.; Ogura, F. *Synt. Met.* **1993**, *57*, 1910.

(10) Yoshida, S.; Fujii, M.; Aso, Y.; Otsubo, T. *J. Org. Chem.* **1994**, *59*, 3077.

(11) Klauk, H. *Chem. Soc. Rev* **2010**, *39*, 2643.

(12) Laquindanum, J. G.; Katz, H. E.; Lovinger, A. J.; Dodabalapur, A. *Adv. Mater.* **1997**, *9*, 36.

(13) Pan, H.; Li, Y.; Wu, Y.; Liu, P.; Ong, B. S.; Zhu, S.; Xu, G. *J. Am. Chem. Soc.* **2007**, *129*, 4112.

(14) Yin, J.; Zhou, Y.; Lei, T.; Pei, J. *Angew. Chem. Int. Ed.* **2011**, *50*, 6320.

(15) Hou, J.; Park, M.-H.; Zhang, S.; Yao, Y.; Chen, L.-M.; Li, J.-H.; Yang, Y. *Macromol.* **2008**, *41*, 6012.

(16) Shi, Q.; Fan, H.; Liu, Y.; Hu, W.; Li, Y.; Zhan, X. *J. Phys. Chem. C* **2010**, *114*, 16843.

(17) Liang, Y.; Feng, D.; Wu, Y.; Tsai, S.-T.; Li, G.; Ray, C.; Yu, L. *J. Am. Chem. Soc.* **2009**, *131*, 7792.

(18) Liang, Y.; Xu, Z.; Xia, J.; Tsai, S.-T.; Wu, Y.; Li, G.; Ray, C.; Yu, L. *Adv. Mater.* **2010**, *22*, E135.

(19) Zhang, Y.; Hau, S. K.; Yip, H.-L.; Sun, Y.; Acton, O.; Jen, A. K.-Y. *Chem. Mater.* **2010**, *22*, 2696.

(20) Najari, A.; Beaupré, S.; Berrouard, P.; Zou, Y.; Pouliot, J.-R.; Lepage-Pérusse, C.; Leclerc, M. *Adv. Funct. Mater.* **2011**, *21*, 718.

(21) Labban, A. El; Bartelt, J. A.; Douglas, J. D.; Mateker, W. R.; Fre, J. M. J.; Mcgehee, M. D.; Beaujuge, P. M. *J. Am. Chem. Soc.* **2013**, *135*, 4656.

(22) Price, S. C.; Stuart, A. C.; Yang, L.; Zhou, H.; You, W. *J. Am. Chem. Soc.* **2011**, *133*, 4625.

(23) Nie, W.; Macneill, C. M.; Li, Y.; Noftle, R. E.; Carroll, D. L.; Coffin, R. C. *Macromol. Rapid Commun.* **2011**, *32*, 1163.

(24) Zhou, N.; Guo, X.; Ortiz, R. P.; Li, S.; Zhang, S.; Chang, R. P. H.; Facchetti, A.; Marks, T. J. *Adv. Mater.* **2012**, *24*, 2242.

(25) Huo, L.; Zhang, S.; Guo, X.; Xu, F.; Li, Y.; Hou, J. *Angew. Chem. Int. Ed.* **2011**, *50*, 9697.

(26) Huo, L.; Hou, J.; Zhang, S.; Chen, H.-Y.; Yang, Y. *Angew. Chem. Int. Ed.* **2010**, *49*, 1500.

(27) Zhang, M.; Gu, Y.; Guo, X.; Liu, F.; Zhang, S.; Huo, L.; Russell, T. P.; Hou, J. *Adv. Mater.* **2013**, *25*, 4944.

(28) Kim, J.-H.; Song, C. E.; Shin, N.; Kang, H.; Wood, S.; Kang, I.-N.; Kim, B. J.; Kim, B.; Kim, J.-S.; Shin, W. S.; Hwang, D.-H. *ACS Appl. Mater. Interfaces* **2013**, *5*, 12820.

(29) Xiao, S.; Zhou, H.; You, W. *Macromol.* **2008**, *41*, 5688.

(30) Zhou, H.; Yang, L.; Price, S. C.; Knight, K. J.; You, W. *Angew. Chem. Int. Ed* **2010**, *49*, 7992.

(31) Qian, D.; Ma, W.; Li, Z.; Guo, X.; Zhang, S.; Ye, L.; Ade, H.; Tan, Z.; Hou, J. *J. Am. Chem. Soc.* **2013**, *135*, 8464.

(32) Zhou, J.; Wan, X.; Liu, Y.; Zuo, Y.; Li, Z.; He, G.; Long, G.; Ni, W.; Li, C.; Su, X.; Chen, Y. *J. Am. Chem. Soc.* **2012**, *134*, 16345.

(33) Zhou, J.; Zuo, Y.; Wan, X.; Long, G.; Zhang, Q.; Ni, W.; Liu, Y.; Li, Z.; He, G.; Li, C.; Kan, B.; Li, M.; Chen, Y. *J. Am. Chem. Soc.* **2013**, *135*, 8484.

(34) Havinga, E. E.; Hoebe, W. ten; Wynberg, H. *Synth. Met.* **1993**, *57*, 299.

(35) Beaujuge, P. M.; Pisula, W.; Tsao, H. N.; Ellinger, S.; Müllen, K.; Reynolds, J. R. *J. Am. Chem. Soc.* **2009**, *131*, 7514.

(36) Beaujuge, P. M.; Amb, C. M.; Reynolds, J. R. *Acc. Chem. Res.* **2010**, *43*, 1396.

(37) Van Mullekom, H. A. M.; Vekemans, J. A. J. M.; Havinga, E. E. *Mater. Sci. Eng.* **2001**, *32*, 1.

(38) Dyer, A. L.; Thompson, E. J.; Reynolds, J. R. *ACS Appl. Mater. Interfaces* **2011**, *3*, 1787.

(39) Mei, J.; Graham, K. R.; Stalder, R.; Reynolds, J. R. *Org. Lett.* **2010**, *12*, 660.

(40) Stalder, R.; Grand, C.; Subbiah, J.; So, F.; Reynolds, J. R. *Polym. Chem.* **2012**, *3*, 89.

(41) Wu, W.; Liu, Y.; Zhu, D. *Chem. Soc. Rev.* **2010**, *39*, 1489.

(42) Mei, C.-Y.; Liang, L.; Zhao, F.-G.; Wang, J.-T.; Yu, L.-F.; Li, Y.-X.; Li, W.-S. *Macromol.* **2013**, *46*, 7920.

(43) O'Regan, B. C.; Grätzel, M. *Nature* **1991**, *353*, 737.

(44) Gerischer, H.; Tributsch, H. *Ber. Bunsen-Ges. Phys. Chem.* **1968**, *72*, 437.

(45) Gerischer, H.; Michel-Beyerele, M. E.; Rebentrost, F.; Tributsch, H. *Electrochim. Acta* **1968**, *13*, 1509.

(46) Hasselman, G. M.; Waston, D. F.; Stromber, J. R.; Bocian, D. F.; Holten, D.; Lindsey, J. S.; Meyer, G. J. *J. Phys. Chem. B* **2006**, *110*, 25430.

(47) Hagfeldt, A.; Boschloo, G.; Sun, L.; Kloo, L.; Pettersson, H. *Chem. Rev.* **2010**, *110*, 6595.

(48) Liang, M.; Chen, J. *Chem. Soc. Rev.* **2013**, *42*, 3453.

(49) Ooyama, Y.; Harima, Y. *Chem. Phys. Chem.* **2012**, *13*, 4032.

(50) Wu, J.; Lan, Z.; Hao, S.; Li, P.; Lin, J.; Huang, M.; Fang, L.; Huang, Y. *Pure Appl. Chem.* **2008**, *80*, 2241.

(51) Roh, D. K.; Chi, W. S.; Jeon, H.; Kim, S. J.; Kim, J. H. *Adv. Funct. Mater.* **2014**, *24*, 379.

(52) Ye, M.; Zheng, D.; Lv, M.; Chen, C.; Lin, C.; Lin, Z. *Adv. Mater.* **2013**, *25*, 3039.

(53) Wang, J.; Lin, Z. *Chem. Asian. J.* **2012**, *7*, 2754.

(54) Yella, A.; Lee, H.-W.; Tsao, H. N.; Yi, C.; Chandiran, A. K.; Nazeeruddin, M. K.; Diau, E. W.-G.; Yeh, C.-Y.; Zakeeruddin, S. M.; Grätzel, M. *Science* **2011**, *334*, 629.

(55) Brabec, C. J.; Durrant, J. R. *MRS Bull.* **2008**, *33*, 670.

(56) Koops, S. E.; O'Regan, B. C.; Barnes, P. R. F.; Durrant, J. R. *J. Am. Chem. Soc.* **2009**, *131*, 4808.

(57) Marinado, T.; Nonomura, K.; Nissfolk, J.; Karlsson, M. K.; Hagberg, D. P.; Sun, L.; Mori, S.; Hagfeldt, A. *Langmuir* **2010**, *26*, 2592.

(58) Ronca, E.; Pastore, M.; Belpassi, L.; Tarantelli, F.; De Angelis, F. *Energy Environ. Sci.* **2013**, *6*, 183.

(59) Bertoluzzi, L.; Ma, S. *Phys. Chem. Chem. Phys.* **2013**, *15*, 4283.

(60) Katoh, R.; Furube, A.; Yoshihara, T.; Hara, K.; Fujihashi, G.; Takano, S.; Murata, S.; Arakawa, H.; Tachiya, M. *J. Chem. Soc. B* **2004**, *108*, 4818.

(61) Beranek, R. *Adv. Phys. Chem* **2011**, *2011*, 1.

(62) Robertson, N. *Angew. Chem. Int. Ed.* **2006**, *45*, 2338.

(63) Mishra, A.; Fischer, M. K. R.; Bäuerle, P. *Angew. Chem. Int. Ed.* **2009**, *48*, 2474.

(64) Pechy, P.; Rotzinger, F. P.; Nazeeruddin, M. K.; Kohle, O.; Zakeeruddin, S. M.; Humphry-baker, R.; Gratzel, M. *J. Chem. Soc., Chem. Comm.* **1995**, *369*, 65.

(65) Bae, E.; Choi, W.; Park, J.; Shin, H. S.; Kim, S. Bin; Lee, J. S. *J. Phys. Chem. B* **2004**, *108*, 14093.

(66) Gillaizeau-Gauthier, I.; Odobel, F.; Alebbi, M.; Argazzi, R.; Costa, E.; Bignozzi, C. a; Qu, P.; Meyer, G. J. *Inorg. Chem.* **2001**, *40*, 6073.

(67) Feldt, S. M.; Lohse, P. W.; Kessler, F.; Nazeeruddin, M. K.; Grätzel, M.; Boschloo, G.; Hagfeldt, A. *Phys. Chem. Chem. Phys.* **2013**, *15*, 7087.

(68) Yum, J.-H.; Baranoff, E.; Kessler, F.; Moehl, T.; Ahmad, S.; Bessho, T.; Marchioro, A.; Ghadiri, E.; Moser, J.-E.; Yi, C.; Nazeeruddin, M. K.; Grätzel, M. *Nat. Comm.* **2012**, *3*, 631.

(69) Wu, W.; Yang, J.; Hua, J.; Tang, J.; Zhang, L.; Long, Y.; Tian, H. *J. Mater. Chem.* **2010**, *20*, 1772.

(70) Choi, H.; Baik, C.; Kang, S. O.; Ko, J.; Kang, M.-S.; Nazeeruddin, M. K.; Grätzel, M. *Angew. Chem. Int. Ed* **2008**, *47*, 327.

(71) Nazeeruddin, M. K.; Kay, A.; Rodicio, I.; Humphry-Baker, R.; Müller, E.; Liska, P.; Vlachopoulos, N.; Grätzel, M. *J. Am. Chem. Soc.* **1993**, 6382.

(72) Zeng, W.; Cao, Y.; Bai, Y.; Wang, Y.; Shi, Y.; Zhang, M.; Wang, F.; Pan, C.; Wang, P. *Chem. Mater.* **2010**, *22*, 1915.

(73) Ning, Z.; Zhang, Q.; Wu, W.; Pei, H.; Liu, B.; Tian, H. *J. Org. Chem.* **2008**, *73*, 3791.

(74) Akitu, K.; Kubo, T.; Uchida, S.; Segawa, H.; Otani, N.; Tomura, M.; Tamura, T.; Matsumura, M. *Jap. J. Appl. Sci.* **2012**, *51*, 10NE04–1.

(75) Fang, Z.; Eshbaugh, A. A.; Schanze, K. S. *J. Am. Chem. Soc.* **2011**, *133*, 3063.

(76) NPD Solarbuzz. *Polysilicon and Water Supply Chain Quarterly*; 2013.

(77) Logitech Solar Keyboard Folio http://www.amazon.com/Logitech-Solar-Keyboard-Folio-generation/dp/B007RNCLBY.

(78) Hardin, B. E.; Snaith, H. J.; McGehee, M. D. *Nat. Photon.* **2012**, *6*, 162–169.

(79) Ball, J. M.; Lee, M. M.; Hey, A.; Snaith, H. J. *Energy Environ. Sci.* **2013**, *6*, 1739.

(80) Burschka, J.; Pellet, N.; Moon, S.-J.; Humphry-Baker, R.; Gao, P.; Nazeeruddin, M. K.; Grätzel, M. *Nature* **2013**, *499*, 316.

(81) Pandey, L. Theoretical Studies of the Structure-Properties Relationships of Hole- and Electron- Transport Materials for Organic Photovoltaic Applications, Georgia Institute of Technology, 2013.

(82) Thomas, L. H. *Proc. Cambridge Phil. Soc.* **1927**, *5*, 542.

(83) Fermi, E. *Rend. Accad. Naz. Lincei* **1927**, *6*, 1049.

(84) Hohenberg, P.; Kohn, W. *Phys. Rev.* **1964**, B864.

(85) Runge, E.; Gross, E. K. . *Phys. Rev. Lett.* **1984**, 997.

(86) Frisch, M. J.; Trucks, G. W.; Schlegel, H. B.; Scuseria, G. E.; Robb, M. A.; Cheeseman, J. R.; Montgomery, J. A.; Vreven, T.; Kudin, K. N.; Burant, J. C.; Millam, J. M.; Iyengar, S. S.; Tomasi, J.; Barone, V.; Mennucci, B.; Cossi, M.; Scalmani, G.; Rega, N.; Petersson, G. A.; Nakatsuji, H.; Hada, M.; Ehara, M.; Toyota, K.; Fukuda, R.; Hasegawa, J.; Ishida, M.; Nakajima, T.; Honda, Y.; Kitao, O.; Nakai, H.; Klene, M.; Li, X.; Knox, J. E.; Hratchian, H. P.; Cross, J. B.; Bakken, V.; Adamo, C.; Jaramillo, J.; Gomperts, R.; Stratmann, R. E.; Yazyev, O.; Austin, A. J.; Cammi, R.; Pomelli, C.; Ochterski, J. W.; Ayala, P. Y.; Morokuma, K.; Voth, G. A.; Salvador, P.; Dannenberg, J. J.; Zakrzewski, V. G.; Dapprich, S.; Daniels, A. D.; Strain, M. C.; Farkas, O.; Malick, D. K.; Rabuck, A. D.; Raghavachari, K.; Foresman, J. B.; Ortiz, J. V; Cui, Q.; Baboul, A. G.; Clifford, S.; Cioslowski, J.; Stefanov, B. B.; Liu, G.; Liashenko, A.; Piskorz, P.; Komaromi, I.; Martin, R. L.; Fox, D. J.; Keith, T.; Laham, A.; Peng, C. Y.; Nanayakkara, A.; Challacombe, M.; Gill, P. M. W.; Johnson, B.; Chen, W.; Wong, M. W.; Gonzalez, C.; Pople, J. A. Gaussian 03, Revision C.02, 2003.

(87) Frisch, M. J.; Trucks, G. W.; Schlegel, H. B.; Scuseria, G. E.; Robb, M. A.; Cheeseman, J. R.; Scalmani, G.; Barone, V.; Mennucci, B.; Petersson, G. A.; Nakatsuji, H.; Caricato, M.; Li, X.; Hratchian, H. P.; Izmaylov, A. F.; Bloino, J.; Zheng, G.; Sonnenberg, J. L.; Hada, M.; Ehara, M.; Toyota, K.; Fukuda, R.; Hasegawa, J.; Ishida, M.; Nakajima, T.; Honda, Y.; Kitao, O.; Nakai, H.; Vreven, T.; Montgomery, J. A.; Peralta, J. E.; Ogliaro, F.; Bearpark, M.; Heyd, J. J.; Brothers, E.; Kudin, K. N.; Straroverov, V. N.; Kobayashi, R.; Normand, J.; Raghavachari, K.; Rendell, A.; Burant, J. C.; Iyengar, S. S.; Tomasi, J.; Cossi, M.; Rega, N.; Millam, J. M.; Klene, M.; Knox, J. E.; Cross, J. B.; Bakken, V.; Adamo, C.; Jaramillo, J.; Gomperts, R.; Stratmann, R. E.; Yazyev, O.; Austin, A. J.; Cammi, R.; Pomelli, C.; Ochterski, J. W.; Martin, R. L.; Morokuma, K.; Zakrzewski, V. G.; Voth, G. A.; Salvador, P.; Dannenberg, J. J.; Dapprich, S.; Daniels, A. D.; Farkas; Foresman, J. B.; Ortiz, J. V.; Cioslowski, J.; Fox, D. J. Gaussian 09, revision b.01, 2009.

(88) ChemCraft Program www.chemcraftprog.com (accessed May 8, 2013).

(89) Cramer, C. J. *Essentials of Computational Chemistry: Theories and Models.*; John Wiley & Sons Ltd, 2002; p. 562.

(90) Becke, A. D. *J. Chem. Phys.* **1993**, *98*, 5648.

(91) Stephens, P. J.; Devlin, F. J.; Chabalowski, C. F. *J. Phys. Chem.* **1994**, *98*, 11623.

(92) Perdew, J. P.; Wang, Y. *Phys. Rev. B* **1992**, *45*, 244.

(93) Becke, A. D. *J. Chem. Phys.* **1993**, *98*, 5648.

(94) Yanai, T.; Tew, D. P.; Handy, N. C. *Chem. Phys. Lett.* **2004**, *393*, 51.

(95) Stephens, P. J.; Devlin, F. J.; Chabalowski, C. F. *J. Phys. Chem.* **1994**, *98*, 11623.

(96) Chai, J.-D.; Head-Gordon, M. *J. Chem. Phys.* **2008**, *128*, 084106.

(97) Tomasi, J.; Mennucci, B.; Cammi, R. *Chem. Rev.* **2005**, *105*, 2999.

(98) Guido, C. a.; Knecht, S.; Kongsted, J.; Mennucci, B. *J. Chem. Theory Comp.* **2013**, *9*, 2209.

(99) Körzdörfer, T.; Sears, J. S.; Sutton, C.; Brédas, J.-L. *J. Chem. Phys.* **2011**, *135*, 204107.

(100) Kitchen, H. J.; Vallance, S. R.; Kennedy, J. L.; Tapia-Ruiz, N.; Carassiti, L.; Harrison, A.; Whittaker, A. G.; Drysdale, T. D.; Kingman, S. W.; Gregory, D. H. *Chem. Rev.* DOI:101.1021/cr4002353.

(101) Mingos, D. M. P.; Baghurst, D. R. *Chem. Soc. Rev.* **1991**, *20*, 1.

(102) Majetich, G.; Hicks, R. J. *Microw. Power Electromag. Energy* **1995**, *30*, 27.

(103) Galema, S. A. *Chem. Soc. Rev.* **1997**, *26*, 233.

(104) De la Hoz, A.; Diaz-Ortiz, A.; Moreno, A. *Chem. Soc. Rev.* **2005**, *34*, 164.

(105) Liu, S. W.; Wightman, J. P. *Appl. Chem. Biotechnol.* **1971**, *21*, 168.

(106) Gedye, R.; Smith, F.; Westaway, K.; Ali, H.; Baldisera, L.; Laberge, L.; Rousell, J. *Tetrahedron Lett.* **1986**, *3*, 279.

(107) Lidstrom, P.; Tierney, J.; Wathey, B.; Westman, J. *Tetrahedron* **2001**, *34*, R55.

(108) Rao, K. J.; Ramesh, P. D. B. *Mater. Sci.* **1995**, *18*, 447.

(109) Schanche, J.-S. *Mol. Divers.* **2003**, *7*, 293.

(110) Dallinger, D.; Kappe, C. O. *Chem. Rev.* **2007**, *107*, 2563.

(111) Anastas, P. T. *Chem. Rev.* **2007**, *107*, 2167.

(112) Kappe, C. O.; Pieber, B.; Dallinger, D. *Angew. Chem. Int. Ed.* **2013**, *52*, 1088.

(113) Dudley, G. B.; Stiegman, A. E.; Rosana, M. R. *Angew. Chem. Int. Ed.* **2013**, *52*, 7918.

(114) Kappe, C. O. *Angew. Chem. Int. Ed.* **2013**, *52*, 7924.

(115) Thompson, B. C. Variable Band Gap Poly(3,4-alkylenedioxythiophene)- Based Polymers for Photovoltaic and Electrochromic Applications, University of Florida, 2005.

(116) Cardona, C. M.; Li, W.; Kaifer, A. E.; Stockdale, D.; Bazan, G. C. *Adv. Mater.* **2011**, *23*, 2367.

(117) Irwin, J. A. Low Oxidation Potential Electrochromic Polymers, University of Florida, 1998.

(118) Galand, E. E. Processable Variable Band Gap Conjugated Polymers for Optoelectronic Devices, University of Florida, 2006.

(119) Würth, C.; Grabolle, M.; Pauli, J.; Spieles, M.; Resch-Genger, U. *Nat. Protoc.* **2013**, *8*, 1535.

(120) Lee, S.-H. A.; Abrams, N. M.; Hoertz, P. G.; Barber, G. D.; Halaoui, L. I.; Mallouk, T. E. *J. Phys. Chem. B* **2008**, *112*, 14415.

(121) Beaujuge, P. M.; Reynolds, J. R. *Chem. Mater.* **2010**, *110*, 268.

(122) Skotheim, T. A.; Reynolds, J. R. *Conjugated Polymers: Theory, Synthesis, Properties and Characterizaion (Handbook of Conducting Polymers)*; 3rd Ed.; CRC Press LLC, 2007.

(123) Letizia, J. A.; Cronin, S.; Ortiz, R. P.; Facchetti, A.; Ratner, M. A.; Marks, T. J. *Chem. - A Eur. J.* **2010**, *16*, 1911.

(124) Mondal, R.; Becerril, H. a.; Verploegen, E.; Kim, D.; Norton, J. E.; Ko, S.; Miyaki, N.; Lee, S.; Toney, M. F.; Brédas, J.-L.; McGehee, M. D.; Bao, Z. *J. Mater. Chem.* **2010**, *20*, 5823.

(125) Getmanenko, Y. A.; Risko, C.; Tongwa, P.; Kim, E.-G.; Li, H.; Sandhu, B.; Timofeeva, T. V.; Brédas, J.-L.; Marder, S. R. *J. Org. Chem.* **2010**, *76*, 2660.

(126) Khor, E.; Ng, S. C.; Li, H. C.; Chai, S. *Heterocycles* **1991**, *32*, 1805.

(127) Nicolas, Y.; Blanchard, P.; Roncali, J.; Allain, M.; Mercier, N.; Demand, A.-L.; Tardy, J. *Org. Lett.* **2005**, *7*, 3513.

(128) Usta, H.; Lu, G.; Facchetti, A.; Marks, T. J. *J. Am. Chem. Soc.* **2006**, *128*, 9034.

(129) Hou, J.; Chen, H.-Y.; Zhang, S.; Li, G.; Yang, Y. *J. Am. Chem. Soc.* **2008**, *130*, 16144.

(130) Babudri, F.; Fiandanese, V.; Marchese, G.; Punzi, A. *Tetrahedron* **1995**, *36*, 7305.

(131) Arroyave, F. A.; Richard, C. A.; Reynolds, J. R. *Org. Lett.* **2012**, *14*, 6138.

(132) Brookins, R. N.; Berda, E.; Reynolds, J. R. *J. Mater. Chem.* **2009**, *19*, 4197.

(133) Fang, Z.; Eshbaugh, A.; Schanze, K. S. *J. Am. Chem. Soc.* **2011**, *133*, 3063.

(134) Lee, K.-H.; Morino, K.; Sudo, A.; Endo, T. *Polym. Bull.* **2010**, *67*, 227–236.

(135) Liu, J.; Kadnikova, E. N.; Liu, Y.; McGehee, M. D.; Fréchet, J. M. J. *J. Am. Chem. Soc.* **2004**, *126*, 9486.

(136) Liu, Y.; Scully, S. R.; McGehee, M. D.; Liu, J.; Luscombe, C. K.; Fréchet, J. M. J.; Shaheen, S. E.; Ginley, D. S. *J. Phys. Chem. B* **2006**, *110*, 3257.

(137) Murphy, A. R.; Liu, J.; Luscombe, C.; Kavulak, D.; Fre, J. M. J.; Kline, R. J.; Mcgehee, M. D. *Chem. Mater.* **2005**, *17*, 4892.

(138) Walczak, R. M.; Brookins, R. N.; Savage, A. M.; van der Aa, E. M.; Reynolds, J. R. *Macromol.* **2009**, 1445.

(139) Liu, J.; Kadnikova, E. N.; Liu, Y.; McGehee, M. D.; Fréchet, J. M. J. *J. Am. Chem. Soc.* **2004**, *126*, 9486.

(140) Mondal, R.; Becerril, H. A.; Verploegen, E.; Kim, D.; Norton, J. E.; Ko, S.; Miyaki, N.; Lee, S.; Toney, M. F.; Bredas, J.-L.; McGehee, M. D.; Bao, Z. *J. Mater. Chem.* **2010**, *20*, 5823.

(141) Malhotra, B. D. *Handbook of Polymers in Electronics*; Smithers Rapra Technology, 2002; p. 104.

(142) Jiang, H.; Taranekar, P.; Reynolds, J. R.; Schanze, K. S. *Angew. Chem. Int. Ed* **2009**, *48*, 4300.

(143) Guo, X.; Zhou, N.; Lou, S. J.; Smith, J.; Tice, D. B.; Hennek, J. W.; Ortiz, R. P.; Navarrete, J. T. L.; Li, S.; Strzalka, J.; Chen, L. X.; Chang, R. P. H.; Facchetti, A.; Marks, T. J. *Nat. Photon.* **2013**, *7*, 825.

(144) Osaka, I.; Abe, T.; Shinamura, S.; Takimiya, K. *J. Am. Chem. Soc.* **2011**, *133*, 6852.

(145) Rieger, R.; Beckmann, D.; Mavrinskiy, A.; Kastler, M.; Müllen, K. *Chem. Mater.* **2010**, *22*, 5314.

(146) He, Y.; Zhou, Y.; Zhao, G.; Min, J.; Guo, X.; Zhang, B.; Zhang, M.; Zhang, J.; Li, Y.; Zhang, F.; Inganäs, O. *J. Polym. Sci. A Polym. Chem.* **2010**, *48*, 1822.

(147) Brookins, R. N.; Berda, E.; Reynolds, J. R. *J. Mat. Chem.* **2009**, *19*, 4197.

(148) He, Y.; Zhou, Y.; Zhao, G.; Min, J.; Guo, X.; Zhang, B.; Zhang, M.; Zhang, J.; Li, Y.; Zhang, F.; Inganäs, O. *J. Polym. Sci. A Polym. Chem.* **2010**, *48*, 1822.

(149) Phillips, K. E.; Katz, T. J.; Jockusch, S.; Lovinger, a J.; Turro, N. J. *J. Am. Chem. Soc.* **2001**, *123*, 11899.

(150) Rieger, R.; Beckmann, D.; Mavrinskiy, A.; Kastler, M.; Müllen, K. *Chem. Mater.* **2010**, *22*, 5314.

(151) Ko, S.; Hoke, E. T.; Pandey, L.; Hong, S.; Mondal, R.; Risko, C.; Yi, Y.; Noriega, R.; McGehee, M. D.; Brédas, J.-L.; Salleo, A.; Bao, Z. *J. Am. Chem. Soc.* **2012**, *134*, 5222.

(152) Boudouris, B. W.; Molins, F.; Blank, D. a.; Frisbie, C. D.; Hillmyer, M. A. *Macromol.* **2009**, *42*, 4118.

(153) Brédas, J.-L. *Mater. Horiz.* **2014**, *1*, 17.

(154) Dyer, A. L.; Craig, M. R.; Babiarz, J. E.; Kiyak, K.; Reynolds, J. R. *Macromol.* **2010**, *43*, 4460.

(155) Hardin, B. E.; Hoke, E. T.; Armstrong, P. B.; Yum, J.; Comte, P.; Tomas, T.; Fréchet, J. M. J.; McGehee, M. D.; Nazeeruddin, K.; Grätzel, M. *Nat. Photon.* **2009**, *3*, 406.

(156) Gao, F.; Wang, Y.; Shi, D.; Zhang, J.; Wang, M.; Jing, X.; Humphry-Baker, R.; Wang, P.; Zakeeruddin, S. M. *J. Am. Chem. Soc.* **2008**, 10720.

(157) Zeng, W.; Cao, Y.; Bai, Y.; Wang, Y.; Shi, Y.; Zhang, M.; Wang, F.; Pan, C.; Wang, P. *Chem. Mater.* **2010**, *22*, 1915.

(158) Fischer, M. K. R.; Wenger, S.; Wang, M.; Mishra, A.; Zakeeruddin, S. M.; Grätzel, M.; Bäuerle, P. *Chem. Mater.* **2010**, *22*, 1836.

(159) Patel, D. G.; Feng, F.; Ohnishi, Y.; Abboud, K. A.; Hirata, S.; Schanze, K. S.; Reynolds, J. R. *J. Am. Chem. Soc.* **2012**, *134*, 2599.

(160) Estrada, L. A.; Neckers, D. C. *J. Org. Chem.* **2009**, *74*, 8484.

(161) Lavigueur, C.; Foster, E. J.; Williams, V. E. *J. Am. Chem. Soc.* **2008**, *130*, 11791.

(162) Shao, F.; Elias, B.; Lu, W.; Barton, J. K. *Inorg. Chem.* **2007**, *46*, 10187.

(163) Turbiez, M.; Frere, P.; Blanchard, P.; Roncali, J. *Tetrahedron Lett.* **2000**, *41*, 5521.

(164) Meyer, A.; Sigmund, E.; Luppertz, F.; Schnakenburg, G.; Gadaczek, I.; Bredow, T.; Jester, S.; Höger, S. *Beilstein J. Org. Chem.* **2010**, *6*, 1180.

(165) Estrada, L. A.; Neckers, D. C. *Org. Lett.* **2011**, *13*, 3304.

(166) Estrada, L. A.; Cai, X.; Neckers, D. C. *J. Phys. Chem. A* **2011**, *115*, 2184.

(167) Lap, D. V; Grebner, D.; Rentsch, S. *J. Phys. Chem. A* **1997**, *5639*, 107.

(168) Parthasarathy, A.; Goswami, S.; Corbitt, T. S.; Ji, E.; Dascier, D.; Whitten, D. G.; Schanze, K. S. *ACS Appl. Mater. Interfaces* **2013**, *5*, 4516.

(169) Moehl, T.; Tsao, H. N.; Wu, K.; Hsu, H.; Chi, Y.; Ronca, E.; Angelis, F. De; Nazeeruddin, M. K.; Grätzel, M. *Chem. Mater.* **2013**, *25*, 4497.

(170) Feng, J.; Jiao, Y.; Ma, W.; Nazeeruddin, M. K.; Grätzel, M.; Meng, S. *J. Phys. Chem. C* **2013**, *117*, 3772.

(171) Favereau, L.; Warnan, J.; Anne, F. B.; Pellegrin, Y.; Blart, E.; Jacquemin, D.; Odobel, F. *J. Mater. Chem. A* **2013**, *1*, 7572.

(172) Zhang, J.; Li, H.-B.; Geng, Y.; Wen, S.-Z.; Zhong, R.-L.; Wu, Y.; Fu, Q.; Su, Z.-M. *Dye. Pigm.* **2013**, *99*, 127.

(173) Haid, S.; Marszalek, M.; Mishra, A.; Wielopolski, M.; Teuscher, J.; Moser, J.-E.; Humphry-Baker, R.; Zakeeruddin, S. M.; Grätzel, M.; Bäuerle, P. *Adv. Funct. Mater.* **2012**, *22*, 1291.

(174) Barea, E. M.; Bisquert, J. *Langmuir* **2013**, *29*, 8733.

(175) Liu, J.; Zhou, D.; Wang, F.; Fabregat-Santiago, F.; Miralles, S. G.; Jing, X.; Bisquert, J.; Wang, P. *J. Phys. Chem. C* **2011**, *115*, 14425.

(176) Shi, P.; Amb, C. M.; Knott, E. P.; Thompson, E. J.; Liu, D. Y.; Mei, J.; Dyer, A. L.; Reynolds, J. R. *Adv. Mater.* **2010**, *22*, 4949.

(177) Amb, C. M.; Chen, S.; Graham, K. R.; Subbiah, J.; Small, C. E.; So, F.; Reynolds, J. R. *J. Am. Chem. Soc.* **2011**, *133*, 10062.

(178) Beaujuge, P. M.; Pisula, W.; Tsao, H. N.; Ellinger, S.; Müllen, K.; Reynolds, J. R. *J. Am. Chem. Soc.* **2009**, *131*, 7514.

(179) Lin, L.-Y.; Tsai, C.-H.; Wong, K.-T.; Huang, T.-W.; Hsieh, L.; Liu, S.-H.; Lin, H.-W.; Wu, C.-C.; Chou, S.-H.; Chen, S.-H.; Tsai, A.-I. *J. Org. Chem.* **2010**, *75*, 4778.

(180) Zeng, W.; Cao, Y.; Bai, Y.; Wang, Y.; Shi, Y.; Zhang, M.; Wang, F.; Pan, C.; Wang, P. *Chem. Mater.* **2010**, *22*, 1915.

(181) Turbiez, M.; Frère, P.; Roncali, J. *J. Org. Chem.* **2003**, *68*, 5357.

(182) Snaith, H. J. *Adv. Funct. Mater.* **2010**, *20*, 13.

(183) Patel, D. G.; Feng, F.; Ohnishi, Y.; Abboud, K. a; Hirata, S.; Schanze, K. S.; Reynolds, J. R. *J. Am. Chem. Soc.* **2012**, *134*, 2599.

(184) Nazeeruddin, K.; Humphry-baker, R.; Liska, P.; Grätzel, M. *J. Phys. Chem. B* **2003**, *107*, 8981.

(185) Haque, S. A.; Handa, S.; Peter, K.; Palomares, E.; Thelakkat, M.; Durrant, J. R. *Angew. Chem. Int. Ed* **2005**, *44*, 5740.

(186) Huang, J.; Fu, H.; Wu, Y.; Chen, S.; Shen, F.; Zhao, X.; Liu, Y.; Yao, J. *J. Phys. Chem. C* **2008**, *112*, 2689.

VITA

CORALIE A. RICHARD

Coralie A. Richard was born in the Olympic city of Albertville, France in 1986. After obtaining her baccalaureat in science, Coralie moved to Lyon to study advanced topics in mathematics, physics and chemistry at the Lycée du Parc. The Concours aux Grandes Ecoles gave her access to the Graduate School of Physics and Chemistry of Bordeaux (ENSCBP) where she spent two years learning the principles of chemical engineering, for which she obtained her Masters in Chemical Engineering in 2009. She enrolled in the graduate chemistry program at the University of Florida in Gainesville, Fl., where she joined the group of Professor John Reynolds, working in the area of organic electronics, and she specialize in the synthesis of conjugated oligomers for dye-sensitized solar cell applications. As Professor Reynolds moved to the Georgia Institute of Technology, Coralie had the opportunity to live in her second Olympic city, Atlanta. She is planning to graduate in 2014 with a doctoral degree from the Georgia Institute of Technology.